Title
Photochemical control of neuronal activity: methods and clinical application

Author
Tochitsky, Ivan

Publication Date
2013

Peer reviewed|Thesis/dissertation

Photochemical control of neuronal activity:

methods and clinical application

by

Ivan Tochitsky

A dissertation submitted in partial satisfaction of the

requirements for the degree of

Doctor of Philosophy

in

Molecular and Cell Biology

in the

Graduate Division

of the

University of California, Berkeley

Committee in charge:

Professor Richard Kramer, Chair

Professor Ehud Isacoff

Professor Diana Bautista

Professor Sheng Luan

Fall 2013

Photochemical control of neuronal activity:

methods and clinical application

By Ivan Tochitsky

Abstract

Photochemical control of neuronal activity: methods and clinical application

by Ivan Tochitsky

Doctor of Philosophy in Molecular and Cell Biology

University of California, Berkeley

Professor Richard Kramer, Chair

Mammalian nervous systems are incredibly complex, with almost 100 billion neurons making up the human brain. Neurons in the brain primarily communicate with one another in one of two ways – electrically, via the flow of ions across the cell membrane, or chemically by releasing and detecting a variety of signaling molecules. In order to understand the function of the nervous system, we need to be able to manipulate it with high spatial and temporal precision. Conventional electrical or chemical stimuli do not allow for such precise control. Thus, a new and orthogonal stimulus modality had to be utilized in order to facilitate the study of the nervous system. The emerging field of optogenetics uses light as such a stimulus since light can be delivered only to a small part of the nervous system, or even a single neuron, and the illumination can be controlled with millisecond time resolution. Optogenetic techniques involve the expression of light-sensitive proteins from microbes in genetically targeted populations of neurons, rendering those neurons sensitive to light. Recent advances in optogenetics have greatly advanced our understanding of the function of the nervous system both in healthy organisms, and in the context of disease. Optogenetics is a powerful technique for investigating neural networks, but this approach primarily studies the function of the nervous system at a system rather than molecular level. The vast complexity of the human brain is created not only by the large number of individual neurons and the intricate connections between them, but also by the dizzying variety of proteins found in the cell membranes of these neurons. These proteins sense and respond to the release of chemical signaling molecules from neighboring cells, or changes in ion concentrations that alter the cell's membrane potential, allowing for the generation and propagation of electrical signals.

We have combined the powers of synthetic chemistry and genetics to develop novel optopharmacological or optochemical genetic methods which enable precise optical control of neuronal function at the molecular level. These strategies involves the generation of light-sensitive "photoswitch" molecules that selectively target a population of either genetically engineered or endogenous membrane proteins – including receptors sensing chemical stimuli, or ion channels responding to electrical potential changes in the cell. The addition of a photoswitch compound to a neuron expressing the target protein makes that protein, and, by extension, the neuron, sensitive to light. We first applied this strategy to generate light regulated neuronal nicotinic acetylcholine receptors, which are a group of proteins that respond to the chemical neurotransmitter acetylcholine. These receptors modulate the activity of other neurons in different parts of the brain and are also sensitive to nicotine, an addictive chemical found in tobacco products. The function of acetylcholine receptors in the brain and their role in nicotine addiction, neuropsychiatric and neurodegenerative disorders is not fully understood, in large part because it quite difficult to chemically manipulate individual receptors without affecting others.

Making light-sensitive, genetically targeted acetylcholine receptors should thus greatly advance our understanding of those receptors' function.

The main rationale for making proteins or neurons light-sensitive is to facilitate the study of the healthy nervous system as well as its malfunction in disease. There are, however, several human diseases where optical methods for controlling neuronal activity could directly provide a clinical benefit. Degenerative blinding diseases such as retinitis pigmentosa or age-related macular degeneration leave the retinas of affected patients either partly or completely insensitive to light by causing the death of light-detecting photoreceptor cells in the eye. Light responses can be restored to a blind retina by making some or all of the remaining retinal neurons sensitive to light. This can be achieved via the expression of light sensitive microbial opsins or engineered receptors in retinal neurons that are not normally light sensitive. Both of these approaches have restored some visual perception to blind mice suffering from retinitis pigmentosa. However, in order to use either optogenetic or optochemical genetic tools in the clinic, the mutant proteins must be artificially expressed in the patient's retina, which requires the use of viral gene therapy. Gene therapy has potential health risks, so we decided to develop a treatment for blinding diseases that would only involve a light-sensitive chemical, without the need for gene therapy or invasive surgery.

To that end, we have developed an optopharmacological therapy for vision restoration by creating photoswitch molecules that block and unblock endogenous voltage-gated ion channels in a light-dependent manner, allowing us to control almost any neuron with light. The first photoswitch tested, called AAQ, restored electrical retinal light responses, the pupillary light reflex, as well as other simple visual behaviors in blind mice. In order to optimize this treatment for clinical use, we generated a compound called DENAQ with improved light sensitivity and persistence in the eye, which responds to broad spectrum white light, similar to what people encounter in natural visual scenes. Furthermore, DENAQ acts selectively on retinas suffering from photoreceptor cell death, but leaves healthy retinas unaffected. This selectivity raises the possibility that we may be able to treat not only patients who are completely blind, but also those suffering from partial vision loss, by restoring light sensitivity only to the parts of the retina experiencing photoreceptor degeneration. The promising preliminary results from animal studies suggest that our optopharmacological strategy for vision restoration may eventually be used in the clinic, in addition to helping researchers understand the function of the nervous system in its normal state and in disease.

Table of Contents

Dedication

To my family:

Thank you for your continued support

Acknowledgements

I would like to begin by thanking my thesis advisor, Richard Kramer, for accepting me into his lab and being an outstanding mentor throughout the last five years. He has provided me with the opportunity to learn about neuroscience and showed me that anything in science is possible with hard work and creativity. I also appreciate the freedom he allowed me to explore various research projects and ideas and the collaborative environment he fostered in the lab. Rich has made me into a much better scientist and prepared me well for my future career.

I would also like to thank my thesis committee members - Ehud Isacoff, Diana Bautista and Sheng Luan - for providing valuable insight and guidance throughout my Ph.D. Their support was very helpful and I enjoyed working with them, both as mentors and as collaborators.

Additionally, I want to thank all of the members of the Kramer lab, past and present, who laid the foundation for my work and assisted in its successful completion. Alexandre Mourot was a wonderful collaborator and mentor in the lab who taught me a lot about ion channel function and electrophysiology. Not only is he a great scientist, but he has become my friend as well, and I hope to continue working with him in the future. Rachel Montpetit and Neil Wilson both provided essential administrative support over the years and helped with various cloning projects, for which I am very grateful. Aleksandra Polosukhina and Tracy Huang introduced me to the vision restoration project and provided very helpful advice and feedback in its early stages. We could not have advanced as far as we have in our search for a cure for blindness in such a short time without their invaluable contributions. I also want to thank all other members of the Kramer lab, including, but not limited to, Christopher Tsang, Christian Herold, Christopher Davenport, Lars Holzhausen, Jeffrey Litt, Caleb Smith and Joe Driscoll. You have made my time in the lab a wonderful and unforgettable experience. I had a lot of fun, not just doing science, but enjoying life and spending time with the friends I have made in the lab.

Last but not least, I would like to thank my friends and family who supported me throughout my Ph.D. I'm not sure I could have completed my work over the past five, sometimes difficult and stressful years without their help. Most of all, I want to thank my parents, Marina and Sergei, for always encouraging me to follow my dreams and do what I enjoyed in life, as well as helping me realize that I really enjoy doing science. I would also like to thank my sister Yana for not letting me get too serious and bringing me down to earth when I needed it and my grandparents, Liudmila and Yasha for their support.

Thesis summary

Chapter 1:

The first chapter of the thesis describes the design and characterization of light activated and light inhibited neuronal nicotinic acetylcholine receptors. The ability to specifically and precisely control the activity of particular neuronal nicotinic receptors with light will allow for much more sophisticated and detailed analysis of these receptors' function in the brain. This study not only describes the photosensitization of an important family of neuronal receptors but also presents a strategy for making virtually any receptor sensitive to light.

Chapter 2:

The second chapter of the thesis describes the use of a light sensitive ion channel blocker, AAQ, to restore visual function in blind mice. This successful proof of principle study introduces a novel pharmacological strategy for treating blindness that could be of great benefit to patients with degenerative retinal disorders like retinitis pigmentosa and age-related macular degeneration.

Chapter 3:

The third chapter of the thesis builds upon our initial successful demonstration of pharmacological vision restoration in blind animals and presents a light sensitive ion channel blocker, DENAQ, which is more suited for clinical use than AAQ. DENAQ photosensitizes blind mouse retinas but has no effect on retinas from sighted mice. The disease-selective action of DENAQ suggests it could target parts of retina which are losing vision without impairing remaining visual function, thus greatly expanding the number of patients that could potentially benefit from our treatment.

Part I: Methods for optical control of neuronal function

Introduction

The study of intricate neural networks requires the ability to manipulate individual neurons as well as genetically defined groups of neurons in a spatially defined region with millisecond temporal precision, in order to be able to generate neural responses approximating those occurring naturally and to minimize confounding effects resulting from the stimulation of other neurons in the system. Conventional pharmacological or electrical stimulation lacks the necessary precision required for such a task. Drugs can diffuse from the site of treatment to affect many different types of neurons and often remain in the tissue for considerable periods of time, making any sort of temporal control challenging. Electrical stimulation allows for only the manipulation of a single neuron at a time or the non-selective excitation of all neurons in a part of the nervous system, limiting its utility. To overcome these shortcomings, neuroscientists have sought to control neuronal activity with orthogonal stimuli distinct from typical modes of neuronal communication and target these stimuli using the tools of molecular biology and genetics, which allow for the expression of genes in selected neuronal populations. Francis Crick has proposed light, especially of a wavelength able to penetrate into tissue, as the ideal modality for controlling neuronal function[1], since it can be delivered with exquisite spatiotemporal precision. Other neuroscientists, aware of the advantages of using light, have developed a variety of tools that use light in order to manipulate neuronal activity.

The various approaches for the optical control of neuronal function can be divided into those taking advantage of natural light-sensitive proteins and compounds, for example the chromophore retinal, which is found in light sensing photoreceptor cells in the eye[2], and those synthesized by chemists to target a particular receptor or ion channel (Fig. 1). Caged compounds, including amino acids, peptides and other biologically active molecules, are one class of synthetic light-sensitive compounds currently being used in neuroscience research. These compounds are typically derivatives of natural signaling molecules that have been covalently modified with a light-cleavable moiety, in such a way that the caged version of the molecule lacks any biological activity. Illumination of the caged compound removes the "cage", allowing the compound to act on its biological target. Some of the first caged molecules included adenosine triphosphate (ATP)[3] and cyclic adenosine monophosphate (cAMP)[4] analogs. The caged compound strategy was later applied to molecules of interest in neuroscience, including neurotransmitters such as acetylcholine[5] and glutamate[6]. More recently, neuropeptides and other signaling molecules have also been modified with photolabile cage groups[7]. The versatility of the caged compound strategy and the advantages of optical control have made these molecules a powerful tool for interrogating various signaling pathways involved in brain function.

One drawback of using caged compounds is the fact that photolysis is irreversible, and, after being released from its protective "cage", the biologically active compound can diffuse from the site of illumination to affect other targets in the tissue being studied. Furthermore, current agonists or antagonists of various receptors often lack specificity, creating the possibility for off-target effects whenever a caged compound is illuminated and the active compound is released. An alternative strategy was thus developed to allow for the reversible photocontrol of genetically defined biological targets. This approach often utilizes compounds, such as azobenzene or

Figure 1

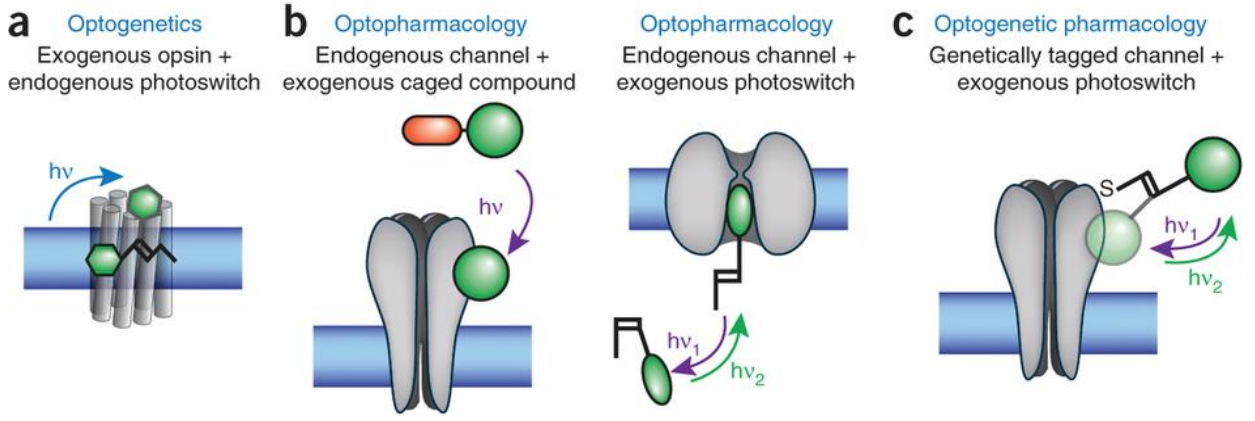

Figure 1: Strategies for controlling neuronal function with light

Schematic representations of **a**) Optogenetic **b**) Caged compound / Optopharmacological and **c**) Optogenetic pharmacological methods for optical control of neuronal function. Reprinted with permission from Kramer *et al*., *Nature Neuroscience* 2013[8].

spiropyran, that possess the unusual property of reversible photoisomerization, where they change their configuration from *trans* to *cis* and vice versa upon illumination with different wavelengths of light[9]. Azobenzene and its derivatives in particular, have become the molecules of choice for groups attempting to control neurons or neuronal receptors with light.

The photoswitch strategy involves the development of a ligand containing the light-sensitive azobenzene core in addition to a biologically active moiety, for example quaternary ammonium[10]. The resulting compound can be synthesized in such a way that only one of its two isomers, *trans* or *cis*, will have biological function at its intended target, or its affinity for its target in its two forms will be dramatically different. By using different wavelengths of light to convert between the two isomers, one can thus reversibly control the activity of the compound's target, typically a receptor or ion channel. In order to achieve genetic specificity, a mutant residue such as cysteine needs to be introduced into the receptor of interest which will then covalently react with a maleimide group that is a part of the photoswitch. By screening various mutations, one can identify residues where covalent conjugation of the photoswitch will result in the biologically active moiety only being able to reach its binding site in either the *trans* or the *cis* configuration. This approach, called chemical optogenetics, was first applied to the Shaker potassium channel from *Drosophila melanogaster*[10], and later extended to ionotropic[11] and metabotropic[12] glutamate receptors.

An alternative, optogenetic strategy for optical control of neuronal activity uses microbial opsin proteins, many of which incorporate the light sensitive molecule retinal. These opsins are ion channels or pumps which allow or block the flow of ions across the cell membrane in a light dependent manner, thus controlling the membrane potential and neuronal activity. Since retinal is already present in the vertebrate nervous system, exogenous expression of the opsin protein

alone in a genetically defined population of neurons makes these neurons light sensitive. The first microbial opsin expressed in mammalian neurons was channelrhodopsin, a depolarizing cation channel sensitive to blue light[13]. Other opsins, such as the hyperpolarizing proton pump, halorhodopsin[14], have expanded the optogenetic tool kit, and the spectral sensitivity as well as other biophysical properties of these opsins have been optimized by mutagenesis[15]. Domains from light sensitive microbial and plant proteins have also been incorporated into membrane receptors to enable optical control of cell signaling[16]. In the last decade, optogenetics has become a powerful and widely used technique in neuroscience, shedding light on the function of the brain in healthy animals and in disease[17].

As mentioned previously, however, the primary utility of optogenetics is in studying the function of the brain at a network or systems level, since it enables the optical manipulation of genetically defined groups of neurons with high spatiotemporal precision. The optochemical genetic strategy is better suited to manipulating the function of individual receptors or ion channels at a molecular level in order to understand their contribution to various cellular processes. In particular, optochemical genetics allows researchers to dissect the role of individual receptor subtypes, which can be composed of various subunits and located in different types of cells or in different cellular compartments. Traditional pharmacology often lacks the specificity needed to determine the function of individual receptor subtypes. Genetic manipulation is gene-specific, but can lead to undesirable compensatory changes or alter the receptor's function in unpredicted ways. Optochemical genetics overcomes these drawbacks by adding an orthogonal optical control modality to a mutant receptor that is almost identical to its endogenous wild-type analog[18]. One family of receptors which can benefit from the application of optochemical genetics are nicotinic acetylcholine receptors, since there dozens of different nicotinic receptor subtypes in the brain whose function is not fully understood[19]. We thus set out to create light regulated nicotinic acetylcholine receptors in order to enable a functional characterization of their role in the brain and demonstrate the broad applicability of optochemical genetics to multiple classes of neurotransmitter receptors.

Chapter 1: Development of light-regulated neuronal nicotinic acetylcholine receptors

The data presented below have been published in the following article which is reprinted in full with permission:

Tochitsky I., Banghart M.R., Mourot A., Yao J.Z., Gaub B., Kramer R.H., Trauner D. "Optochemical control of genetically engineered neuronal nicotinic acetylcholine receptors". *Nature Chemistry* 2012 Jan 10;4(2):105-11.

Author contribution

M.R.B., A.M., R.H.K. and D.T. designed the research. M.R.B. and J.Z.Y. synthesized the ligands. I.T., A.M., and B. G. performed the research and analyzed data. I.T., M.R.B. and D.T. wrote the paper.

Abstract

Advances in synthetic chemistry, structural biology, molecular modeling, and molecular cloning have enabled the systematic functional manipulation of transmembrane proteins. By combining genetically manipulated proteins with light-sensitive ligands, innately "blind" neurobiological receptors can be converted into photoreceptors, allowing them to be photoregulated with high spatiotemporal precision. Here, we present the optochemical control of neuronal nicotinic acetylcholine receptors (nAChRs) with photoswitchable tethered agonists and antagonists. Using structure-based design, we have produced heteromeric α3β4 and α4β2 nAChRs that can be activated or inhibited with deep violet light but respond normally to acetylcholine in the dark. The generation of these engineered receptors should facilitate the investigation of the physiological and pathological functions of neuronal nAChRs and open a general pathway to photosensitizing pentameric ligand-gated ion channels.

Introduction

Acetylcholine (ACh) and its receptors have always been at the forefront of new developments in physiology. With its isolation as "Vagusstoff" in 1921, Otto Loewi established that a small diffusible molecule could mediate nervous activity and shaped the concept of a neurotransmitter[20]. Nicotinic ACh receptors (nAChRs) were among the first ion channels investigated long before the advent of molecular cloning and heterologous expression[21]. Numerous techniques in biophysics and chemical biology, including patch clamp electrophysiology[22], cryo-electron microscopy[23], and the expansion of the genetic code[24], were developed using nAChRs, and the powerful methods of molecular cloning were applied to nAChRs early on[25,26]. These studies established that nAChRs are pentameric ligand-gated cation channels that are expressed throughout the mammalian nervous system and at the neuromuscular junction[20]. The neuronal nAChR subtypes are composed of α2-α10 and β2-β4 subunits and can assemble both as heteromeric [e.g. $(\alpha4)_2(\beta2)_3$] and homomeric [e.g. $(\alpha7)_5$] pentamers[20]. Whereas the function of muscle nAChRs is well established, the physiological roles of neuronal nAChRs are still being unraveled. For instance, they have been strongly implicated in the pathophysiology of several psychiatric disorders as well as nicotine addiction and Alzheimer's disease[19,20]. However, progress in this regard has been held back by the lack of subtype-selective nAChR pharmacology and the difficulties associated with selectively targeting nAChRs in different parts of the brain.

These issues can be addressed using an approach called "Optochemical Genetics"[18,27]. In essence, this is an effort to photosensitize innately "blind" receptors using synthetic photoswitches. These can be covalently attached as photoswitchable tethered ligands (PTLs), which require a reactive functional group for bioconjugation - typically the sulfhydryl group of a cysteine[9,10]. By introducing the cysteine through genetic manipulation, these receptors can be targeted in a subtype-selective manner based on the subunit that contains the mutation[28]. Furthermore, the mutant receptors can be expressed in specific cell types in the brain and controlled with the millisecond precision and subcellular spatial resolution only light can provide[9,10]. This has already been achieved with voltage-gated ion channels and glutamate receptors. We now demonstrate that our approach towards photosensitizing Nature's molecular machines can be applied to pentameric ligand-gated ion channels as well, introducing the genetically targeted, Light-controlled nAChR (LinAChR).

Results

Photoswitchable tethered ligand design.

The development of LinAChR first required the design and synthesis of proper PTLs. Our PTLs typically consist of a maleimide as a cysteine reactive group, an azobenzene photoswitch, and a ligand head group that resembles known receptor agonists or antagonists. Three compounds known to interact with nAChRs guided the choice of the ligand: the photoaffinity label **AC-5** (**1**), the agonist homocholine phenyl ether (**HoChPE**) (**2**), and the antagonist **MG-624** (**3**). The presence of an aromatic ring separated by 7 atoms from the ACh moiety in **AC-5** (Fig. 1a), which acts as a full agonist at muscle nAChRs[29], suggests that the steric bulk of an azobenzene photoswitch may be tolerated in PTLs that act as tethered agonists. Although the much shorter molecule **HoChPE** is an agonist of nAChRs[30,31], the stilbene derivative **MG-624** is a potent antagonist of neuronal receptors[32]. Based on the steric similarity of stilbenes and azobenzenes, we therefore anticipated that corresponding PTLs could function as antagonists. Based on these model compounds, we synthesized Maleimide-Azobenzene-AcylCholine (**MAACh**) (**4a,b**) (Fig. 1a), a putative photoswitchable agonist for nAChR. We also synthesized Maleimide-Azobenzene-HomoCholine (**MAHoCh**) (**5a,b**) (Fig. 1b), wherein the choline moiety was replaced with homocholine and the spacer was removed to resemble **MG-624**. **MAACh** and **MAHoCh** were prepared by multistep total synthesis, as detailed in Supplementary Fig. S1. By taking absorbance measurements of the ligands in solution, we determined that both molecules can be maximally converted to their *cis* isomer by illumination with 380nm light and can then be reset to the *trans* isomer by 500nm illumination or thermal relaxation in the dark (Supplementary Fig. S2).

Preferably, a photosensitive receptor would be inactive in the dark, where azobenzene photoswitches generally reside in a *trans* configuration (Fig. 1c). Illumination with 380nm light would produce the *cis* configuration of the azobenzene and activate the receptor. Deactivation could then be achieved through conversion of the photoswitch back to its inactive *trans* configuration by illumination with 500nm or by thermal relaxation in the dark. Likewise, a tethered antagonist should block the receptor in its *cis* configuration (i.e. at 380nm), but should leave the receptor unimpaired in its *trans* configuration (at 500nm or in the dark), allowing it to be activated by free acetylcholine (Fig. 1d).

Attachment site screening.

These functional requirements can be met by the proper choice of cysteine attachment sites, which we decided to place on the β2 or β4 subunits of heteropentameric neuronal nAChRs. Using the X-ray structure of an acetylcholine binding protein (AChBP) in complex with carbamylcholine (PDB ID:1uv6)[33] and the model of AC-5 docked into the *Torpedo* nAChR[29] we identified an antiparallel beta sheet in the β subunit facing the ligand-binding site as a potential region for PTL attachment. Based on the calculated structures of our PTLs and distance measurements in the protein structures, we decided to install cysteines in positions S32, R34, E61, T63, R113, N115, and S117 of the β4 nAChR subunit. Homologous residues with identical numbering were chosen for β2. These residues are shown mapped onto a homology model of the

Figure 1

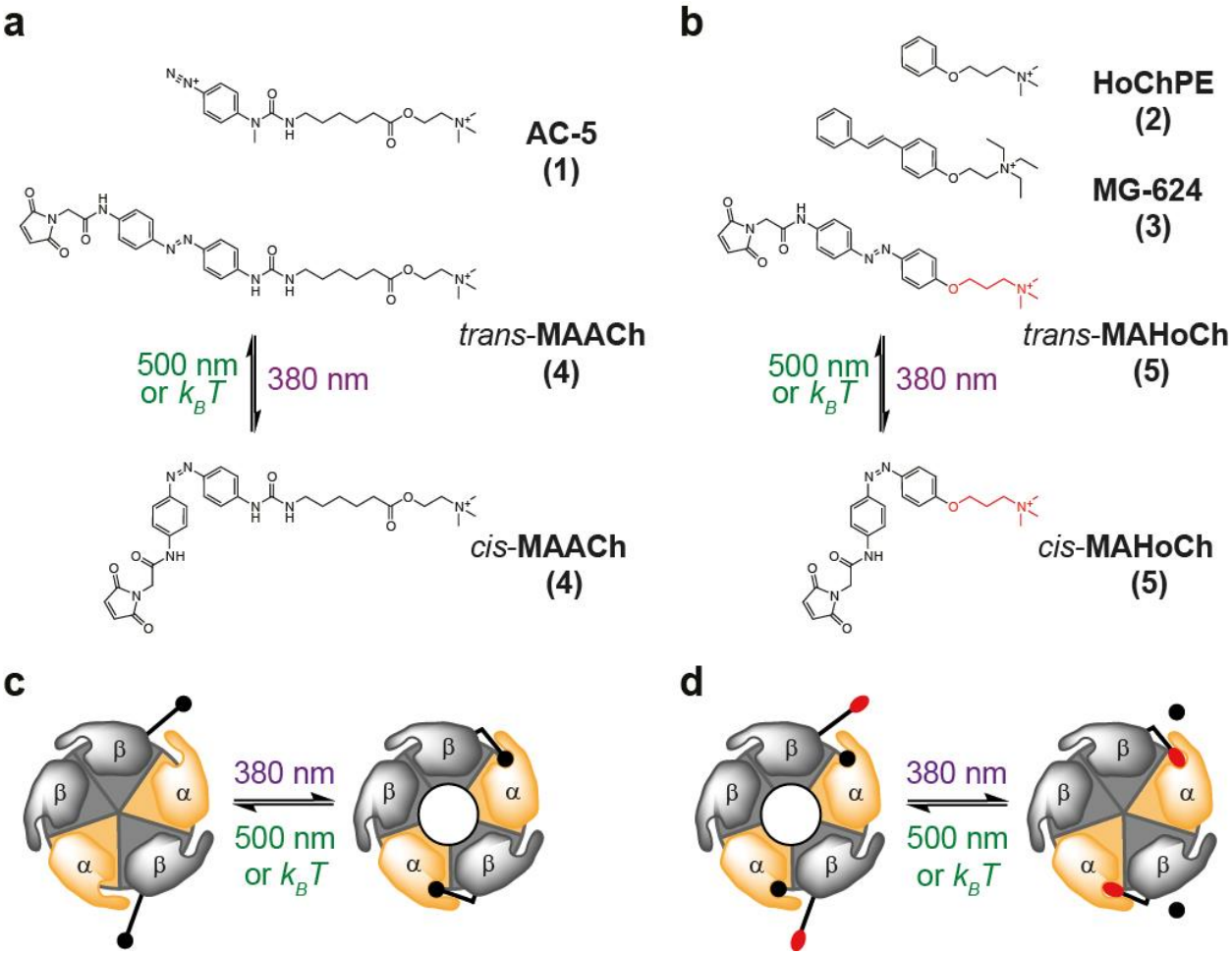

Figure 1: Photoswitchable ligand design for the optical control of neuronal nicotinic acetylcholine receptors.

(**a, b**) Structures of **AC-5** and **MAACh** (**a**) as well as **HoChPE, MG-624** and **MAHoCh** (**b**). The PTL molecules photoisomerize from *trans* to *cis* upon illumination with 380nm light and revert to *trans* under 500nm light or in the dark.
(**c**) A tethered agonist is converted from its *trans* to its *cis* configuration under 380nm light, thus activating heteropentameric nicotinic ACh receptors. Illumination with 500nm light or thermal relaxation deactivates the receptor.
(**d**) A tethered antagonist is converted from its *trans* to its *cis* configuration under 380nm light, blocking heteromeric nicotinic ACh receptors from binding to ACh (black). Illumination with 500nm light or thermal relaxation unblocks the receptor, allowing it to be activated by the neurotransmitter.
α4β2 receptor[34] (PDB ID:1ole) (Figs. 2a,b), based on the structure of AChBP[35]. A sequence alignment that relates these positions on various complementary subunits to AChBP is also provided (Supplementary Fig. S3).

Our choice of cysteines was further validated by molecular docking studies, which were carried out using the same homology model (Fig. 2c). Unconstrained *cis*-**MAACh** and *trans*-**MAACh** were docked into the α4β2 model, while allowing rotatable bonds in the ligand to move freely. We found that the maleimide moiety of **MAACh** comes very close to several of the engineered cysteine mutants shown in Fig. 2b in the *cis* form of the azobenzene photoswitch, in particular to cysteines in positions 61, 63 and 117 (Fig. 2c), but extends past most of them in its *trans* form (Fig. 2d). Molecular modeling studies with **MAHoCh** were not undertaken due to the lack of ligand similarity in the antagonist-bound AChBP structures[36] and the absence of a homology model of an antagonist-bound heteromeric neuronal nAChR.

To test our predictions experimentally, we first introduced the seven independent cysteine mutations into the β4 subunit. We then screened α4β4 mutant nAChRs heterologously expressed in *Xenopus* oocytes, since this particular heteropentamer desensitizes very slowly compared to nAChRs composed of other neuronal subunits[37]. The oocyte system was chosen for its robust expression of heteromeric nAChRs and the lack of endogenous receptors. By contrast, non-neuronal mammalian cell lines often express nAChRs poorly and many neuronal mammalian cell lines possess endogenous nAChRs, which would complicate the screening process.

Using two-electrode voltage clamp recordings, we screened these α4β4 mutants for *cis*-agonism by treating oocytes with **MAACh** in the dark and then looking for current induction upon illumination with 380nm light. We identified three cysteine mutations on the β4 subunit where **MAACh** could evoke a photoactivatable current in the *cis* but not the *trans* configuration: E61C, R113C, and S117C. In the structure of carbamylcholine-bound AChBP[33], the distances from the alpha carbons of each of the three positions and the carbonyl carbon of carbamylcholine were very similar (10.43 Å, 11.28 Å and 12.11 Å for the E61C, R113C, and S117C mutants, respectively). The remaining residues were farther away (19.03 Å, 14.28 Å, 16.39 Å, and 16.54 Å for S32C, R34C, T63C, and N115C, respectively).

Photoactivation of engineered nicotinic acetylcholine receptors.

For comprehensive electrophysiological analysis, these mutant β4 subunits were expressed as α3β4 heteropentamers, which have a more established presence in the nervous system[38]. After labeling the α3β4 E61C receptor with **MAACh**, illumination with 380nm light produced an inward current that could be reversed with 500nm light (Fig. 3a). The amplitude of the photoactivatable current was 6.8±1.3 % (mean±SEM, n=10) of the saturating cholinergic current and the receptor still responded normally to perfusion of ACh in the dark. Neither the E61C mutation nor **MAACh** conjugation greatly changed the EC50 of the receptor for ACh (Fig. 3b, Supplementary Table S1)). **MAACh** labeling at the other two residues, β4R113C and β4S117C also produced photoactivatable currents of similar magnitude (Supplementary Fig. S4).

Next, we transposed the E61C mutant from the β4 to the β2 subunit, and tested whether **MAACh** conjugation at the β2E61C position could photoactivate the neuronal α4β2 receptor. Indeed, the **MAACh**-labeled α4β2E61C receptor also produced an inward current under 380nm light, which could be terminated with 500nm light (Fig. 3c). The amplitude of the photoactivatable current was 16.1±2.1% (mean±SEM, n=15) of the saturating cholinergic current. The E61C mutation

Figure 2

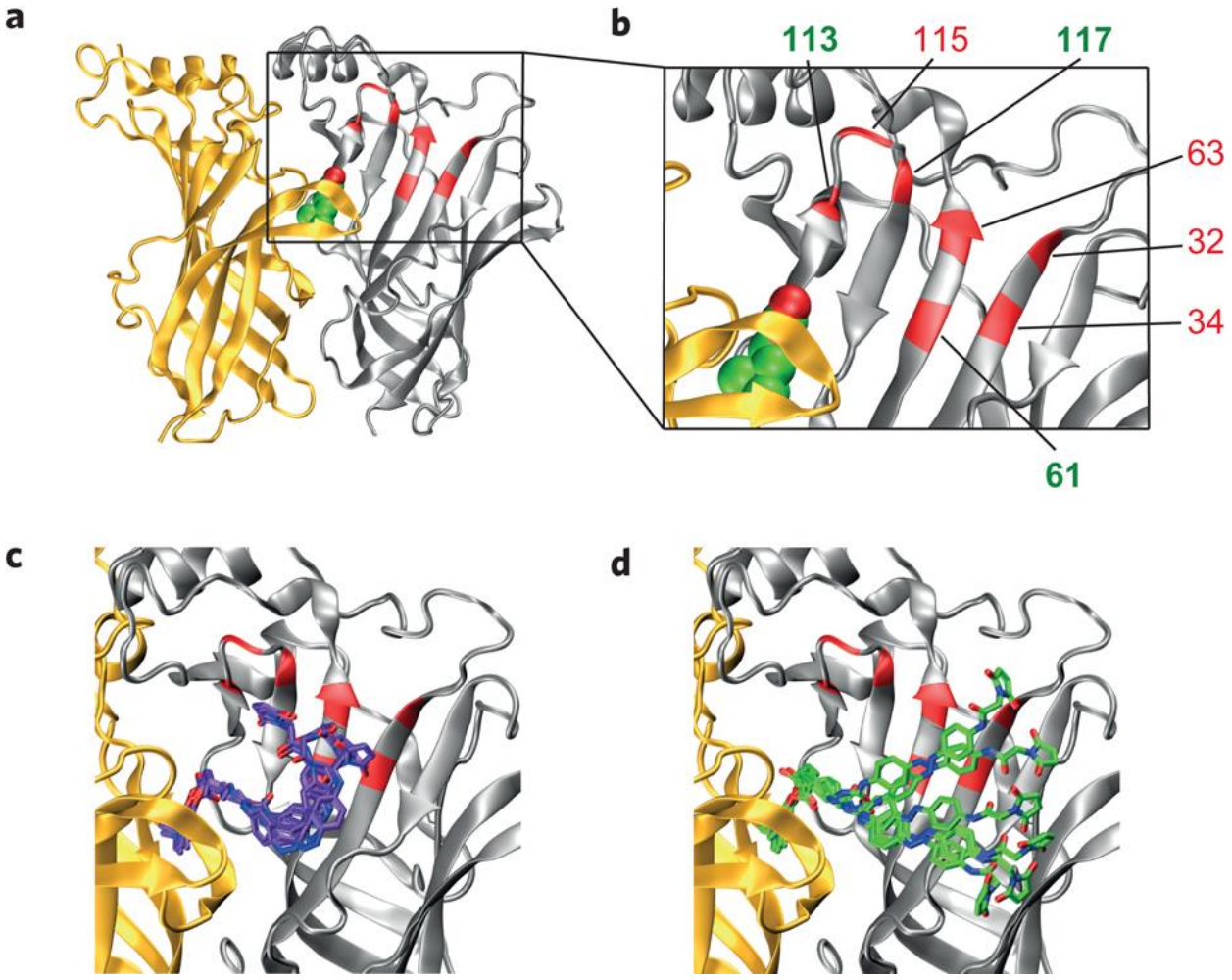

Figure 2. Choice of cysteine attachment sites for photoswitchable ligand conjugation.

(**a**, **b**) Homology model of the α4β2 nAChR with ACh (green and red spheres) docked in the binding site and the engineered cysteine mutants shown in red and numbered in the zoomed in view of the receptor (**b**). Only one α/β (α-yellow, β-grey) interface is shown for clarity.
(**c**, **d**) Docking results with unconstrained *cis*-**MAACh** (violet) (**c**) and *trans*-**MAACh** (green) (**d**) in the α4β2 homology model. Six of the most energetically favorable conformations are shown

Figure 3

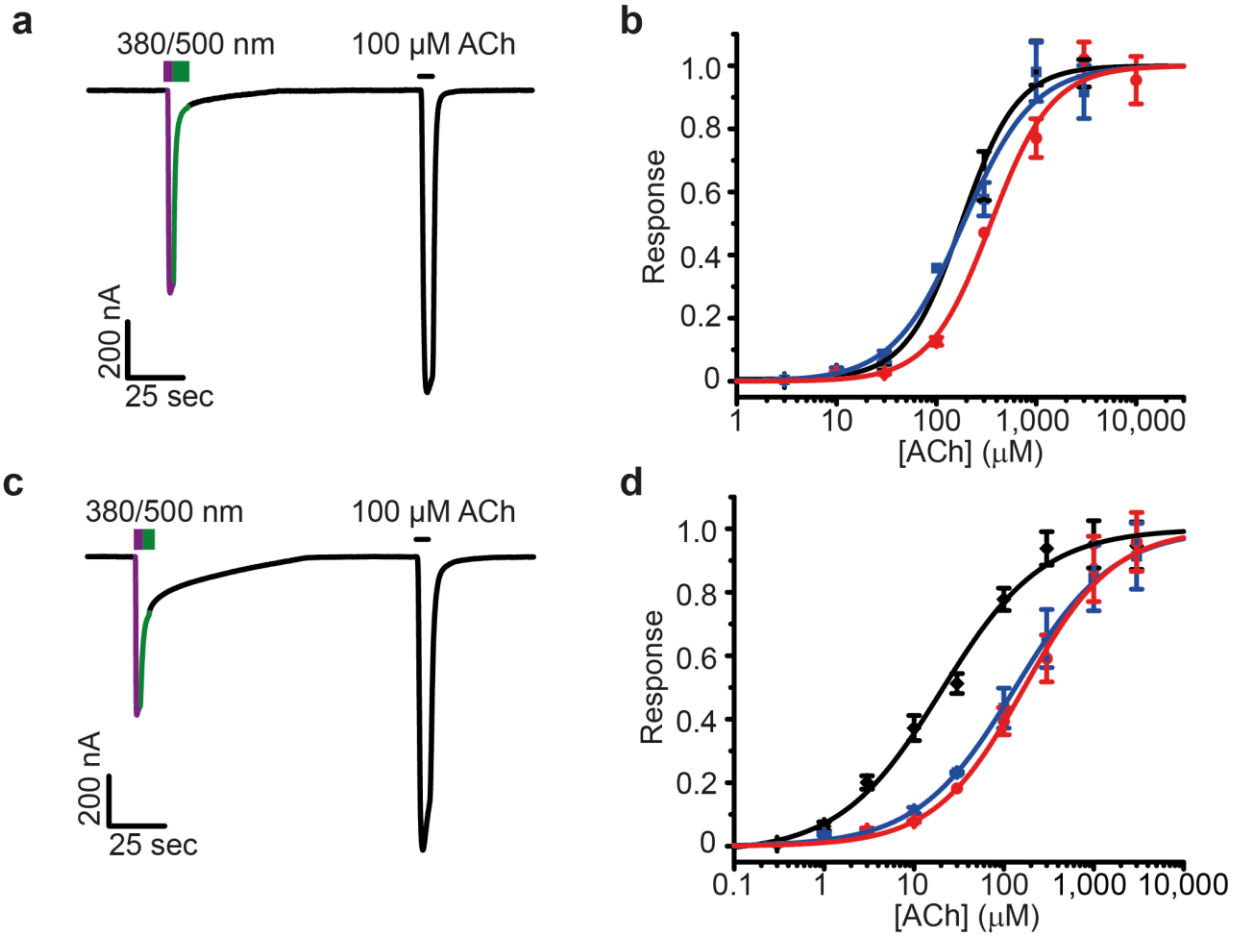

Figure 3. Photoactivation of nicotinic acetylcholine receptors with a tethered agonist.

(**a**, **c**) Photoactivation of the α3β4E61 (**a**) and the α4β2E61C (**c**) mutant receptors by tethered **MAACh** in *Xenopus* oocytes. 380nm light (violet) triggers photoactivatable current and 500nm light (green) shuts it off.
(**b**, **d**) ACh dose response curves for the α3β4 (**b**) and the α4β2 (**d**) wild type (black), E61C mutant (blue) and the E61C mutant with tethered **MAACh** in the dark (red). Data are mean±SEM, n=5.

increased the EC50 of the α4β2 receptor for ACh. Labeling with **MAACh** did not change this EC50 further (Fig. 3d, Supplementary Table S1).

The prominence of the E61C mutant motivated us to carry out another molecular docking study, wherein the maleimide moiety of **MAACh** was "virtually tethered" to be in the proximity of the sulfhydryl group of the E61C residue (Figs. 4a,b). Allowing the remainder of the PTL to move about freely resulted in docking of the ligand head group into the ligand-binding site in all conformations. By contrast, none of the tethered *trans*-**MAACh** conformations reached the ligand-binding site (Figs. 4a,b; Supplementary Fig. S5). These molecular docking studies corroborate our finding that the agonist is only able to reach the ligand-binding site and activate the receptor in its *cis* but not its *trans* configuration.

Photoinhibition of engineered nicotinic acetylcholine receptors.

We then proceeded to test the effect of **MAHoCh** attached to the three *cis*-agonist active cysteine mutants in α3β4 heteromeric nAChRs. After treating oocytes with the PTL in the dark, we determined that illumination with 380nm and 500nm light did not produce photoactivatable current with any of the three mutants (Supplementary Fig. S6). Instead, illumination with 380nm light dramatically reduced the response of the α3β4E61C receptor to ACh, while 500nm light restored the initial response to ACh (Fig. 5a). This indicates that tethered **MAHoCh** acts as a *cis*-antagonist of the α3β4E61C receptor. ACh-evoked currents were not substantially modulated by illumination at the α3β4R113C and α3β4S117C receptors (data not shown). To characterize the light-dependent block of the α3β4E61C receptor at different concentrations of ACh, we compared the amount of current observed under 380nm and 500nm illumination for the same cells. The percentage of current blocked under 380nm light ranged from 80±5% at 30μM ACh to 68±4% at a saturating 10mM ACh (mean±SEM, n=5) (Fig. 5b). Tethering **MAHoCh** at the α4β2E61C receptor produced a similar photoinhibition of the cholinergic current (Fig. 5c). The percentage of current blocked under 380nm light at the α4β2 receptor ranged from 75±10% at 100μM ACh to 81±7% at a saturating 3mM ACh (mean±SEM, n=5) (Fig. 5d).

In control experiments, we did not observe any photoactivation after treating oocytes expressing either α3β4E61C or α4β2E61C nAChRs with **AcAACh** (**6a,b**), a non-reactive analogue of **MAACh** (Supplementary Fig. S7). Furthermore, treatment of wild type receptors with either **MAACh** or **MAHoCh** did not impart any photosensitivity (Supplementary Fig. S6). These results confirm that covalent modification at the genetically introduced cysteine residue is required for the optical control of LinAChR function and suggest that off-target actions of these ligands at endogenous neuronal receptors should be minimal.

Thermal relaxation of the photoswitchable ligands.

Azobenzene PTLs can be converted from their *cis* configuration to their *trans* configuration by 500nm illumination, but they also spontaneously convert to the more stable *trans* isomer *via* thermal relaxation in the dark[39]. Thus, the **MAACh**-labeled α4β2E61C receptor can be activated by 380nm light and the photoactivatable current decays over time in the dark (Fig. 6a). To investigate whether tethering the PTL to a receptor affects the rate of *cis*-isomer thermal relaxation, we compared the half-life of **MAACh** in solution, measured by changes in absorption

at 380nm, to the calculated half-life of the decay of the photoactivatable current (Fig. 6b). The half-life of **MAACh** in solution was 28 seconds, close to the previously reported value of 26 seconds for a urea-azobenzene derivative[40]. In contrast, the thermal decay of the photoactivatable current could only be fit with a biexponential decay curve, with a fast half-life of 4.7 seconds and a slow half-life of 94 seconds, indicating that ligand binding increases the stability of *cis*-**MAACh**. The **MAHoCh**-labeled α4β2 E61C receptor can be blocked by 380nm light and the amount of block also decays slowly in the dark (Fig. 6c). We measured the half-life of *cis*-**MAHoCh** in solution to be 74.4 minutes (Fig. 6d). The long half-life of *cis*-**MAHoCh** is likely due to the alkoxy substituent on the azobenzene, which does not destabilize the *cis* configuration to the same extent as the urea substituent in **MAACh**[39]. The thermal relaxation rate of tethered *cis*-**MAHoCh** appears to be of the same order of magnitude as *cis*-**MAHoCh** in solution.

Figure 4

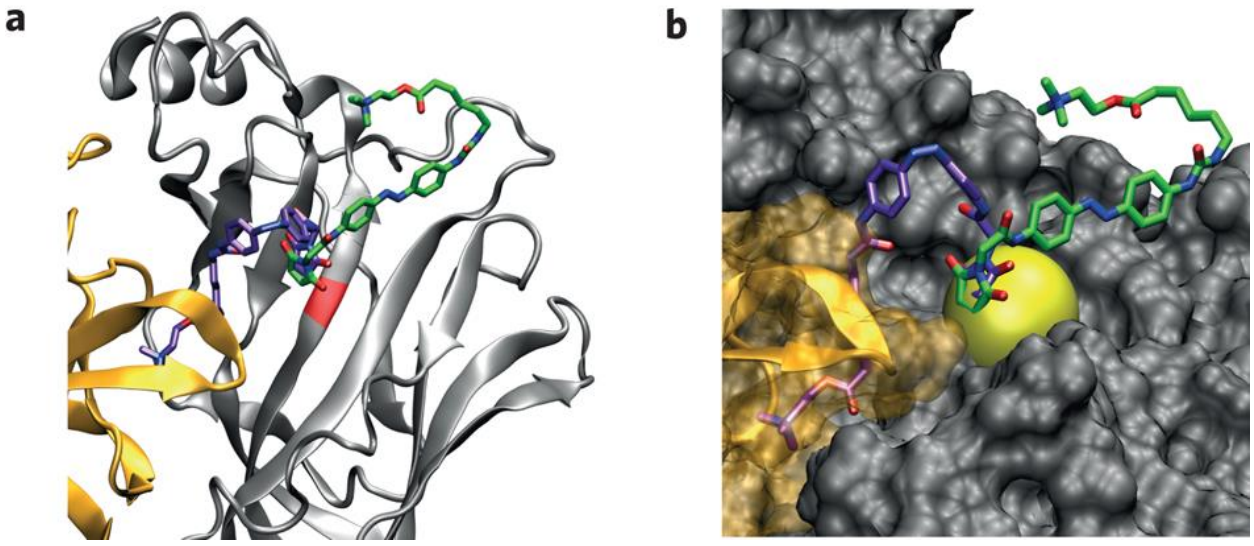

Figure 4: Molecular model of a nicotinic acetylcholine receptor with a virtually tethered photoswitchable agonist.

(**a**, **b**) Docking results with constrained *cis*-**MAACh** (violet) and *trans*-**MAACh** (green) in the α4β2 homology model. The maleimide is constrained to be near the sulfhydryl group of C61. Ribbon (**a**) and surface (**b**) views of the minimum energy conformations are shown. The positional constraint (sphere) is shown in bright yellow.

Figure 5

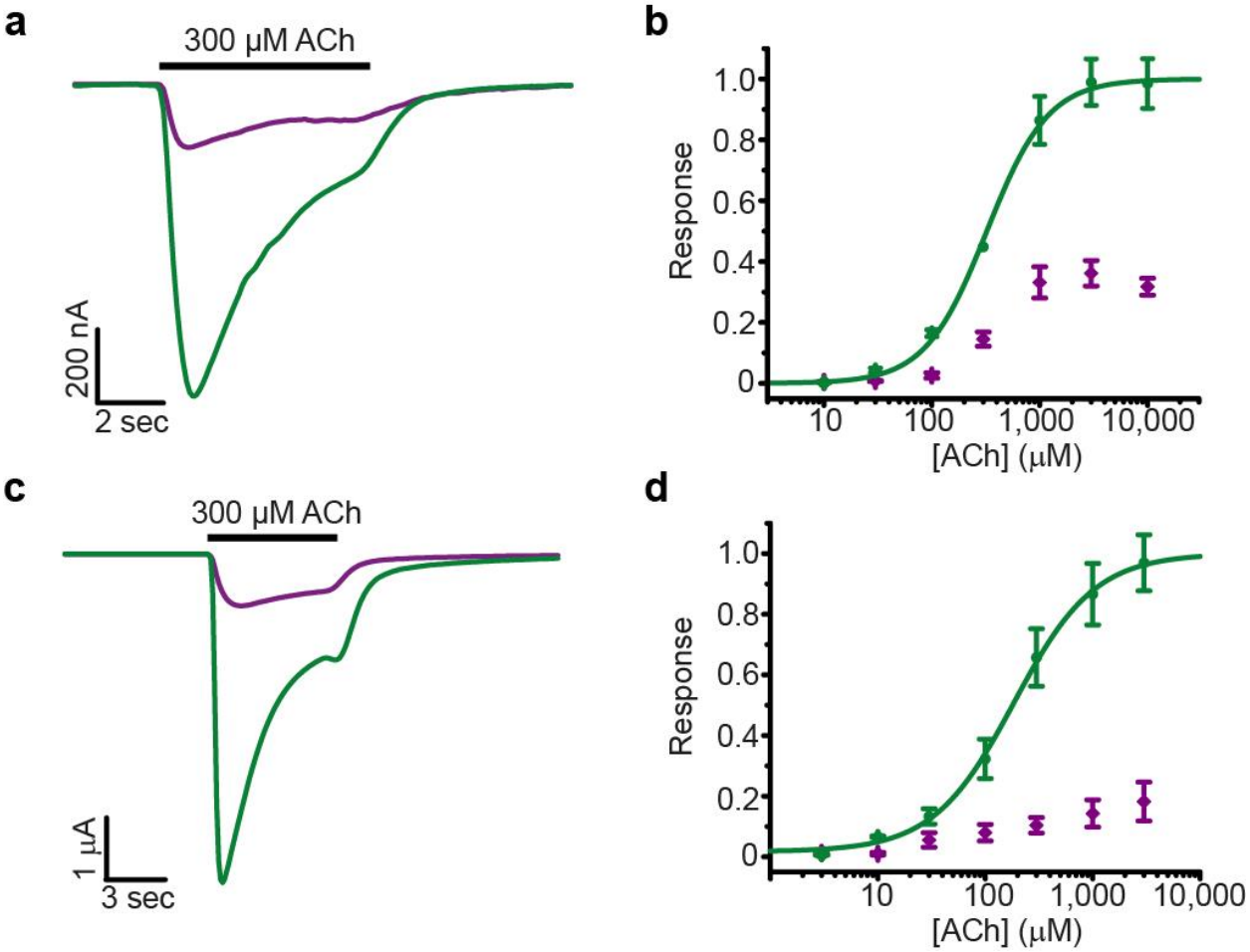

Figure 5: Photoinhibition of nicotinic acetylcholine receptors with a tethered antagonist.

(**a**, **c**) Photo-block of the cholinergic current of the α3β4E61C (**a**) and α4β2E61C (**c**) mutant receptors by tethered **MAHoCh**. Current is shown in response to 300µM ACh under 380nm light (violet) and 500nm light (green).
(**b**, **d**) ACh dose response curves for the α3β4E61C (**b**) mutant and the α4β2E61C (**d**) mutant with tethered **MAHoCh** under 500nm light (green) and 380nm light (violet). Data are mean±SEM, n=5.

Figure 6

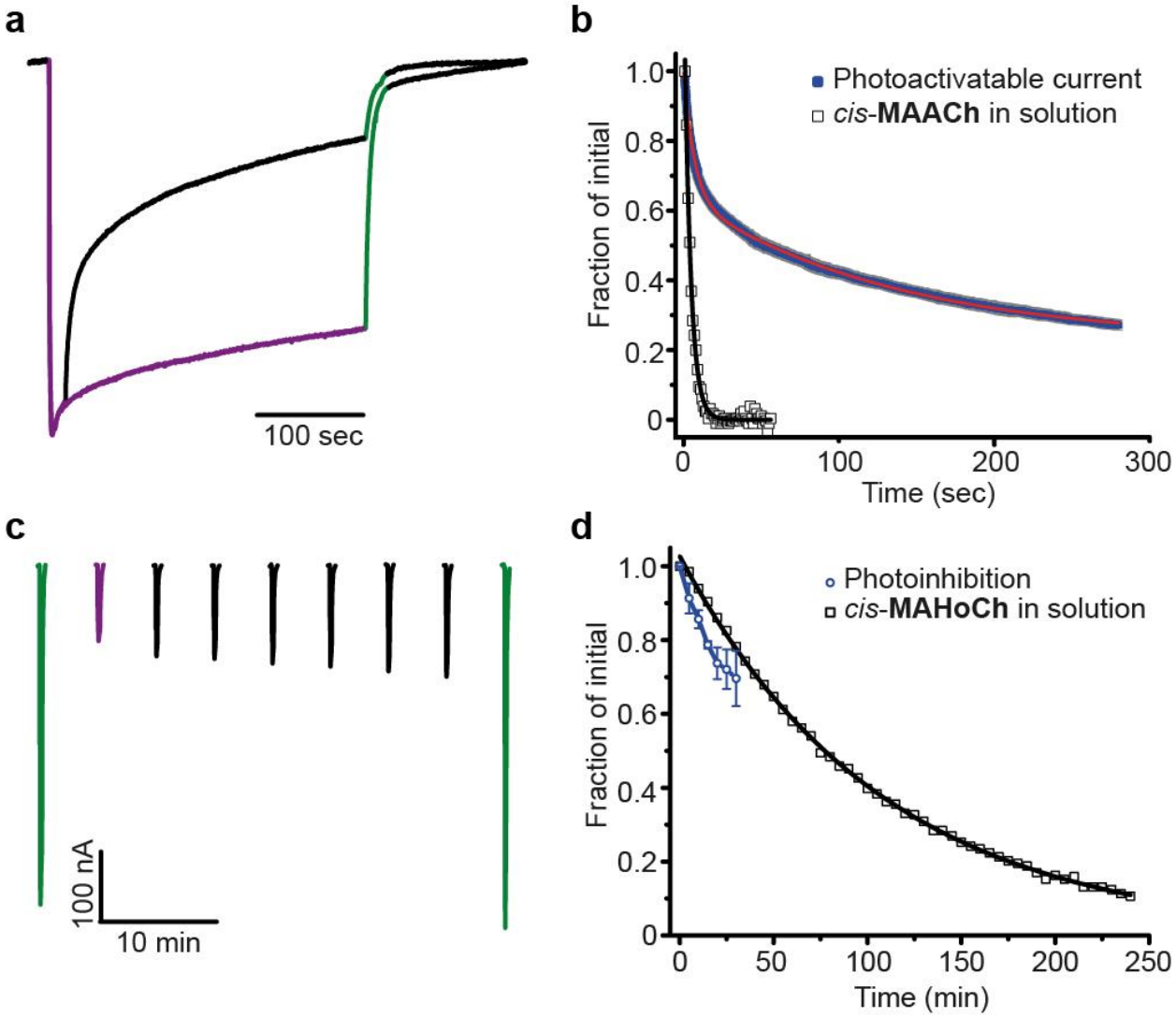

Figure 6: Thermal relaxation of the photoswitchable agonist and antagonist.
(**a**) Normalized photoactivatable current decay of the α4β2E61C receptor in the dark with tethered **MAACh**. Decay of the photoactivatable current over time under 380nm illumination (violet) and in the dark (black).
(**b**) Thermal relaxation of *cis*-**MAACh** in phosphate-buffered saline (open squares) fitted with a monoexponential decay function (black) ($t_{1/2}$ = 28sec). Decay of the photoactivatable current (mean (blue) ± SEM (gray), n=4) fitted using a biexponential decay function (red, $t_{1/2}(1)$ = 4.7sec, A(1) = 0.36, $t_{1/2}(2)$ = 94sec, A(2) = 0.41). Both measurements are normalized.
(**c**) Decay of the photo-block of cholinergic current of the α4β2E61C receptor in the dark with tethered **MAHoCh** measured in *Xenopus* oocytes. 100µM ACh is perfused under 500nm (green) light, 380nm (violet) light and in the dark (black).
(**d**) Thermal relaxation of *cis*-**MAHoCh** in phosphate-buffered saline (open squares) fitted with a monoexponential decay function (black) ($t_{1/2}$ = 74.4min). Decay of the photo-block of cholinergic current of the α4β2E61C receptor with **MAHoCh** (blue) (mean±SEM, n=4).

Discussion

In a classic set of studies carried out in the late 1970s and early 80s, Erlanger and colleagues demonstrated that azobenzene photoswitches could provide photosensitivity to endogenous muscle nAChRs[41,42]. These pentameric ligand-gated ion channels naturally possess a disulfide bond at the tip of the so-called C-loops in their α-subunits[20], which is in close proximity to the ligand-binding site. This disulfide could be reduced, providing a reactive thiol for covalent attachment of a PTL, although such treatment also reduced the affinity of the receptor for agonists by up to 100-fold[43]. The PTL**,** called **QBr**, consisted of a benzylic bromide (the electrophile), an azobenzene photoswitch and a benzylic trimethylammonium moiety. Once attached, **QBr** activated the channel in its *trans* form, i.e. at 500nm or in the dark, but could be switched to an inactive *cis* form by irradiation with 330nm light. The resulting light-activated nAChR could be used to reversibly stimulate *Electrophorus* electroplaques, frog muscles and rat myoballs with light[41,42,44,45]. At the time these studies were carried out, however, receptors could not be genetically manipulated and heterologously expressed and the impact of synthetic photoswitches on neuroscience research remained limited.

Due to the enormous progress of molecular biology since the 1980s, it is now possible to heterologously express mutant receptors in *Xenopus* oocytes, mammalian cells, neurons and even transgenic animals[10,11,46]. Once expressed in a cell, our engineered LinAChR (E61C) can be conjugated with either an agonist or an antagonist, providing for powerful, bidirectional control of receptor activity. Both variants of LinAChR behave like normal nAChRs in the dark but can be turned on in the absence of ACh or off in the presence of the neurotransmitter, respectively, upon irradiation with 380nm. The red-shifted PTL action spectra (compared to **QBr**) should also minimize potential phototoxic effects. In principle, their spectral sensitivity could be further moved toward lower energies through appropriate substitution of the azobenzene photoswitch[47,48].

Another field that has undergone remarkable progress in recent years is the structural biology of pentameric ligand gated ion channels (Cys-loop receptors)[49]. Several X-ray structures of homopentameric ligand-gated ion channels are now available[50,51], as are high-resolution structures of acetylcholine binding proteins (AChBPs) bound to a variety of agonists and antagonists[33,35]. Without these, it would have been difficult to design functional PTLs and choose appropriate sites for their attachment. The X-ray structure of carbamylcholine bound to AchBP[33] and the homology models of the neuronal receptors[34] proved to be most relevant for our design and computational evaluation of PTLs and were particularly helpful for identifying residues suited for the attachment of the photoswitchable agonist **MAACh**. Our molecular docking studies correctly identified positions 61 and 117 as suitable sites of attachment. The predicted site 63 turned out to be unsuitable, however, highlighting the importance of functional screening as a complement to *in silico* models.

The antagonist action of tethered **MAHoCh** is more difficult to explain based on the available X-ray structures but is consistent with the known pharmacology of nAChRs (see Fig. 1). It is also consistent with the "foot in the door" mechanism of nAChR antagonism, wherein an antagonist binds but prevents the complete conformational contraction of the ligand binding site required for receptor activation[52]. Apparently, the elongation of **HoChPE** with a diazene unit bearing an

aryl group is sufficient to prevent the C-loop of the receptor α-subunit from closing in sufficiently to activate the receptor. This also makes sense given the structural similarity of the azobenzene **MAHoCh** with the stilbene **MG-624**, and timethylammonium derivatives thereof, which also function as antagonists[32]. Our data demonstrate that once an attachment site is chosen, it is possible to convert a tethered photoswitched agonist into a tethered photoswitched antagonist by altering the structure of the tether and the ligand head group. This matches previous observations by Cohen *et al*. who established that elongation of a covalently attached agonist by a single methylene group could turn it into an antagonist[53]. Conversely, it might be possible to use the same tethered ligand and two different sites of attachment to achieve either photoagonism or photoantagonism[53].

The diversity of neuronal nAChRs and their structural similarities complicates the pharmacological selective targeting of specific nAChR subtypes. This study reports the reversible photoactivation and inhibition of common neuronal α4β2 and α3β4 nAChRs using light following the genetically targeted conjugation of photoswitchable tethered ligands. This initial study should enable the rational design of other light-regulated pentameric ligand-gated ion channels, homopentameric α7 nAChRs, and neuromuscular nAChRs. The lessons learned in this study should also facilitate the design of photosensitive $GABA_A$ receptors, GlyRs, $5HT_3$ or GluCl receptors. Based on the recent X-ray structure of GluCl[54] and our expertise with photoswitchable tethered glutamate derivatives[11], for instance, it should be possible to develop a hyperpolarizing light-gated chloride channel. It is also conceivable that photoswitchable tethered agonists and antagonists could be extended to muscarinic ACh receptors, which have not yet been characterized in atomic detail but for which extensive pharmacology exists[55].

In future physiological investigations, LinAChRs will be expressed in dissociated neurons, intact neuronal tissues and live animals. We expect them to function well in these systems, perhaps even better than in *Xenopus* oocytes, whose opacity makes it impossible to photoregulate receptors on the entire surface of the cell. In any case, the amount of photoactivation should be sufficient to replicate the major type of cholinergic transmission in the mammalian brain. Neuronal nAChRs are mostly located extrasynaptically and respond to low micromolar concentrations of acetylcholine diluted after synaptic release (i.e. volume transmission)[56]. Expression of the cysteine-containing subunit alone should produce functional LinAChRs in neurons that possess endogenous nicotinic receptors, which would then allow for optical manipulation of receptor function *in vitro* and *in vivo*[57]. Alternatively, native nAChR subunits can be replaced by cysteine mutants using a knock-in strategy[58], which would preserve the endogenous pattern and level of receptor expression. We intend to pursue these strategies to study the physiological and pathological roles of heteromeric nAChRs in the brain and periphery and will report the results of that investigation in due course.

Materials and methods

Synthesis of MAACh and MAHoCh: See Figure S1 and Supplementary Methods.

Molecular cloning:
Rat nicotinic ACh receptor subunit cDNAs in the pNKS2 vector (generously provided by Dr. Annette Nicke, Max Planck Institute for Brain Research, Frankfurt am Main, Germany) were used for all experiments. To minimize non-specific labeling, the C-terminal α4C594 and the β4C75 residues were both mutated to serine. These mutations do not affect the function of the receptor[59]. These mutants were then used as a background for PTL attachment site screening. For nomenclature simplicity, the WT receptors are named in this article α3β4WT and α4β2WT, whereas the α4C594Sβ2 and the α3β4C75S background receptors are named α4β2 and α3β4, respectively. DNA was linearized with XbaI and RNA was transcribed using the mMessage mMachine SP6 transcription kit (Ambion). Surgically extracted *Xenopus laevis* oocytes were injected with 2–20 ng of channel RNA (50 nL). The cells were incubated in oocyte Ringer's solution [96 mM NaCl, 2 mM KCl, 1.8 mM $CaCl_2$, 1 mM $MgCl_2$ and 5 mM HEPES (pH 7.4)] at 18 °C for 24–48 h before experiments.

Molecular Modeling:
Molecular models of α4β2 neuronal nAChR (PDB ID: 1ole)[34] and of the *Torpedo californica* nAChR[29] were used to identify endogenous cysteine residues accessible from the extracellular medium. The X-ray structure of AChBP in complex with carbamylcholine[33] was used to estimate the distance between the ammonium group of the ligand and the beta carbon of the engineered cysteine residues. The numbering of the residues in the homology model is not consistent with the protein sequence. See Supplementary Fig. S3 for sequence alignment and residue numbering. *Cis* and *trans* ligands were docked to the homology model of the α4β2 receptor after the addition of hydrogen atoms and the removal of non-protein moieties using Glide 5.7 as implemented in Maestro 9.2[60]. The docking consisted of a spatial fit of the ligand to the receptor grid, followed by minimization and scoring of hits based on a discretized ChemScore function[61,62]. Ligands were flexibly docked to a rigid receptor using standard precision and the top hits were examined. Docking of the constrained ligands contained an additional positional constraint that restricted the alkenyl carbons of the maleimide moiety to a shell with an inner radius of 1Å and an outer radius of 3.5Å centered at the sulfhydryl group of the C61 cysteine residue.

Photoswitch conjugation:
All photoswitch compounds were dissolved in DMSO to make a 10 mM stock solution and diluted in oocyte Ringer's solution to 25μM for conjugation. For all recordings, the DMSO concentration was <0.25% (vol/vol). Oocytes were incubated in the photoswitch compound solution for 20 minutes in the dark at room temperature before electrophysiological recordings. Photoswitch conjugation was followed by a 5 minute wash in oocyte Ringer's solution.

Electrophysiology:
All electrophysiology experiments were conducted at room temperature. Two-electrode voltage-clamp (TEVC) experiments were performed using an OC-725C amplifier (Warner Instruments), DigiData 1200 interface, and pClamp 8.0 software. The oocytes were placed in a perfusion chamber for recordings. All recordings were performed in oocyte Ringer's solution [96 mM

NaCl, 2 mM KCl, 1.8 mM $CaCl_2$, 1 mM $MgCl_2$, 10 mM HEPES (pH 7.4)]. For each experiment, the oocyte membrane potential was held at −80 mV. An 8-line perfusion system with a VC-8 valve controller (Warner Instruments) was used for perfusion of ACh into the chamber. Data were sampled at 1 kHz, and filtered at 10 Hz. Cells were illuminated using a Lambda-LS illuminator containing a 125W xenon arc lamp (Sutter Instruments) equipped with narrow-band-pass (±10 nm) filters. The incident light intensity was 20 mW/cm^2 for both 380nm and 500nm light, measured at the aperture using a handheld optical power meter (1918-C, Newport, Inc).

Data Analysis:
Dose response curves were created using the following equation:
$y = A_1 + (A_2-A_1)/(1 + 10^{((LOGx0-x)*p)})$, where p = Hill coefficient and 10^{LOGx0} = EC50.

Absorption spectra:
UV-Vis spectra of the photoswitch compounds were obtained using the SmartSpec Plus Spectrophotometer (BioRad Laboratories) in PBS at pH 7.4. The change in absorbance of the compounds at 380nm over time following photoconversion to the *cis* configuration was used to determine the kinetics of thermal relaxation. The light source used for photoconversion of the ligands was the same as the one used in electrophysiological recordings.

Supplemental Information

Figure S1

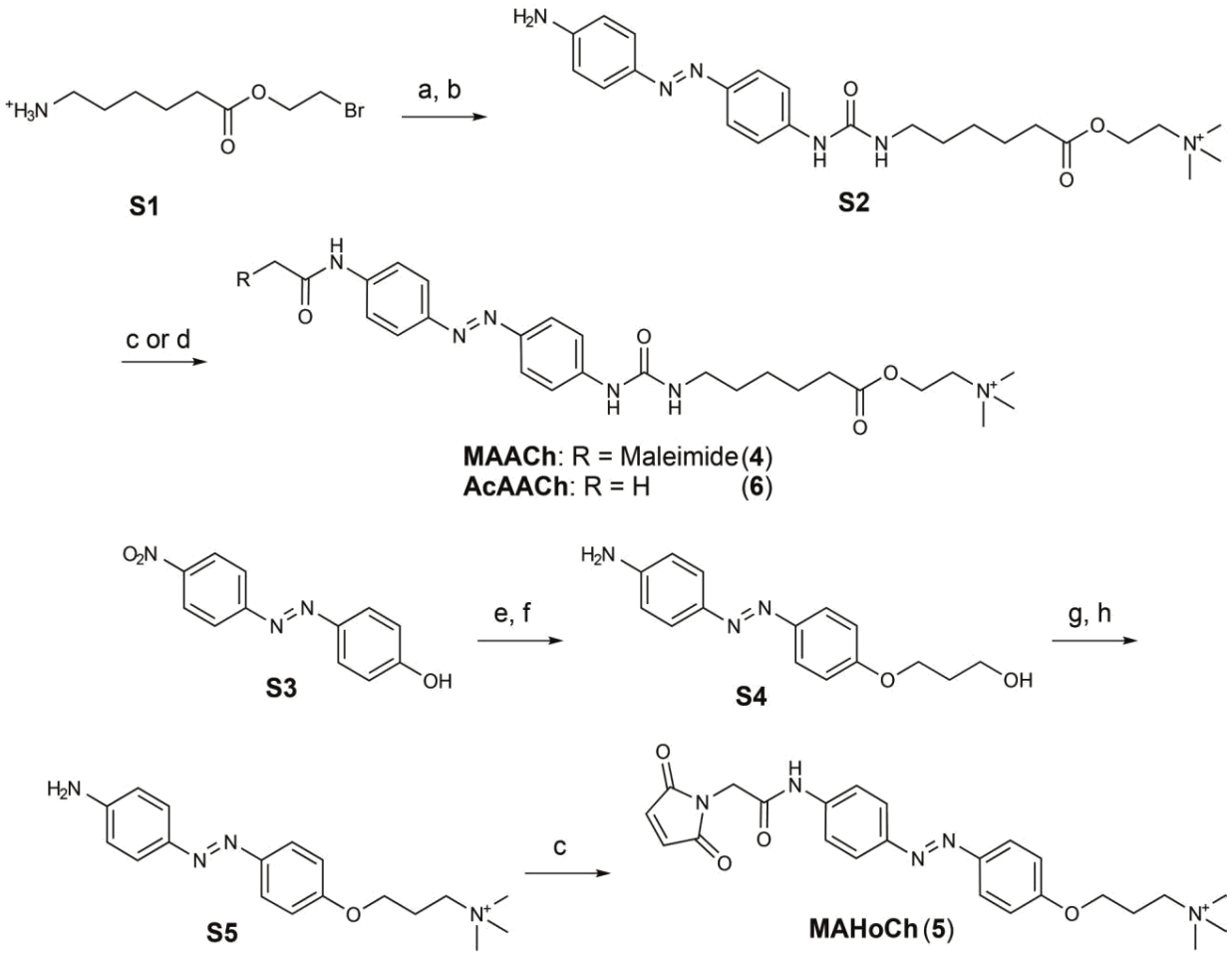

Figure S1. Synthesis of the photoswitchable tethered ligands.

Synthesis of **MAACh**, **AcAACh** and **MAHoCh**. Reagents and conditions: a - triphosgene, $NaHCO_3$, H_2O/DCM, then 4,4'-azodianiline (33%); b - Me_3N, DMF (84%); c - maleoylglycyl chloride, DIPEA, DMF (50%); d - acetyl chloride, DIPEA, DMF (54%); e - 3-bromopropanol, cat. KI, K_2CO_3, acetone (99%); f - $(NH_4)_2S$, Na_2CO_3, H_2O/THF (87%); g - CBr_4, PPh_3, imid. THF (40%); h - Me_3N, THF (quant.).

Figure S2

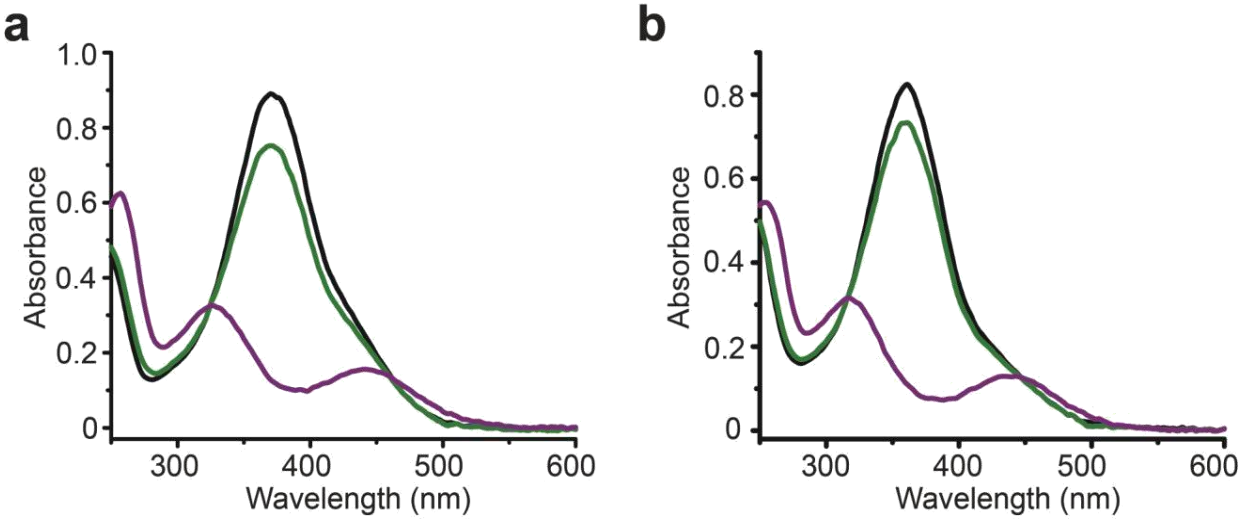

Figure S2. UV-Vis absorption spectra of the photoswitchable tethered ligands.

(**a**, **b**) UV-Vis absorption spectra of **MAACh** (**a**) and **MAHoCh** (**b**) in phosphate buffered saline (PBS) in the dark (black), under 500nm light (green) and 380nm light (violet).

Figure S3

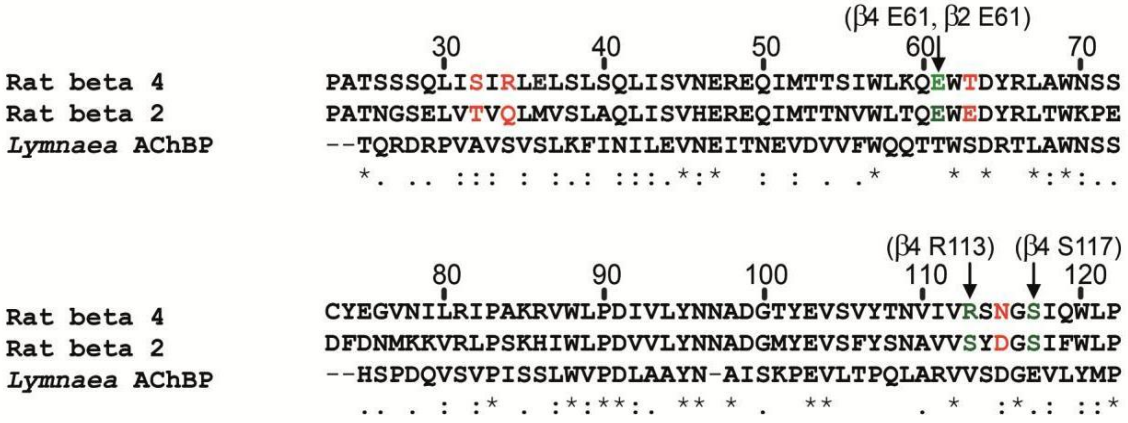

Figure S3. Sequence alignment showing the introduced nicotinic receptor cysteine mutants.

Sequence alignment for *Rattus norvegicus* nAChR β4, β2 subunits and the *Lymnaea stagnalis* acetylcholine binding protein (AChBP), with the cysteine mutations that produced *cis*-activation with **MAACh** colored green and the ones that didn't produce *cis*-activation in red. Alignment was performed using ClustalW 2.0[63,64]

Figure S4

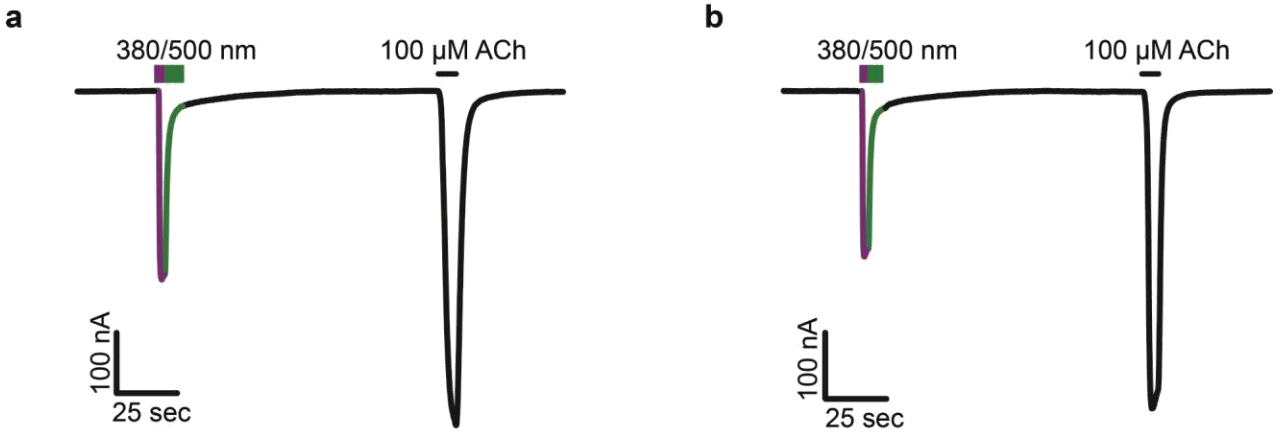

Figure S4. Photoactivation of additional mutant α3β4 nicotinic acetylcholine receptors with a tethered agonist.
(**a**, **b**) Photoactivation of the α3β4R113C (**a**) and the α3β4S117C (**b**) mutant receptors by tethered **MAACh**. 380nm light (violet) triggers photoactivatable current and 500nm light (green) shuts it off. Representative traces, similar behavior in three other cells.

Figure S5

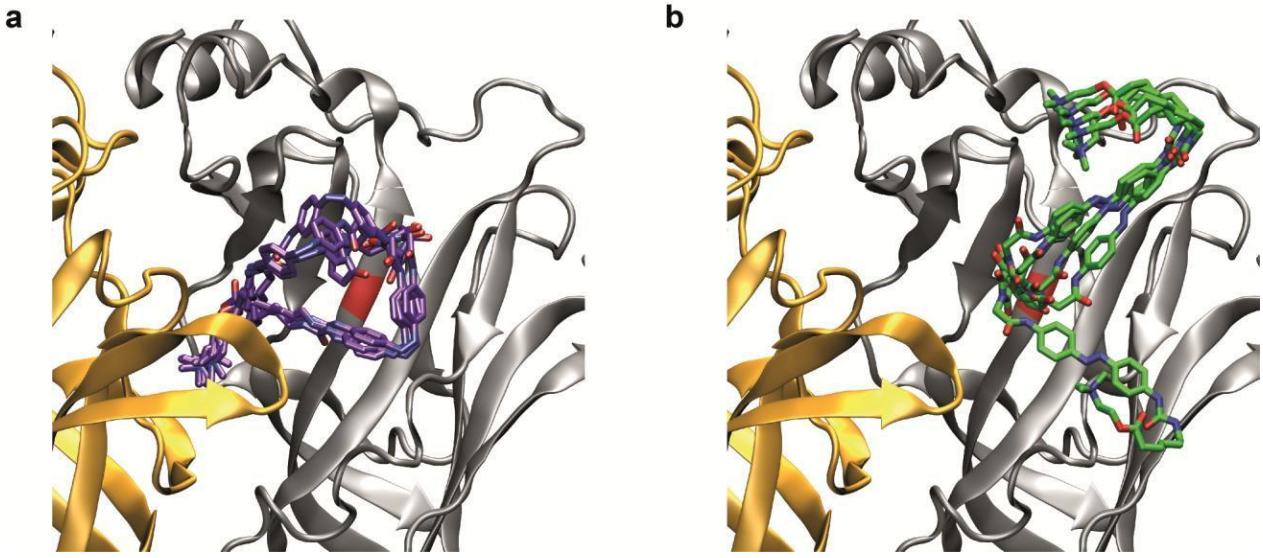

Figure S5. Molecular model of a nicotinic receptor with a virtually tethered photoswitchable agonist.
(**a**, **b**) Docking results with constrained *cis*-**MAACh** (violet) (**a**) and *trans*-**MAACh** (green) (**b**) in the α4β2E61C homology model. The maleimide is constrained to be near the sulfhydryl group of C61. Six of the lowest energy conformations are shown.

Figure S6

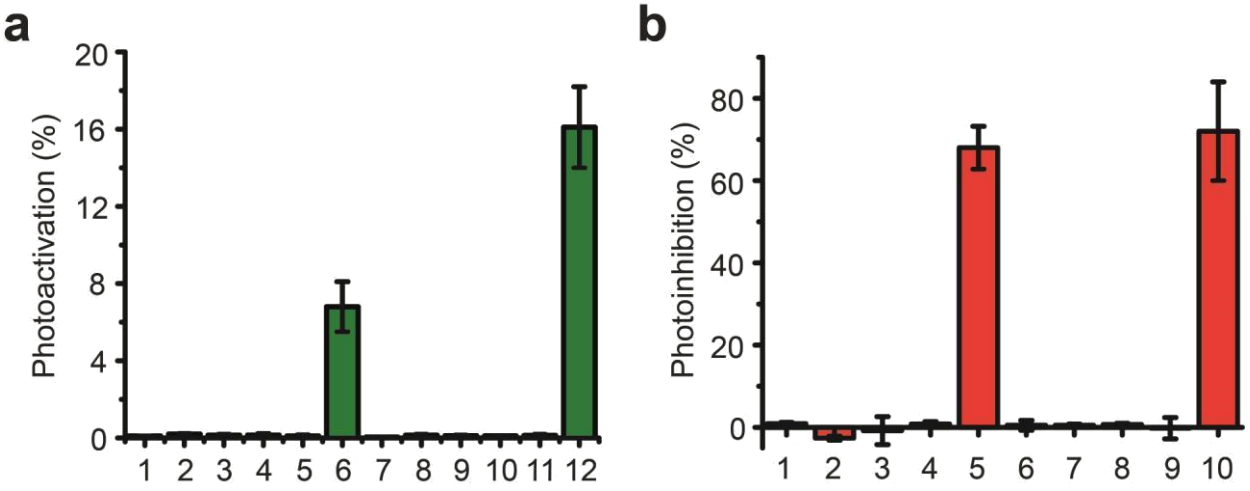

Figure S6. Photoregulation of nicotinic acetylcholine receptors with photoswitchable tethered ligands.

(**a**) Photoactivation of heteromeric nAChRs in *Xenopus* oocytes by various PTLs. 1: α3β4WT+ **MAACh**, 2: α3β4 + **MAACh**, 3: α3β4 + **MAHoCh**, 4: α3β4E61C + **AcAACh**, 5: α3β4E61C + **MAHoCh**, 6: α3β4E61C + **MAACh**, 7: α4β2WT + **MAACh**, 8: α4β2 + **MAACh** 9: α4β2 + **MAHoCh**, 10: α4β2E61C + **AcAACh**, 11: α4β2E61C + **MAHoCh**, 12: α4β2E61C + **MAACh**. Photoactivation is shown as percent of maximum ACh current. Data are mean±SEM, n=3-15.
(**b**) Photoinhibition of heteromeric nAChRs in *Xenopus* oocytes by various PTLs. 1: α3β4WT + **MAHoCh**, 2: α3β4 + **MAACh**, 3: α3β4 + **MAHoCh**, 4: α3β4E61C + **AcAACh**, 5: α3β4E61C + **MAHoCh**, 6: α4β2WT + **MAHoCh** 7: α4β2 + **MAACh**, 8: α4β2 + **MAHoCh**, 9: α4β2E61C + **AcAACh**, 10: α4β2E61C + **MAHoCh**. Photoinhibition is shown as percent of ACh current blocked under 380nm light upon perfusion of 300μM ACh for the α3β4 nAChRs and 100μM ACh for the α4β2 nAChRs. Data are mean±SEM, n=3-5.

Figure S7

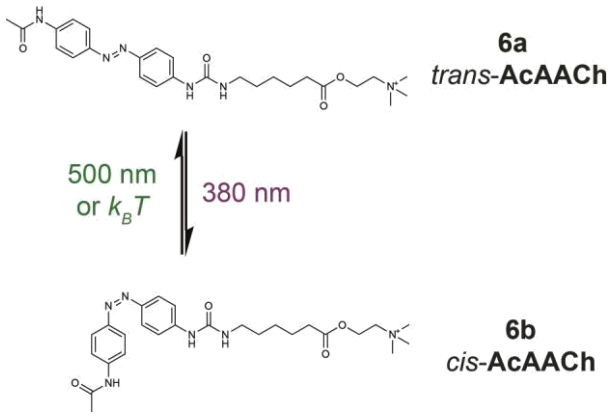

Figure S7. Structure of a non-cysteine reactive analog of the photoswitchable tethered agonist .

Structure of Acetamide-Azobenzene-AcylCholine (**AcAACh**) (**6a**, **b**), a non-cysteine reactive analog of the PTL **MAACh**. **AcAACh** is photoisomerizable, but does not photosensitize cysteine-mutant nAChRs after treatment and wash.

Table S1

Receptor	Acetylcholine EC50 (μM)	Hill coefficient
α3β4WT	178±22	1.56±0.24
α3β4E61C	186±52	1.24±0.3
α3β4E61C + **MAACh**	350±54	1.41±0.23
α3β4E61C + **MAHoCh**	323±13	1.52±0.09
α4β2WT	20±4	0.77±0.08
α4β2E61C	134±11	0.80±0.03
α4β2E61C + **MAACh**	169±39	0.87±0.11
α4β2E61C + **MAHoCh**	185±12	1.16±0.07

Table S1. Characterization of cysteine-mutant and photoswitchable ligand-conjugated nicotinic acetylcholine receptors.

Acetylcholine EC50 values and Hill coefficients of the dose-response curves for the wild-type, cysteine-mutant and PTL-conjugated cysteine mutant α3β4 and α4β2 nAChRs. All data are mean±SEM, n=5.

Supplemental Methods

Chemical Synthesis

General methods. Reactions were carried out under N_2 atmosphere in flame dried glassware. Tetrahydrofuran (THF) was distilled from Na/benzophenone immediately prior to use. Acetonitrile (MeCN), and diisopropylethylamine (DIPEA) were distilled from CaH_2 immediately prior to use. All other reagents and solvents were used without further purification from commercial sources. Flash column chromatography was carried out with EcoChrom ICN SiliTech 32–63 D 60 Å silica gel. Reverse-phase chromatography was carried out with Waters Preparative C18 Silica Gel WAT010001 125 Å and Waters Sep-Pak Vac 20 cc C18 Cartridge s WAT036925. Reactions and chromatography fractions were monitored with either Merck silica gel 60F254 plates or Analtech C18 silica gel RPS-F 52011 plates, and visualized with 0.1N HCl. NMR spectra were measured specified solvents and calibrated from residual solvent signal on a Bruker DRX spectrometer at 500 MHz for ^{1}H spectra and 125 MHz for ^{13}C spectra and either a Bruker AVB or Bruker AVQ spectrometer at 400 MHz for ^{1}H spectra and 100 MHz for ^{13}C spectra. IR spectra were measured with a Genesis FT-IR spectrometer by thin film.

6-(2-bromoethoxy)-6-oxohexan-1-aminium (**S1**)**.** Compound **S1** was prepared from 6-aminohexanoic acid according to the procedure of Chatrenet et al[65].

(*E*)-2-((6-(3-(4-((4-aminophenyl)diazenyl)phenyl)ureido)hexanoyl)oxy)-*N*,*N*,*N* trimethylethanaminium (**S2**)**.** To a biphasic mixture of DCM (15 ml) and saturated aqueous $NaHCO_3$ (15 ml) was added triphosgene (108 mg, 0.36 mmol). Compound **S1** was dissolved in H_2O (5 ml) and then added dropwise over 10 min to mixture, which was allowed to stir at room temperature for 1 hr and then transferred to a separatory funnel with DCM. After extracting 3 times with DCM (15 ml) the organics were combined, washed with brine (20 ml), dried over Na_2SO_4, filtered, and removed of solvent *in vacuo*. The brown oil was dissolved in THF (3 ml), and cannulated into a solution of 4,4'-azodianiline (460 mg, 2.18 mmol) dissolved in THF (6 ml) under N_2. The flask containing isocyanate **S1** was rinsed with additional THF (3 ml), which was also cannulated into the mixture. The reaction was refluxed overnight, cooled, diluted with additional THF (25 ml) and dry-loaded onto silica gel (2 g). Silica gel chromatography through a wide column (25% EtOAc in DCM gradient to 50%) provided the primary bromide as a yellow-brown solid (170 mg, 0.36 mmol, 33% yield): ^{1}H (d_6-DMSO, 300MHz): 1.33 (s, 2H); 1.44 (s, 2H); 1.57 (s, 2H); 2.35 (s, 2H); 3.09 (s, 2H); 3.36 (s, 1H); 3.66 (s, 2H); 4.34 (s, 2H); 5.95 (s, 2H); 6.23 (s, 1H); 6.65 (s, 2H); 7.54–7.64 (m, 6H), 8.78 (s, 1H). HRMS (FAB+): calc'd for $C_{21}H_{26}BrN_5O_3$ – 475.1219, found – 475.1229 (M+).

The primary bromide (154 mg, 0.31 mol) was dissolved in DMF (3 ml) and cooled on an ice bath under N_2. The N_2 line was removed and a gentle stream of Me_3N gas was bubbled through the solution while stirring and venting into a solution of 10% HCl for about 1 min or until a small volume increase was observed. After removal of the Me_3N stream, the reaction vessel was sealed and allowed to stir at room temperature overnight. A stream of N_2 gas was then bubbled through the reaction while stirring and vented into a solution of 10% HCl to remove the excess Me_3N, followed by addition of formic acid (1 ml) to protonate the remaining Me_3N. After removal of solvent *in vacuo*, reverse phase silica gel chromatography (15% MeCN: 0.1% formic acid in H_2O

gradient to 33% MeCN) provided **S2** as a yellow solid (128 mg, 0.26 mmol, 84% yield): ^{1}H (MeOD, 400MHz): 1.29 (s, 2H); 1.43 (s, 2H); 1.53 (s, 2H); 2.30 (t, 2H, J=7.6); 3.06-3.11 (m, 1H); 3.55 (s, 2H); 4.39 (s, 2H); 6.60 (d, 2H, J=8.8); 7.36 (d, 2H, J=8.8); 7.54 (d, 2H, J=8.8); 7.60 (d, 2H, J=8.4); 8.42 (bs, 1H). HRMS (FAB+): calculated for $C_{24}H_{35}N_6O_3^+$ – 455.2771, found – 455.2761 (M+).

Maleoylglycyl chloride. Maleoylglycyl chloride was prepared from N-maleoyl glycine[66] by treatment with oxalyl chloride (1.05 eq.) and DMF (cat.) immediately prior to use. A suspension of the acid and oxalyl chloride in DCM was cooled in an ice bath followed by addition of a drop of DMF. The reaction was vented under gentle positive pressure from N_2 gas and allowed to warm to room temperature. After stirring for at least 15 min, the solvent was removed *in vacuo*. The white residue was dissolved in DMF for use without further purification.

(*E*)-2-((6-(3-(4-((4-(2-(2,5-dioxo-2,5-dihydro-1*H*-pyrrol-1 yl)acetamido)phenyl)diazenyl)phenyl)ureido)hexanoyl)oxy)-*N*,*N*,*N*-trimethylethanaminium (**4a**) (**MAACh**)**.** To a solution of compound **S2** (10 mg, 20 µmol) and DIPEA (16 µl, 92 µmol) in DMF (1 ml) was added maleoylglycyl chloride (14 mg, 80 µmol of N-maleoyl glycine) in DMF (0.5 ml). The reaction was stirred for several hours, followed by removal of solvent *in vacuo*. Reverse phase silica gel chromatography (1% MeCN: 0.1% formic acid in H_2O gradient to 20% MeCN) provided **4a** (**MAACh**) as a yellow solid (6.4 mg, 10 µmol, 50% yield): ^{1}H (MeOD, 400MHz): 1.29 (s, 2H); 1.44 (s, 2H); 1.56 (s, 2H); 2.30 (t, 2H, J=7.6); 3.07-3.09 (m, 1H); 3.56 (s, 2H); 4.25 (s, 2H); 4.40 (s, 2H); 6.82 (s, 2H); 7.41 (d, 2H, J=8.8); 7.59 (d, 2H, J=8.8); 7.69-7.71 (m, 4H); 8.29 (bs, 1H). HRMS (ES+): calculated for $C_{30}H_{38}N_7O_6^+$ – 592.2884, found – 592.2878 (M+)**.**

(*E*)-2-((6-(3-(4-((4-acetamidophenyl)diazenyl)phenyl)ureido)hexanoyl)oxy)-*N*,*N*,*N*-trimethylethanaminium (**6a**) (**AcAACh**)**.** To a solution of compound **S2** (23 mg, 46 µmol) and DIPEA (16 µl, 92 µmol) in DMF (1 ml) was added acetyl chloride (6.5 µl, 92 µmol) in DMF (0.5 ml). The reaction was stirred for several hours, followed by removal of solvent *in vacuo*. Reverse phase silica gel chromatography (1% MeCN: 0.1% formic acid in H_2O gradient to 33% MeCN) provided **6a** (**AcAACh**) as a yellow solid (14 mg, 25 µmol, 54% yield): ^{1}H (MeOD, 400MHz): 1.31 (s, 2H); 1.43 (s, 2H); 1.55 (s, 2H); 2.03 (s, 3H); 2.30 (t, 2H, J=7.6); 3.07-3.11 (m, 1H); 3.57 (s, 2H); 4.41 (s, 2H); 7.42 (d, 2H, J=8.8); 7.60 (d, 2H, J=8.8); 7.69-7.72 (m, 4H); 8.31 (bs, 1H). HRMS (ESI+): calculated for $C_{26}H_{37}N_6O_4^+$ – 497.2871, found – 497.2853 (M+).

(E)-4-((4-nitrophenyl)diazenyl)phenol (**S3**)**.** Compound **S3** was prepared from 4-nitroaniline and phenol according to the method in Haghbeen *et al*.[67]

(*E*)-3-(4-((4-aminophenyl)diazenyl)phenoxy)propan-1-ol (**S4**)**.** A mixture of **S3** (200 mg, 0.82 mmol), K_2CO_3 (567 mg, 4.10 mmol), KI (~ 1 mg), and 3-bromopropanol (0.37 ml, 4.1 mmol) in acetone (25 ml) was refluxed for 4.5 hrs with stirring under N_2. After cooling, the reaction was transferred to a separatory funnel with EtOAc (50 ml), extracted twice with H_2O (20 ml), once with brine (20 ml) followed by drying of the organic layer over Na_2SO_4 and removal of solvent *in vacuo*. Silica gel chromatography (33% EtOAc in Hex gradient to 50%) provided the nitro-bromide as an orange solid (246 mg, 0.82 mmol, 99% yield): ^{1}H ($CDCl_3$, 500MHz): 1.69 (s, 1H); 2.08 (dt, 2H, J=5.5, 6.0); 3.88 (t, 2H, J=5.5); 4.21 (t, 2H, J=6.0); 7.02 (d, 2H, J=9.0); 7.92-7.96

(m, 4H); 8.32 (d, 2H, J=9.0). ^{13}C ($CDCl_3$, 125MHz): 31.9, 59.8, 65.7, 114.9, 123.1, 124.7, 125.6, 146.9, 148.2, 155.9, 162.5. HRMS (FAB+): calculated for $C_{15}H_{16}N_3O_4^+$ – 302.1141, found – 302.1146 (MH+).

To a mixture of the nitro alcohol (205 mg, 0.68 mmol), and Na_2CO_3 (324 mg, 3.06 mmol) in 1:1 THF:H_2O (30 ml) was added a solution of 20% $(NH_4)_2S$ in H_2O (0.68 ml, 2.04 mmol). The reaction was refluxed for 1 hr followed by careful acidification to pH 7 with dilute HCl deep in the hood as to prevent exposure to highly toxic H_2S gas. After cooling, the reaction was transferred to a separatory funnel with EtOAc (50 ml) and extracted three times with EtOAc (25 ml). The combined organics were washed once with H_2O (20 ml), once with sat. aq. $NaHCO_3$ (20 ml) and once with brine (20 ml) followed by drying over Na_2SO_4 and removal of solvent *in vacuo*. Silica gel chromatography (15% EtOAc in DCM gradient to 50%) provided **S4** as an orange solid (150 mg, 0.55 mmol, 81% yield): ^{1}H (CD_3CN, 500MHz): 1.96 (t, 2H); 2.69 (bs, 1H); 3.69 (s, 2H); 4.15 (t, 2H); 4.72 (bs, 2H); 6.73 (d, 2H, J=9.0); 7.04 (d, 2H, J=9.0); 7.68 (d, 2H, J=9.0); 7.78 (d, 2H, J=9.0). ^{13}C (CD_3CN, 125MHz): 32.0, 58.1, 65.1, 113.9, 114.7, 123.6, 124.4, 144.3, 146.9, 151.1, 160.6. HRMS (FAB+): calculated for $C_{15}H_{18}N_3O_2^+$ – 272.1399, found – 272.1407 (MH+).

(*E*)-3-(4-((4-aminophenyl)diazenyl)phenoxy)-*N*,*N*,*N*-trimethylpropan-1-aminium (**S5**)**.** To a solution of **S4** (143 mg, 0.53 mmol) in THF (10 ml), cooled on an ice bath was added, in the following order, PPh_3 (566 mg, 2.16 mmol), imidazole (180 mg, 2.65 mmol) and CBr_4 (211 mg, 0.64 mmol) with stirring under N_2 and subsequently warmed to room temperature. After about 10 min, a white precipitate began to form, which completely dissolved after 1 hr. After 3 hrs, an additional 0.5 eq. CBr_4 and 2 eq. PPh_3 were added and the reaction was allowed to stir overnight. The reaction was then transferred to a separatory funnel with EtOAc (60 ml), washed twice with H_2O (30 ml) and once with brine (30 ml) followed by drying over Na_2SO_4 and removal of solvent *in vacuo*. Silica gel chromatography (25% EtOAc in Hex gradient to 50%) provided the amino-bromide as an orange solid (70 mg, 0.21 mmol, 40% yield): ^{1}H (CD_3CN, 400MHz): 2.29 (dt, 2H, J=5.5, 6.0); 3.64 (t, 2H, J=6.0); 4.14 (t, 2H, J=5.5); 4.73 (bs, 2H); 6.73 (d, 2H, J=9.0); 7.04 (d, 2H, J=9.0); 7.68 (d, 2H, J=9.0); 7.78 (d, 2H, J=9.0). ^{13}C (CD_3CN, 100MHz): 30.3, 32.0, 65.7, 113.9, 114.8, 123.6, 124.5, 144.3, 147.1, 151.2, 160.2. HRMS (FAB+): calculated for $C_{15}H_{16}BrN_3O$ – 333.0477, found – 333.0482 (M+).

The amino-bromide (49 mg, 0.15 mmol) was dissolved in THF (3 ml) and cooled on an ice bath under N_2. The N_2 line was removed and a gentle stream of Me_3N gas was bubbled through the solution while stirring and venting into a solution of 10% HCl for about 1 min or until a small volume increase was observed. Orange precipitate began to form immediately. After removal of the Me_3N stream, the reaction vessel was sealed and allowed to stir at room temperature overnight. A stream of N_2 gas was then bubbled through the reaction while stirring and vented into a solution of 10% HCl to remove the excess Me_3N. After removal of solvent *in vacuo*, reverse phase silica gel chromatography (5% MeOH:H_2O gradient to 50% MeOH) provided **S5** as an orange solid (61 mg, 0.15 mmol, quantitative yield): ^{1}H (MeOD, 500MHz): 2.32 (s, 2H); 3.20 (s, 9H); 3.60 (s, 2H); 4.17 (s, 2H); 6.74 (d, 2H); 7.05 (d, 2H); 7.67 (d, 2H); 7.77 (d, 2H). ^{13}C (MeOD, 125MHz): 22.9, 52.3, 63.9, 64.5, 113.8, 114.4, 123.3, 124.3, 144.1, 146.8, 151.3, 159.4. HRMS (ES+): calculated for $C_{18}H_{25}N_4O^+$ – 313.2023, found – 313.2019 (M+).

(*E*)-3-(4-((4-(2-(2,5-dioxo-2,5-dihydro-1*H*-pyrrol-1-yl)acetamido)phenyl)diazenyl)phenoxy)-*N*,*N*,*N*-trimethylpropan-1-aminium (**5a**) (**MAHoCh**)**.** To a solution of compound **S5** (27 mg, 69 µmol) and DIPEA (24 µl, 133 µmol) in DMF (1 ml) was added maleoylglycyl chloride (14 mg, 80 µmol of N-maleoyl glycine) in DMF (0.5 ml). The reaction was stirred for several hours, followed by removal of solvent *in vacuo*. Reverse phase silica gel chromatography chromatography (1% MeOH: 0.1% formic acid in H_2O gradient to 25% MeOH) provided **5a** (**MAHoCh)** as a yellow solid (17 mg, 35 µmol, 51% yield): ^{1}H (MeOD, 500MHz): 2.35 (s, 2H); 3.31 (s, 9H); 3.59-3.63 (m, 2H); 4.21 (t, 2H); 4.38 (s, 2H); 6.95 (s, 2H); 7.10 (d, 2H, J=9.0); 7.73 (d, 2H, J=9.0); 7.85-7.90 (m, 4H); 8.27 (bs, 1H). HRMS (ESI+): calculated for $C_{24}H_{28}N_5O_4^+$ – 450.2136, found – 450.2132 (M+).

Part II: Restoration of visual function to blind mice

Introduction

Blinding diseases resulting from the degeneration of light-sensing photoreceptor cells (Fig. 1) affect millions of patients around the world. Approximately 1.5 million people worldwide suffer from inherited disorders such as retinitis pigmentosa and 15 million patients in the United States alone eventually experience vision loss from age-related macular degeneration and other ageing diseases[68,69]. There is currently no treatment to restore vision to patients suffering from one of these degenerative blinding diseases. A number of strategies are being explored to address this unmet clinical need. They can be broadly divided into two categories - those attempting to replace cells missing from the degenerated retina, and those attempting to control the activity of remaining retinal neurons through either electrical or optical stimulation, with the goal of transmitting visual information to the downstream areas of the brain.

The first strategy involves the use of stem cells - cells that possess the ability to differentiate into many other cell types found in the human body, including, for example, photoreceptor cells in the retina. A number of groups have attempted to use stem cells to derive photoreceptor precursor cells[70] or retinal pigment epithelial cells essential for photoreceptor survival[71] and then implant those cells into the eyes of patients suffering from degenerative disease. Under the right conditions, these stem-cell-derived cells can integrate into the retina and replace the cells lost due to degeneration. Stem cell therapy have improved visual function in animal models of retinal degeneration[72] and produced some promising preliminary results in stage I clinical trials in human patients[73]. Despite these encouraging results, much more work needs to be done to understand the fundamental biology and potential adverse effects of implanted stem cells or stem cell derived cells in the eye before this strategy can be widely used in the clinic.

An alternative strategy for vision restoration is to control the activity of remaining retinal neurons by electrical stimulation. While retinal degenerative diseases result in the loss of photoreceptor cells, other neurons in the retina, and the connections from the retina to the rest of the brain, remain relatively intact even in advanced stages of degeneration[74]. Thus, it is possible that generating electrical signals in those remaining neurons would allow those signals to propagate to the rest of the brain and thus restore visual perception. In order to stimulate remaining retinal neurons electrically, an electronic retinal prosthetic can be implanted into the eye[75]. These retinal prosthetics can be placed either above or below the retina and stimulate neighboring cells indiscriminately by delivering electrical pulses through a series of electrodes arranged in a grid. The stimulation pattern can be configured in such a way as to represent the outlines of simple objects observed by patients thus effectively allowing them to perceive their surroundings. These retinal prosthetics have restored some visual perception to human patients[76] and have recently been approved for clinical use by the Food and Drug Administration. At present, however, this approach can only confer vision with a very limited spatial resolution due to the relatively small number of stimulating electrodes (60 electrodes in the Argus II implant and 1500 in the Alpha IMS implant) present in the retinal prosthetic. Furthermore, the implantation of a retinal prosthetic can damage the patient's eye or cause other adverse side effects[77].

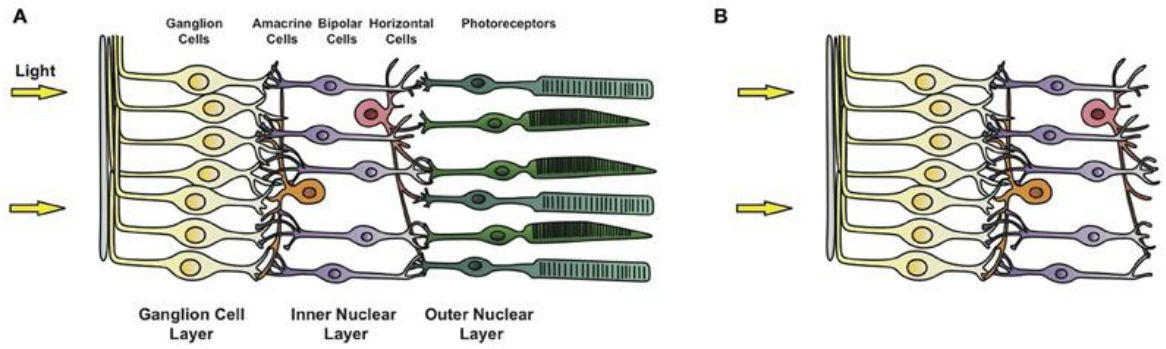

Figure 1: Retinal degeneration results in the loss of rod and cone photoreceptors

A) Structure of a healthy retina and **B**) structure of a retina where the photoreceptors have been lost due to degeneration. Reprinted with permission from Mourot *et al*., 2013[78].

Given these drawbacks of using retinal implants, and electrical stimulation in general, researchers began to develop other strategies and stimulus modalities for vision restoration. Optogenetic approaches for controlling neuronal function with light have quickly gained widespread acceptance in neuroscience. It is thus not surprising that researchers attempted to express light-sensitive microbial opsins in various cell types in the retina of blind animals in an attempt to determine whether optical control of neuronal function could restore vision. Indeed, animal trials of optogenetic therapies in blind mice rescued visual function in those animals and allowed them to perform visual behaviors[79]. Optical stimulation offers a number of advantages over electrical stimulation for vision restoration. First, light has the ability to stimulate virtually all remaining cells of a particular type in the retina with much higher spatial precision. Additionally, optogenetic treatment, consisting of a single intraocular injection of the viral vector, is much less invasive than the surgical procedure required for implantation of retinal prosthetics. However, optogenetic or chemical optogenetic strategies still require the use of viral gene therapy to deliver the desired microbial opsin to the retina. Gene therapy has potential serious adverse side effects[80] and the use of microbial opsins may generate an immune response in human patients.

Thus, we set out to develop a way of controlling the activity of surviving retinal neurons with light that does not require gene therapy, but relies only on a light-sensitive chemical that can be introduced into the eye by a relatively simple surgical procedure. Unlike chemical optogenetic tools, which require the expression of a mutant protein, optopharmacological approaches aim to control the function of endogenous ion channels or receptors with light by the addition of a light-sensitive ligand. These ligands, which can be agonists, antagonists or blockers of certain channels[8], can be designed not only to be selective for particular receptors, but also to possess certain physicochemical properties, such sensitivity to relatively dim, visible light as well as long-term persistence in tissue, that would be desirable in a drug used for clinical vision restoration. We have tested a series of these light-sensitive compounds in animal models of retinal degeneration and found that they restore retinal light responses and visual behaviors in formerly blind animals.

Chapter 2: The light-sensitive chemical AAQ restores visual function to blind mice

The data presented below have been published in the following article which is reprinted in full with permission:

Polosukhina A., Litt J., Tochitsky I., Nemargut J., Sychev Y., De Kouchkovsky I., Huang T., Borges K., Trauner D., Van Gelder R.N., Kramer R.H. "Photochemical restoration of visual responses in blind mice". *Neuron* 2012 Jul 26;75(2):271-82.

Author contribution

A.P., J.L., I.T., J.N, Y.S., T.H, I.D.K., and K.B. conducted the *in vitro* and *in vivo* experiments. D.T. designed and synthesized chemical reagents. R.H.K. and R.V.G. coordinated the research and wrote the manuscript. R.H.K. initiated the research and supervised the program.

Abstract

Retinitis pigmentosa (RP) and age-related macular degeneration (AMD) are degenerative blinding diseases caused by the death of rods and cones, leaving the remainder of the visual system intact but largely unable to respond to light. Here we show that, AAQ, a synthetic small molecule photoswitch, can restore light sensitivity to the retina and behavioral responses *in vivo* in mouse models of RP without exogenous gene delivery. Brief application of AAQ bestows prolonged light sensitivity on multiple types of retinal neurons, resulting in synaptically amplified responses and center-surround antagonism in arrays of retinal ganglion cells (RGCs). Intraocular injection of AAQ restores the pupillary light reflex and locomotory light avoidance responses in mice lacking retinal photoreceptors, indicating reconstitution of light signaling to brain circuits. AAQ and related photoswitch molecules present a new drug strategy for restoring retinal function in degenerative blinding diseases.

Introduction

Inherited degenerative diseases of the retina including retinitis pigmentosa (RP) affect 1 in 3,000 people worldwide. As differentiation of rods and cones ceases soon after birth in mammals, disorders resulting in photoreceptor degeneration lead to a permanent visual deficit. At present, there is no effective treatment for preventing this degenerative process and without some means of restoring photoreception, patients with advanced RP face the prospect of irreversible blindness.

Retinal ganglion cells (RGCs) are the sole output neurons of the retina. Hence all of the visual information that reaches the brain is encoded by the spatial and temporal pattern of RGC action potentials. Several strategies have been advanced to enable light to alter RGC firing in the absence of rods and cones, with the goal of restoring visual function after the photoreceptors are lost[81-84]. Biomedical engineers have developed surgically implanted retinal "chip" prosthetics[85-87], which can be electronically controlled by an external camera to enable optical stimuli to trigger RGC firing. Retinal implants have restored simple shape discrimination to blind patients[88,89] indicating that artificial stimulation of RGCs *in vivo* can create a useful visual experience. Second, genes encoding optogenetic tools, including light-activated ion channels[90-92], transporters[79] or receptors[93,94] can be introduced with viruses to bestow light-sensitivity on retinal neurons that survive after the natural photoreceptive cells have degenerated. Expression of optogenetic proteins in RGCs[92,93], bipolar cells[91], and remnant cones[79] can reinstate light-elicited behavioral responses in mouse models of RP. Third, embryonic stem cells can be differentiated into photoreceptors *in vitro*[94]. Injecting stem cell-derived retinal progenitors into blind animals results in integration of photoreceptors and restoration of some electrical activity in response to light[95].

Each of these strategies has shown promise for restoring visual function, but they all require highly invasive and/or irreversible interventions that introduce hurdles to further development as a therapeutic approach. Implantation of retinal chips or stem cell-derived photoreceptors requires invasive surgery, while exogenous expression of optogenetic tools leads to permanent genetic alterations in retinal neurons. Retinal chip prosthetics rely on extracellular electrical stimulation of RGCs, which when excessive can be cytotoxic[96]. Stem cell therapies carry potential for teratoma formation[97]. Viruses that deliver optogenetic tools can have off-target effects and may elicit inflammatory responses[98]. While the potential permanence of optoelectronic, stem cell, or optogenetic interventions could be favorable in the absence of complications, any deleterious effects of these treatments could be very difficult or impossible to reverse.

Here we report an alternative strategy for restoring visual function, based on a small molecule "photoswitch" that bestows light sensitivity onto neurons without requiring exogenous gene expression. The photoswitch is injected into the vitreous cavity of the eye, but unlike the other strategies, it does not require highly invasive surgical interventions and its actions are reversible. We used AAQ (acrylamide-azobenzene-quaternary ammonium), a K^+ channel photoswitch that enables optical control of neuronal excitability[99,100]. AAQ was originally thought to conjugate to K^+ channels[100], but recent work shows that the molecule interacts non-covalently with the cytoplasmic side of the channels, similar to the mechanism of action of local anesthetics[99]. The *trans* form of AAQ blocks K^+ channels and increases excitability, whereas photoisomerization to

the *cis* form with short wavelength light (e.g. 380 nm) unblocks K^+ channels and decreases excitability. Relaxation from *cis* to *trans* occurs slowly in darkness, but much more rapidly in longer-wavelength light (e.g. 500 nm), enabling rapid bi-directional photocontrol of neuronal firing with different wavelengths.

We show that AAQ confers robust light responses in RGCs in retinas from mutant mice that lack rods and cones. Moreover, after a single intraocular injection, AAQ restores light-driven behavior in blind mice *in vivo*. Because it is a rapid and reversible drug-like small molecule, AAQ represents a class of compounds that has potential for the restoration of visual function in humans with end-stage photoreceptor degenerative disease.

Results

Imparting light sensitivity on *rd1* mouse retina with AAQ

We tested whether AAQ can impart light sensitivity on retinas from 6-month old *rd1* mice, a murine model of retinitis pigmentosa (RP). The homozygous *rd1* mouse (*rd1*/*rd1*) has a mutation in the gene encoding the β-subunit of cGMP phosphodiesterase-6 (PDE-6), essential for rod phototransduction. Rods and cones in these mice degenerate nearly completely within 3 months after birth, leading to a loss of electrical and behavioral light responses[101]. We placed the *rd1* mouse retina onto a multi-electrode array (MEA) that enables simultaneous extracellular recording from many RGCs[102]. Before AAQ application, light generated no measurable change in RGC firing. However, after 30 min treatment with AAQ, nearly all RGCs responded to light (Figure 1A). Photosensitization increased with AAQ concentration (Figure S1, Table S1), but we used 300 μM for our standard *ex vivo* treatment. Light responses slowly diminished, but were still robust for >5 hours after removing AAQ from the bathing medium, (Figure S2a). Light responses could also be detected in 3 of 4 recordings from retinas removed from *rd1* mice that 12 hours previously had received *in vivo* intravitreal AAQ injections (Figure S2a). The degree of photosensitivity varied, reflecting inaccurate injection in the small intravitreal volume of the mouse eye (2-3 ml).

Most RGCs exhibited an increase in firing rate in response to 380 nm light and a decrease in 500 nm light, opposite to AAQ-mediated light responses in neurons in culture[100]. To quantify the effects of light, we calculated a Photoswitch Index (PI) representing the normalized change in firing rate upon switching from darkness to 380 nm light. Positive or negative PI values reflect an increase or decrease, respectively, of firing. Before AAQ treatment, RGCs had almost no light response (median PI = 0.02); but after treatment, nearly all were activated by 380 nm light (median PI = 0.42) (Figure 1B). The rare light responses before AAQ treatment might result from melanopsin-containing intrinsically photosensitive RGCs (ipRGCs), which account for ~3% of the RGCs in the adult mouse retina[103]. Significant photosensitization was observed in each of 21 AAQ-treated retinas. On average, we observed an 8-fold increase in RGC firing rate in response to 380 nm light (Figure 1C).

AAQ acts on RGCs, bipolar, and amacrine cells in *rd1* retinas

We were surprised that 380 nm light stimulated RGC firing because this wavelength unblocks K^+ channels which should reduce neuronal excitability. However, since RGCs receive inhibitory input from amacrine cells, RGC stimulation might be indirect, resulting from amacrine cell-dependent disinhibition. To test this hypothesis, we applied antagonists of receptors for GABA and glycine, the two inhibitory neurotransmitters released by amacrine cells. Photosensitization of RGCs by AAQ persisted after adding inhibitors of $GABA_A$, $GABA_C$, and glycine receptors (Figure 2A), but the polarity of photoswitching was reversed, with nearly all neurons inhibited rather than activated by 380 nm light (Figure 2B). These results indicate that photoregulation of amacrine cells is the dominant factor that governs the AAQ-mediated light response of RGCs.

After blocking amacrine cell synaptic transmission, the remaining light response could result from photoregulation of K^+ channels intrinsic to RGCs and/or photoregulation of excitatory

Figure 1

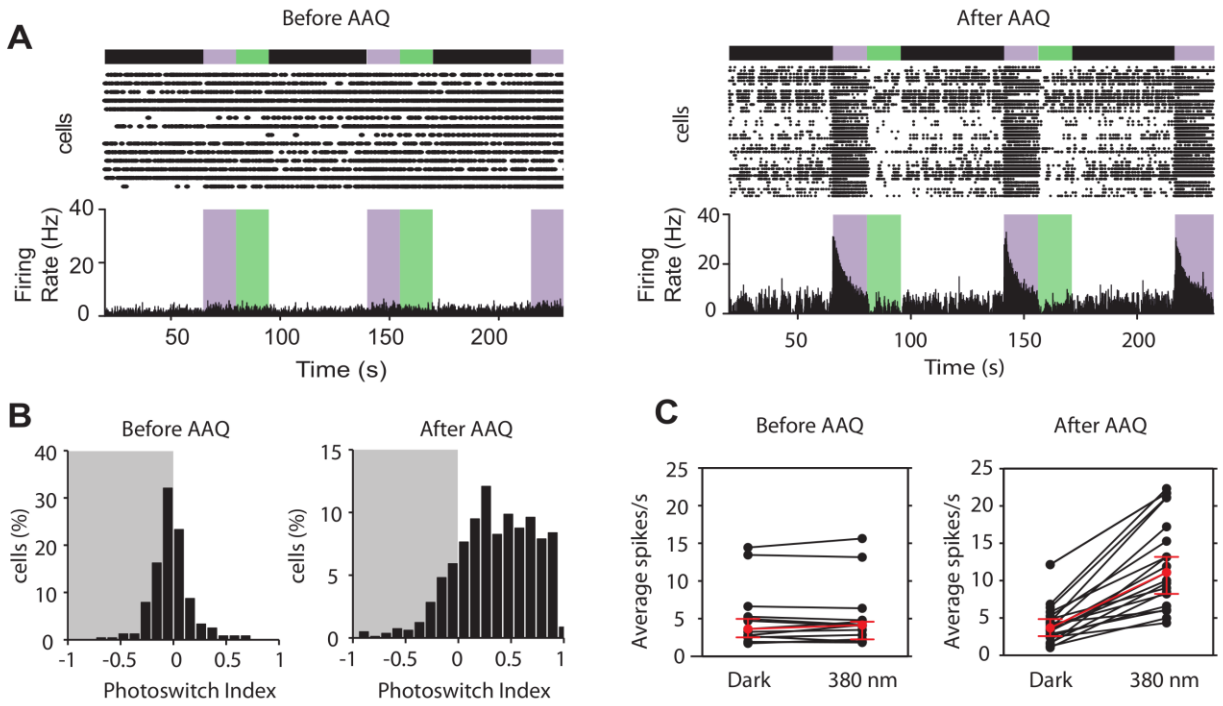

Figure 1. AAQ imparts light sensitivity onto blind retinas from *rd1* mice.

(**A**) Multi-electrode recordings from flat-mounted *rd1* mouse retinas before and after treatment with AAQ (300 μM for 25 min, followed by washout). Top, raster plot of spiking from RGCs; bottom, average RGC firing rate calculated in 100 msec time bins. Color bars represent illumination with 380 nm (violet) or 500 nm light (green), separated by periods of darkness.
(**B**) Analysis of photoswitching of the entire population of RGCs from all untreated retinas and all AAQ-treated retinas. Untreated retinas (n=12) had PI values near 0, indicating no photoswitching, AAQ-treated retinas (n=21) had PI values >0, indicating an increase in firing frequency after switching from darkness to 380 nm light.
(**C**) AAQ-mediated photosensitivity results from an increase in firing rate in 380 nm light. Average RGC firing rates in untreated retinas and AAQ-treated retinas in darkness and during the first 5 s in 380 nm light. Note that untreated retinas (n=12) fail to respond to light, but AAQ-treated retinas have RGCs that increase firing rate with 380 nm light. Red symbols show median values and error bars represent 95% confidence intervals for untreated and treated retinas ($p < 0.0001$, Mann-Whitney test).

Figure 2

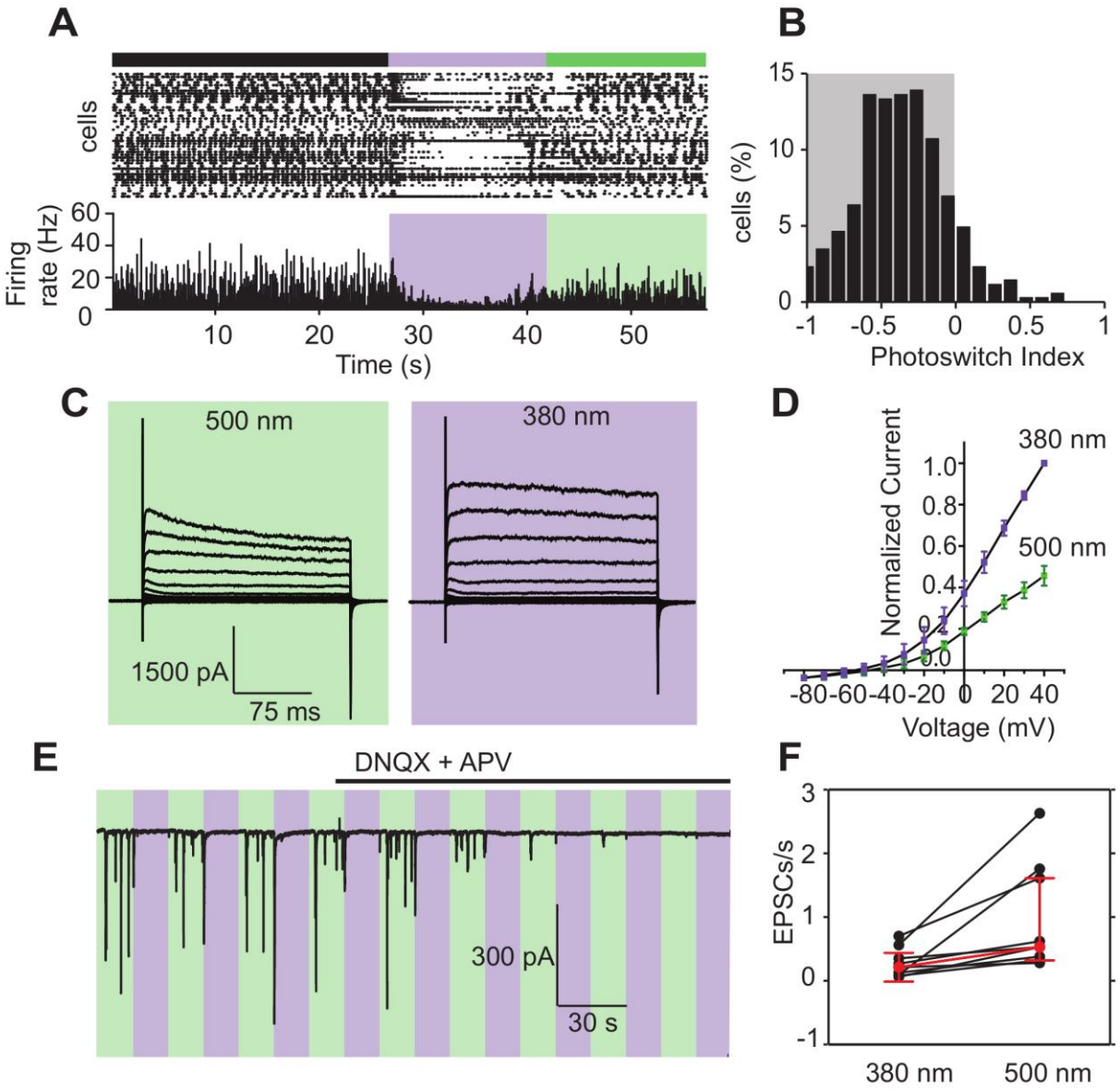

Figure 2. Multiple types of retinal neurons contribute to the AAQ-mediated light response of RGCs.

(**A**) Amacrine cell-mediated synaptic inhibition dominates the RGC light response. MEA recording with antagonists of $GABA_A$ (gabazine; 4 μM), $GABA_C$ (TPMPA; 10 μM), and glycine receptors (strychnine; 10 μM). Top, raster plot of RGC spiking. Bottom, average RGC firing rate. After blocking inhibition, PI values show a decrease in firing frequency upon switching from darkness to 380 nm light (n=11 retinas).

(**B**) After blocking inhibition, PI values show a decrease in firing frequency upon switching from darkness to 380nm light (n=11 retinas).

(**C**) Endogenous K^+ channels contribute to the RGC light response. Whole-cell patch clamp

recording from an RGC. Currents were evoked by voltage steps from -80 to +40 mV in 20-mV increments in 380 nm and 500 nm light. Inhibitory GABAergic and glycinergic inputs were blocked as in (**A**), and excitatory glutamatergic inputs were blocked with DNQX (10 μM) and AP5 (50 μM).

(**D**) Photoregulation of endogenous K^+ channels evaluated in steady-state I-V curves obtained in 380 and 500 nm light (n = 5 RGCs). Current is normalized to the maximal value at +40 mV (380 nm light). Variability among data is expressed as mean ± SEM.

(**E**) Bipolar cell-mediated synaptic excitation also contributes to the RGC light response. Whole-cell patch clamp recording from an RGC. Blockade of inhibitory synaptic inputs (as in panel **A**) and endogenous RGC K^+ channels (as in panel **C**) reveals photoregulation of EPSCs. Note the disappearance of EPSCs after superfusion with glutamate receptor antagonists DNQX (10 μM) and AP5 (50 μM). Holding potential = -60 mV.

(**F**) Average EPSC rate in 380 nm and 500 nm light. Note the significant increase in EPSC rate in 500 nm light ($p < 0.05$, Mann-Whitney test; n=9 cells). Red symbols show median values and error bars represent 95% confidence intervals.

inputs from bipolar cells. To explore the contribution of intrinsic K^+ channels, we obtained whole-cell patch clamp recordings from RGCs and pharmacologically blocked nearly all synaptic inputs (glutamatergic, GABAergic, and glycinergic). Depolarizing voltage steps activated outward K^+ currents that were smaller and decayed more rapidly in 500 nm light than in 380 nm light (Figure 2C). Comparison of current vs. voltage (I-V) curves shows that the current was reduced by ~50% in 500 nm light (Figure 2D), similar to previous results[100]. However, MEA recordings indicate that photoregulation of RGC firing was nearly eliminated by blocking all excitatory and inhibitory synaptic inputs (Figure S3), suggesting that the light response is driven primarily by photoregulation of upstream neurons synapsing with RGCs.

To examine directly the contribution of retinal bipolar cells to the RGC light response, we blocked RGC K^+ channels with intracellular Cs^+ and added GABA and glycine receptor antagonists to block amacrine cell inputs. Flashes of 500 nm light triggered excitatory post-synaptic currents (EPSCs) in RGCs and 380 nm light suppressed these events (Figures 2E and 2F). Blocking glutamate receptors eliminated these events and bipolar cells provide the only known glutamatergic input to RGCs. Hence, we conclude that inputs from amacrine cells, bipolar cells, and to a lesser extent, the intrinsic K^+ conductances of RGCs, all combine to shape and amplify the AAQ-mediated RGC light response.

Spatial localization and center-surround antagonism of RGC light responses in AAQ-treated retina

Visual acuity is determined by the size of receptive fields of neurons in the visual system. In the healthy retina, the receptive field of an RGC is defined by the spatial extent of all of the photoreceptors that influence its activity. By definition, the receptive fields of RGCs in *rd1* mice are eliminated after the photoreceptors have degenerated. However because AAQ makes presynaptic neurons light-sensitive, it is possible to measure the spatial extent of their light-driven influence on RGC firing. While this is not a conventional measurement of the RGC receptive field, it does indicate the spatial precision of the AAQ-mediated RGC light response.

We illuminated AAQ-treated retinas with small spots (60 μm diameter) of 380 nm light centered on one of the 60 electrodes in an MEA (Figure 3A). In the example shown in Figure 3A, upon switching from 500 to 380 nm light, the average RGC activity increased in the targeted electrode by ~81%, but not in the surrounding electrodes. In each of a total of 8 targeted spots from 3 different retinas, only neurons near the targeted electrode exhibited a significant increase in firing (median PI=0.517; Figure 3B). Since RGCs are detected by only one electrode and they are spaced 200μm apart, this puts an upper limit on the radius of the AAQ-mediated RGC collecting area of 100μm.

Analysis of electrodes outside the illuminated spot showed that 380 nm light significant decreased RGC firing. Decreased firing was detected in electrodes centered at 300, 500, and 700 μm from the mid-point of the targeted electrode (Figure 3C, Table 1). Hence RGCs in the center of an illuminated spot are stimulated, whereas those in a surrounding annulus (from 200 to 800 μm) are inhibited. Inhibition in the surrounding RGCs implies that a sign-inverting synapse from a laterally-projecting neuron is involved in transmitting information from the center illuminated area to the surround. Amacrine cells are known to form a mutually inhibitory network, making them the likely source of the inhibitory signal.

Figure 3

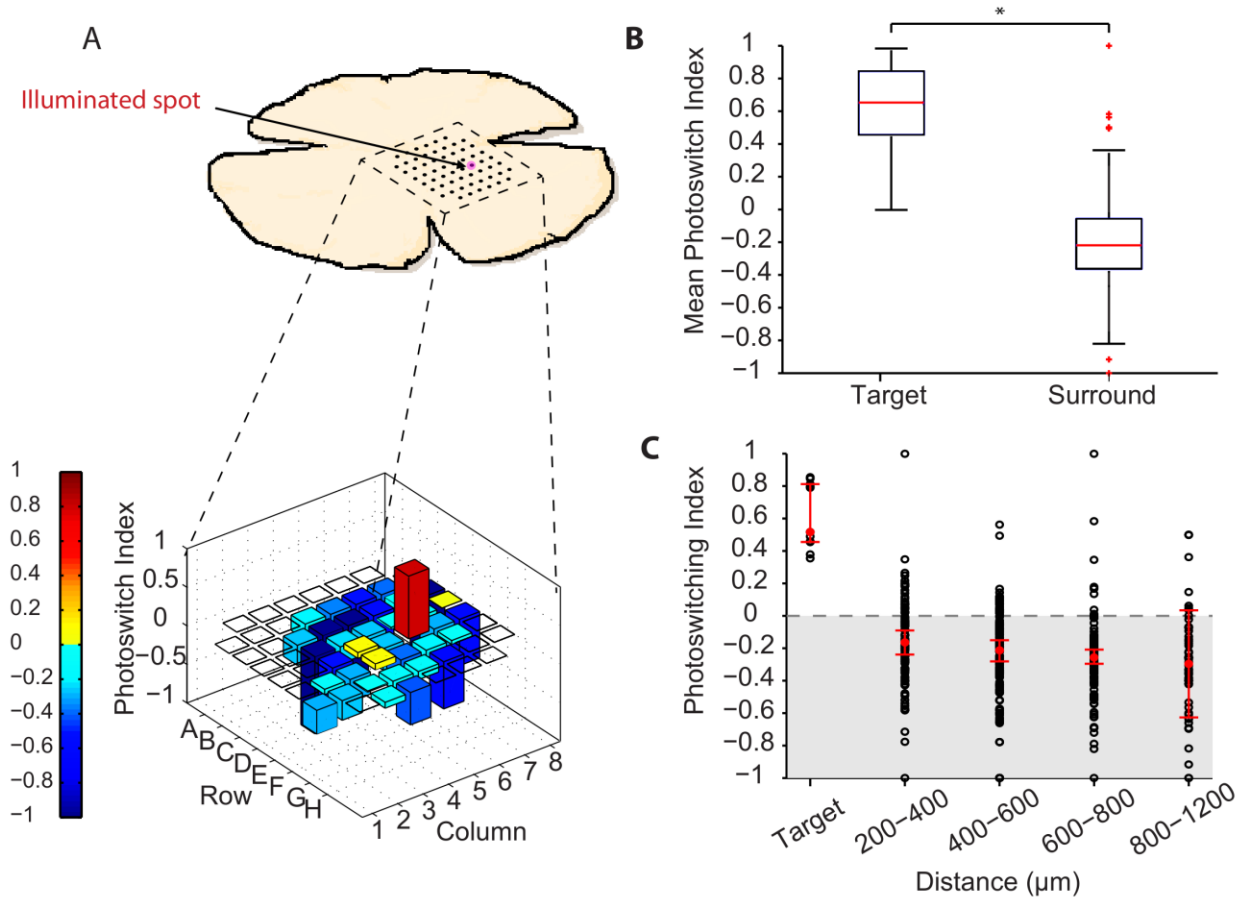

Figure 3: The AAQ treated retina generates spatially precise light responses.

(**A**) Targeted illumination of a portion of the retinal centered on a single MEA electrode (top). The target (electrode E6) was exposed to 3 s flashes of alternating 380 and 500 nm light. ,Spot size = 60 μm in radius, inter-electrode spacing = 200 μm. Only the targeted electrode records an increase in RGC firing in response to 380 nm light (bottom). PI values are color-coded (scale at left) and also represented by bar height. Red bar is electrode E6 (PI = 0.812; n = 1 cell) and blue electrodes are the surround (PI = -0.209; n = 56 cells). Empty squares are electrodes on which no action potentials were recorded.

(**B**) Targeted illumination results from 3 retinas, displayed in a box plot. PI values for the target and the surround RGCs are significantly different from one another ($p < 0.005$, Mann-Whitney test

(**C**) Targeted illumination results in opposite responses in center and surround RGCs (n = 11 cells and n = 385 cells, respectively, from 3 retinas. PI values of RGCs (open circles) as a function of distance from the target electrode, displayed in 200 um bins. The red diamonds indicate the median plus or minus the bootstrapped 95% confidence intervals.

Table 1

Distance (μm)	Number of Cells	Median PI	95% Confidence Interval
Target	11	0.517	0.455 to 0.812
200-400	95	-0.165	-0.239 to -0.090
400-600	143	-0.213	-0.284 to -0.150
600-800	97	-0.256	-0.294 to -0.206
800-1200	50	-0.296	-0.626 to 0.034

Spectral requirements of AAQ-mediated light responses

We determined the optimal wavelength for turning off RGC firing when the AAQ photoswitch is driven from the *cis* to the *trans* configuration. First, a conditioning 380 nm stimulus was used to turn on firing and then we measured suppression of firing in response to test flashes of different wavelengths. We found that 500 nm light is best at suppressing activity (Figure 4A), as expected from previous results[100]. To determine which wavelengths are best at triggering firing when AAQ photoisomerizes from *trans* to *cis*, we again applied test flashes of different wavelengths, but to ensure that the photoswitch started maximally in the *trans* configuration, the stimulation protocol began with a reset flash of 500 nm light followed by a period of darkness. We found that the optimal wavelength for stimulating firing was 380 nm under these conditions. However, robust firing could also be activated with 420 or 460 nm light (Figure 4B), and even 500 nm light could trigger an increase in firing frequency, if the preceding dark interval was sufficiently long. The history-dependence of photoswitching is a consequence of the initial ratio of the *cis* and *trans* photoisomers. Starting with all molecules in the *trans* state, even 500 nm light can increase the fraction of *cis* molecules. Hence UV light is not essential for eliciting retinal responses. We also found that broad spectrum white light can trigger an increase in firing frequency in RGCs (Figures 4C and 4D).

We measured the absolute light intensity required to photoregulate AAQ-treated retinas from *rd1* mice. The threshold intensity required to induce RGC firing was $2.6*10^{15}$ photons/cm^2/s of 380 nm light (Figure 4E). RGC firing rate increased progressively with brighter light, up to 10^{17} photons/cm^2/s, but even this intensity did not saturate the response. By comparison, retinas from *rd1* mouse expressing ChR2 in bipolar cells[91] have RGCs that exhibit a firing threshold of $6*10^{15}$ photons/cm^2/s.

Restoring behavioral light responses *in vivo* with AAQ

Given that AAQ can bestow photosensitivity onto blind retinas *ex vivo*, we asked whether it can confer light-induced behavior in blind mice *in vivo*. Although *rd1* mice lose all morphologically recognizable rods and cones, a small fraction of cones with altered morphology can survive, allowing correct performance of a visual discrimination task under some illumination conditions[104]. *Rd1* mice also exhibit a pupillary light reflex (PLR), but this behavior is completely absent from *rd1* mice lacking melanopsin, the photopigment found in the small percentage (~3%) of RGCs that are intrinsically photosensitive[103,105] (ipRGCs). Therefore, we tested the PLR of adult *rd1* mice lacking the melanopsin gene (*opn4*$^{-/-}$ *rd1/rd1*)[105]. After 3 months of age, no PLR could be elicited in any of the mice that we tested, even with brightest light available (Figure 5A). However, in a subset of these mice (9 / 25), intravitreal injection of AAQ resulted in a substantial PLR, with a maximal pupillary constriction ~65% as large as wild-type. Control experiments showed no restoration of the PLR following sham injection of vehicle alone (n=4; Figure S4). The AAQ-mediated response was attributable to the retina, as direct application of AAQ to the isolated iris *in vitro* did not produce light-elicited constriction. In the remaining mice, suboptimal intravitreal placement or leakage resulting from puncture damage may have limited retinal access to injected AAQ, precluding effective photosensitization.

Figure 4

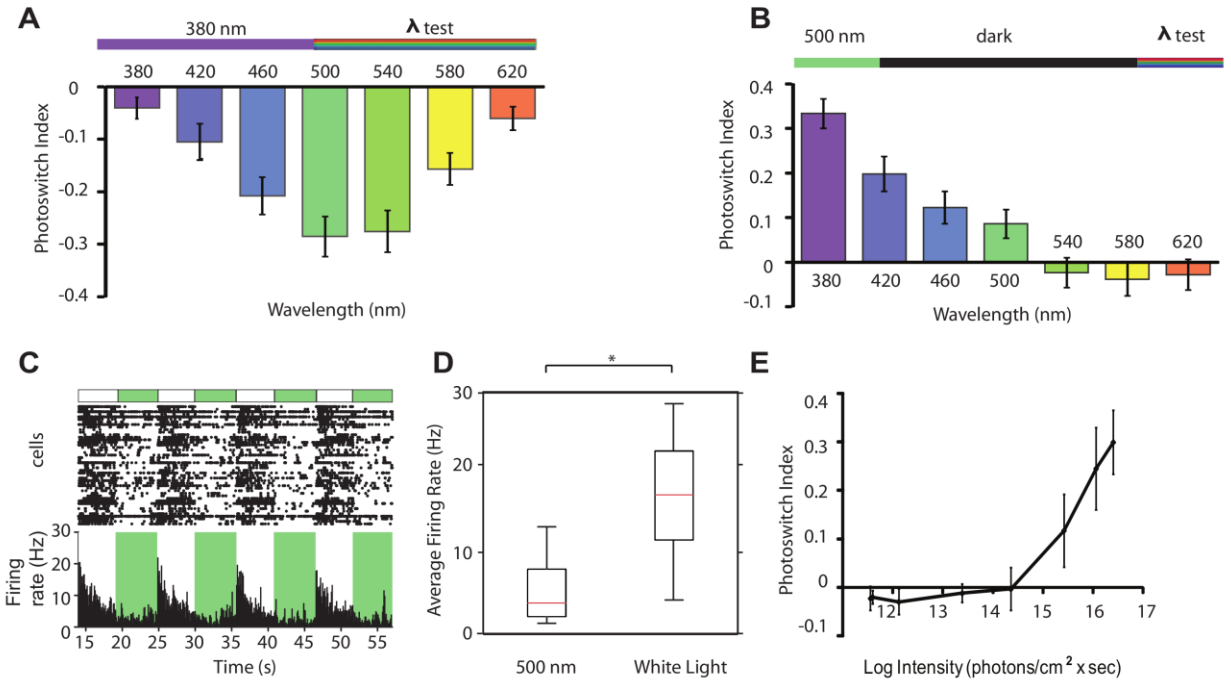

Figure 4. Spectral and illuminance sensitivity of AAQ-mediated photocontrol of RGC firing.

(**A**) Spectral sensitivity of light-elicited suppression of RGC firing. Top: Light stimulation protocol. AAQ was first driven into its *cis* configuration with 380 nm light (5 s) and various test wavelengths triggered photoisomerization to the *trans* configuration. Bottom: PI values reveal the effectiveness of different wavelengths in suppressing RGC firing (n=5 retinas).
(**B**) Spectral sensitivity of light-elicited activation of RGC firing. Top: Light stimulation protocol. AAQ was first driven into its *trans* configuration with 500 nm light (15 s). After an additional dark period (45 s) various test wavelengths triggered photoisomerization to the *cis* configuration. Bottom: PI values reveal the effectiveness of different wavelengths in stimulating RGC firing (n = 5 retinas). For **A** and **B** the PI was measured over the first 1 s after applying the test wavelength.
(**C**) Stimulation of RGC firing in an AAQ-treated retina with white light. Top, raster plot of spiking from RGCs; bottom, average RGC firing rate.
(**D**) Box plot representation of increased firing rate in white light vs. 500 nm. White light significantly increases peak firing rate (*p* < 0.05, Mann-Whitney test, *n* = 5).
(**E**) Light intensity-response relationship for AAQ-treated *rd1* mouse retinas exposed to different intensities of 380 nm light. Minimum light intensity needed for photoswitching is $2.6*10^{15}$ photons/cm^2/sec.

Figure 5

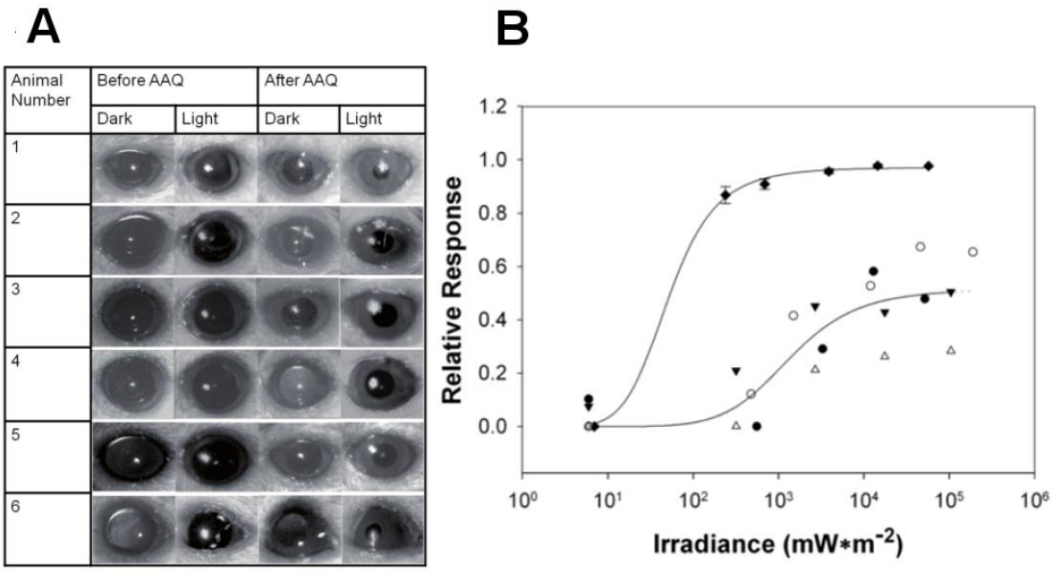

Figure 5. AAQ restores the pupillary light response in mice lacking all retinal photoreceptors.

(**A**) Pupillary light responses to 5.5 * 10^4 mW/m^2 white light in *opn4*$^{-/-}$ *rd/rd* mice, before (left) and 3 hours after (right) intravitreal injection of AAQ (1 µl of 80 mM in DMSO). Dark images taken 5 s before light stimulus; light images represent maximal pupillary constriction during 30 s light exposure. Images were taken with an infrared-sensitive camera under infrared illumination.
(**B**) Irradiance-dependence of pupillary light responses to white light. Irradiance response for wild-type mice (plotted as mean ± STD, n = 5) (♦) and four *opn4*$^{-/-}$ *rd/rd* mice injected with AAQ (plotted individually: ●○▼Δ). Data were fitted with a three parameter Hill equation.

The AAQ-mediated PLR in *opn4*$^{-/-}$ *rd1/rd1* mice could be triggered by photopic irradiance levels normally encountered during daytime, but the PLR threshold was 2-3 log units higher than the normal PLR in wild-type mice (Figure 5B). The AAQ-mediated PLR was slower than in wild-type mice (see Supplemental Movie 1) and AAQ induced some basal pupillary constriction in darkness. Nonetheless, these results show that light responses in AAQ-treated retina can drive brain circuits, leading to a behavioral response that is absent from untreated blind animals.

We next tested whether locomotory light-avoidance behavior[106,107] could be restored in blind *opn4*$^{-/-}$ *rd1/rd1* mice treated with a unilateral intravitreal injection of AAQ. We placed a mouse into a narrow cylindrical transparent tube and recorded behavior with an infrared video camera (Figure 6A). An automated image analysis system was used to detect the mouse and measure how quickly it moved away from the illuminated end of the tube, toward the center. The latency to movement was significantly shorter in light than in darkness in wild-type mice (n=13, 26 trials, $p < 0.01$), but not in *opn4*$^{-/-}$ *rd1/rd1* mice (n=7, 14 trials) indicating light-avoidance in the wild-type but not in the mutant mice. AAQ reinstated the light vs. dark latency difference, measured 2 hours after injection (n=7, 14 trials, $p < 0.02$), indicating restoration of light avoidance. At 24 hours after AAQ injection, there was no difference in latency in light vs. darkness, consistent with dissipation of the AAQ. These results indicate that an active light-avoidance behavior can be elicited by AAQ following a single injection into the eye.

Wild-type mice exhibit a decrease in open-field locomotion in response to light, which corresponds to a decrease in exploratory drive (Bourin et al., 2003). In contrast, *rd1* mice exhibit no change in locomotion over at least a 10 minute period of illumination (Lin et al., 2008). In order to determine if AAQ leads to light modulated exploratory behavior in *rd1* mice, we carried out open field experiments. We placed a mouse into a circular test chamber and monitoring movement during 5 min in darkness followed by 5 min in 380 nm light. Figure 7A and 7B show an example of the effect of AAQ on one *rd1* mouse (See also Movie S2 and Movie S3). Before AAQ, light had no effect on movement trajectory (Figure 7A) or total distance traveled (Figure 7B). After AAQ, light caused an almost immediate decrease in exploratory behavior, quantified as diminished distance traveled. Average data from 8 *rd1* mice showed no light vs dark difference in movement before AAQ (Figure 7C). However, after AAQ there was a decrease in movement that occurred within 30 seconds of light onset. This decrease was sustained throughout the illumination period. Before AAQ there was no statistically significantly change in the speed of locomotion in light as compared to darkness (Figure 7D), but after AAQ injection, light caused a significant 40% slowing of locomotion. Sham injections with vehicle alone elicited no significant change in light modulated behavior ($n = 4$, $p > 0.6$). Further analysis of the 8 mice showed that 7 of them exhibited significant light-evoked slowing of locomotion after AAQ injection (Figure 7E).

After termination of the behavioral test, mice were sacrificed and retinas were placed on the MEA for electrophysiological analysis. In 5 cases, we successfully obtained MEA recordings and we were able to directly compare the AAQ-mediated photosensitization of the retina *ex vivo* with the behavioral responses *in vivo*. The one mouse that failed to exhibit light-modulated behavior (mouse A in Figure 7F) also failed to exhibit light-sensitive retinal responses. For all of the other 4 mice, light-elicited behavior corresponded with a light-elicited change in firing rate. *Rd1* mice possess ipRGCs, which should respond to the light used in this behavioral test.

However, previous studies (Lin et al., 2008) show that ipRGCs do not mediate short-term light-elicited changes in exploratory behavior. Moreover, in our open field experiments mice exhibited no light modulated behavior prior to AAQ injections, suggesting that alone, the intrinsically photosensitive RGCs are not sufficient to evoke this behavior.

Figure 6

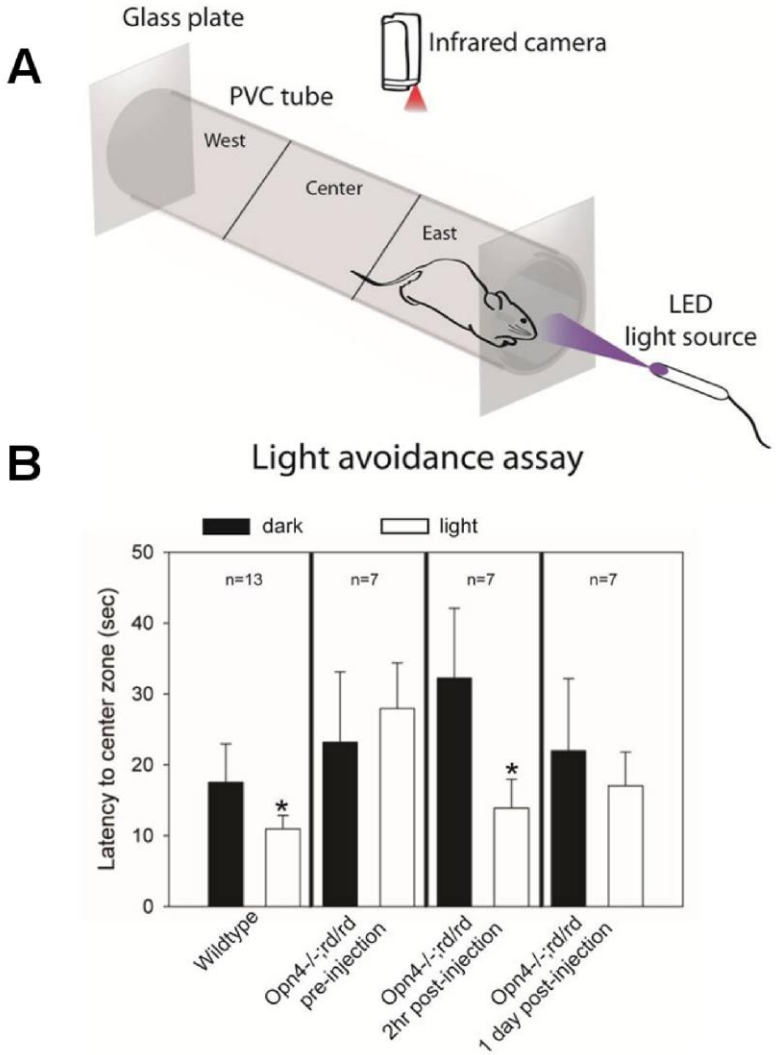

Figure 6. AAQ restores active light avoidance behavior in mice lacking all retinal photoreceptors.

(**A**) Schematic diagram of the locomotory light-avoidance test chamber.
(**B**) Restoration of light avoidance behavior in *opn4*$^{-/-}$ *rd/rd* mice following AAQ injection. Bars represent mean latency of movement from the "East" to the "Center" third of the tube (plotted as ± STD).

Figure 7

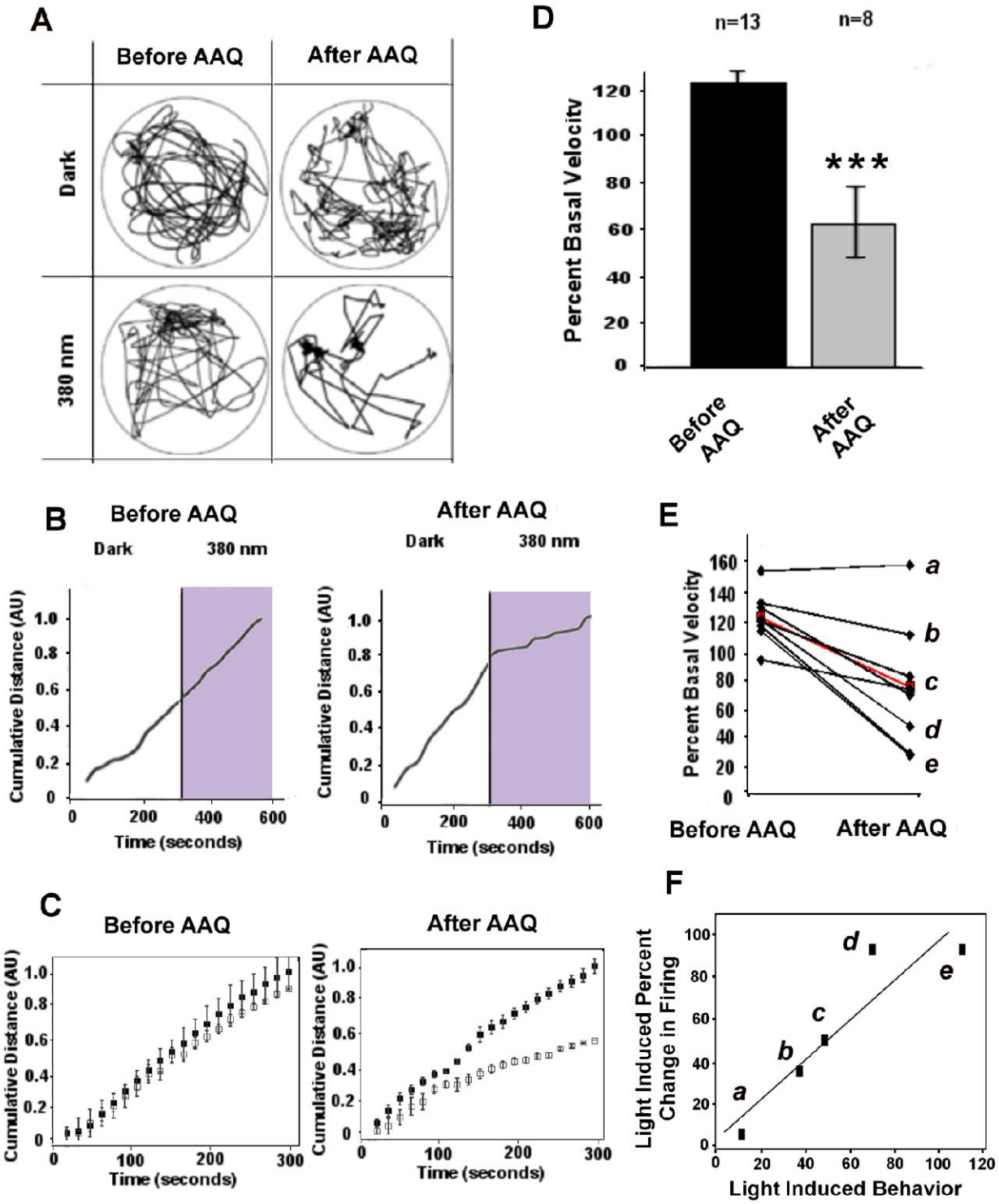

Figure 7: AAQ restores light-modulated locomotor behavior in an open-field test

(**A**) Paths traveled by an *rd1* mouse before and after injection with AAQ in darkness and with 380 nm illumination.

(B) Cumulative distance traveled by the mouse in darkness and in 380 nm light, before and after AAQ.
(**C**) Average cumulative distance traveled of all mice in darkness and 380 nm light, before and after AAQ. Closed squares represent time spent in darkness while open squares represent time spent in 380 nm light. (mean ± SEM, n = 8).
(**D**) Mean locomotory velocity in light normalized to basal velocity in darkness. Velocity decreases significantly in light ($n = 8$, $p < 0.0006$).
(**E**) Light evoked change in the velocity of each of the eight mice, before and after AAQ. Red line shows the mean light evoked change, before and after AAQ.
(**F**) Light induced behavior is correlated with the light induced change in firing rate. Data were from the five mice for which both *in vivo* behavioral measurement and *ex vivo* retinal MEA recordings were obtained (as labeled in panel (**E**)). The light induced percent change in firing rate was calculated from the aggregate light response for all units recorded with the MEA upon switching from darkness to 380 nm light. The light induced behavior represents percent change in velocity upon switching from darkness to 380 nm light.

Discussion

The ultimate goal of vision restoration research is to recreate as closely as possible the activity of the entire population of RGCs in response to a natural visual scene. Since only a small fraction of RGCs are intrinsically light-sensitive[105,108], photosensitivity must be conferred artificially by directly or indirectly making the neurons sensitive to light. Ideally, the kinetics and absolute sensitivity to light should be equivalent to natural RGC responses. The healthy retina has a remarkably broad operating range owing to light-adaptation mechanisms, so the artificial system should include gain adjustment and range extension capabilities. Ideally, the system would replicate normal encoding of contrast and color and highlight movement, with certain RGCs being directionally selective, accomplished with a minimally invasive and safe technology. To date, no restorative technology is close to meeting these criteria, but new developments are providing reason for optimism.

Broadly, three approaches have been suggested for restoring visual function to the eye in the absence of rods and cones: optoelectronic engineering with retinal chip prosthetics; genetic engineering with viral-mediated delivery of optogenetic tools; and cellular engineering, with rod or cone progenitors differentiated from stem cells *in vitro*. We now describe a fourth approach, photochemical engineering with a small molecule photoswitch. The following functional considerations suggest that the photoswitch approach would compare favorably with other methods for restoring visual function. and offers some practical advantages.

Kinetics

AAQ-mediated retinal light responses are rapid. MEA recordings show that the median response latency of RGC spiking is 45 msec in the AAQ-treated *rd1* mouse retina, compared to ~50 msec[109] to several hundred msec[110] for photopic light responses from RGCs in wild-type retina. Retinal chips electrically stimulate RGCs directly, and therefore can elicit spikes with latencies of several msec. For optogenetic tools, depending on which retinal cell type expresses the tool the response latency of RGCs ranges from several msec to 150 msec[79,90,91]. Stem-cell based therapies would presumably restore wild-type kinetics assuming the differentiated rods and cones have full function.

Sensitivity

MEA recordings *in vitro* and PLR measurements *in vivo* indicate that the AAQ-treated *rd1* mouse retina responds under bright photopic conditions, comparable to levels achieved in natural outdoor illumination. This is similar to light sensitivity conferred onto RGCs by optogenetic tools[90,104]. Exogenous expression of NpHR in cone remnants can result in higher light sensitivity[79]. However, it is unclear whether many patients with advanced RP have sufficient cone remnants to allow this to be a broadly applicable approach[111]. High sensitivity can also be conferred by exogenously expressing melanopsin in RGCs that are not normally light-sensitive[94], but the responses are variable and slow (on the order of seconds). Stem cell-based therapies in theory might recapitulate the wild-type sensitivity of rods and cones. However, the human retina normally contains >100,000,000 rods and cones, and whether a significant fraction can be restored with stem cells remains unclear.

Spatial resolution and extent of retinal functional restoration

AAQ-mediated retinal responses have a high spatial resolution. Our spot illumination experiments places a 100 µm radius upper limit on the AAQ-mediated receptive field size. Amacrine cells, which predominate in driving RGC responses, can project over several hundred um, but mutual inhibition between these cells presumably spatially constrains RGCs responses to a smaller area. Because AAQ is a diffusible small molecule, in principle it should reach the entire retina and confer light sensitivity on all RGCs. In practice, we observed robust light responses in almost all RGCs when AAQ was applied *in vitro*, but intravitreal injections *in vivo* were less effective, with only 25-36% of injections resulting in behavioral responses to light. Drug delivery via intravitreal injections in mice can be unreliable because of the very small vitreal volume (~5 µl), which is <1,000-fold the vitreal volume of the human eye (~5.5 ml). Further experiments using animals with larger vitreal volumes are needed to better test and optimize the effectiveness of intravireal AAQ administration.

In contrast to the relatively high spatial resolution that could be conferred by AAQ, the spatial resolution of a retinal chip is limited by the relatively large size of the stimulating electrodes and the spread of current emanating from each electrode. While the healthy human retina contains ~1.2 million RGCs, current retinal chips have 16-64 electrodes spaced 100-200 micrometers apart[96]. Chips with electrodes more densely packed exhibit crosstalk between electrodes, limiting their effectiveness. At present, the resolution that could be provided by retinal chip stimulation is several orders of magnitude lower than the theoretical limits imposed by RGC density in the macula, crucial for high-acuity vision. The area of RGC stimulation is limited by the physical size of the chip implant, which typically covers only the central 20 degrees of vision in the macula[85]. Larger chips are possible, but there are challenges in power delivery and achieving stable adherence to the retina.

Similar to photoswitches, the spatial resolution conferred by optogenetic tools is defined by the size of the cell type targeted for expressing a given light-activated protein. In principle, the smaller the cell type and the more densely they are packed together, the higher the spatial resolution. In practice, viral transduction with current vectors has resulted in expression of optogenetic tools in a minority of targeted cells (e.g. ~5% of bipolar cells in mice[91]; and 5-10% of RGCs in marmosets[112], but it is possible that new viral vectors will be developed that improve transduction efficiency[113]. Viral transduction of NpHR has resulted in more efficient transduction (50-75%) of remnant cones in blind mice[79], but this approach is only appropriate for the few patients thought to possess remnant cones. Viral transduction of cones requires subretinal injection, which involves local detachment of a portion of the retina from the underlying retinal pigment epithelium. Effective viral gene transfer is limited to the detached area[114].

Stem cell approaches offer the potential for greater spatial resolution but this is dependent on having a high density of differentiated photoreceptor cells that form functional and anatomically correct synapses with appropriate retinal neuron partners, and at present only a very low density of cells has been achieved[95].

ON and OFF retinal output channels

Optogenetic tools have the advantage of being genetically-targetable to particular types of neurons to generate the appropriate stimulation or inhibition of firing, for example to ON- or OFF-RGCs[79,91]. Moreover, ChR2 and NpHR can be co-expressed in the same RGC and trafficked to different compartments to restore antagonistic center-surround responses[115]. In contrast, all RGCs in AAQ-treated retina respond with the same polarity light response. While this pattern of responsiveness is different than the normal retina, it may not preclude a useful visual experience. Behavioral studies in primates demonstrate that selective pharmacological blockade of ON neurons does not severely impair recognition of shapes or detection of light decrements[116]. Moreover, in RP patients, electronic retinal prosthetics can restore shape recognition, even though the devices stimulate ON- and OFF-RGCs indiscriminately[117]. Hence while two channels of visual information flow are important for normal vision, simultaneous activation of ON- and OFF-pathways is sufficient for visual perception. AAQ treatment enables RGCs surrounding an illuminated area to respond with the opposite polarity to those in the center. Since all RGCs respond with the same polarity light response to full-field illumination (Figure 1A), the opposite center vs. surround responses to spot illumination suggests that inhibitory neurons that project laterally invert the sign of the response. It seems likely that the opposite center vs. surround response would enhance perception of spatial contrast and facilitate edge detection in downstream visual regions of the brain. But ultimately, the evaluation of the quality of images produced by photoswitch activation of retinal cells will require study in primates or human patients.

Spectral sensitivity

In AAQ-treated retinas, RGCs respond most strongly to short wavelength light, consistent with the photochemical properties of the molecule[100]. Although 380 nm light is optimal for enhancing firing frequency, longer wavelengths (up to 500 nm) can still generate excitatory light responses, reflecting the spectral range of *trans* to *cis* azobenzene photoisomerization. This is important, because unlike in the mouse, the human lens minimally transmits 380 nm light[118]. Newly-developed red-shifted azobenzene derivatives allow K^+ channel regulation with even longer wavelengths of light and chemical modification of the azobenzene moiety results in compounds with improved quantum efficiency[48]. Ideally, second-generation AAQ derivatives would enable photostimulation of the retina with intensities and wavelengths experienced during normal photopic vision. Alternatively, a head-mounted optoelectronic visual aid[119] designed to intensify and transform the palette of visual scenes to a blue-shifted wavelength could enhance the effectiveness of AAQ and related agents. Such a device would also allow switching of individual RGCs ON and OFF by rapid modulation of shorter- and longer-wavelength light. Except for some of the optogenetic tools, the other vision restoration methods pose no particular spectral challenges. NpHR and ChR2 respond optimally to 580 and 470 nm light, respectively[14,120], but newly discovered red-shifted homologs[121] expand the toolkit for potential use for photosensitizing retinal neurons. Since they are driven by images captured by an external camera, retinal chip prosthetics can be engineered to operate over the entire visual spectrum. Similarly, assuming stem-cell derived photoreceptors express the full complement of cone opsins, these should be responsive to a broad range of wavelengths.

Invasiveness, safety, and reversibility

The phototswitch approach has the advantage of being relatively non-invasive and readily reversible. We envision photoswitch molecules being administered therapeutically by intravitreal injection, a safe and frequent procedure for treating macular degeneration with anti-vasoproliferative agents. Because AAQ photosensitization dissipates within 24 hrs, it may be possible to titrate the most effective dose with repeated intravitreal injections. The reversibility of AAQ will allow for "upgrades as newer agents become available, perhaps with improved spectral or kinetic properties. Longer-term therapy would require an extended release formulation. We estimate that a several month supply of AAQ could be packaged into an intravitreal device like those currently used for long-term steroid treatment of ocular inflammation[122].

In contrast, retinal chip prosthetics require invasive intraocular surgery. Optogenetic treatment of remnant cones and stem cell therapy both require subretinal injection, a risky procedure that begins with iatrogenic retinal detachment, which could further damage the retina. These three approaches are essentially irreversible. Should they produce undesired effects (such as chronic photophobia or disturbing visual sensations) there is no ready means for reversal of either stem cell implantation or gene therapy, and removal of chip prosthetics would require additional significant surgery.

Both retinal chip prosthetics and human gene replacement therapy have received investigational new device/drug status and have been tested in human patients under research protocols[123,124], without significant toxicity. However, microbial optogenetic tools would require trans-specific gene therapy, which is unprecedented. Viral gene expression in the eye can elicit late-onset inflammation, indicating an immune reaction[98]. Because the unitary conductance of ChR2 and NpHR is quite small[14,125,126], photosensitivity requires very high levels of exogenous expression, raising concerns about an immune response to the microbially-derived protein or cytotoxicity. While long-term safety of AAQ or similar compounds will require toxicology studies, to date we have not seen acute toxicity of AAQ on neural function *in vitro*[100] *or in vivo* (Figure S2). The pathway for evaluating photoswitch compounds for toxicity is straightforward and will mirror those that have been followed for other approved, intravitreal agents. Finally, in addition to its potential clinical use, AAQ has utility as a scientific tool for understanding normal retinal function and development. Using AAQ the firing activity of single cells or small regions of the retina can be controlled with high temporal and spatial resolution. This may be useful for better understanding information processing by the retina and for studying developmental plasticity in animals before rods and cones are functional[127]. AAQ-mediated photocontrol of retinal neurons also provides a unique way to investigate circuit remodeling after the rods and cones have degenerated in mouse models of RP[82].

Materials and methods

Animals

Wild-type mice (C57BL/6J strain, Jackson Laboratories) and homozygous *rd1* mice (C3H/HeJ strain, Charles River Laboratories) >3 months old were used for the experiments. All animal use procedures were approved by the UC Berkeley or University of Washington Institutional Animal Care and Use Committee (See Supplemental Experimental Protocols).

Electrophysiology and pharmacology

Mouse retinas were dissected and kept in physiological saline at 36 °C containing (in mM): 119 NaCl, 2.5 KCl, 1 KH_2PO_4, 1.3 $MgCl_2$, 2.5 $CaCl_2$, 26.2 $NaHCO_3$, 20 D-glucose, aerated with 95% O_2/5% CO_2. For extracellular recording, the retina was placed ganglion cell layer down onto a multielectrode array system (model number MEA 1060-2-BC, Multi-Channel Systems).

The MEA array electrodes were 30 µm in diameter and arranged on an 8 x 8 rectangular grid. Extracellular spikes were high-pass filtered at 200 Hz and digitized at 20 kHz. A spike threshold of 4SD was set for each channel. Typically, each electrode recorded spikes from 1-3 RGCs. Principal component analysis of spike waveforms was used for sorting spikes generated by individual cells (Offline Sorter; Plexon). Only cells with interspike intervals of < 1 msec were included in the analysis.

Borosilicate glass electrodes of 6-11 MΩ were used for whole-cell voltage-clamp recordings. Current records were low-pass filtered at 2 kHz. For measuring voltage-gated K^+ currents, electrodes contained (in mM): 98.3 K^+ gluconate, 1.7 KCl, 0.6 EGTA, 5 $MgCl_2$, 40 HEPES, 2 ATP-Na, 0.3 GTP-Na (pH =7.25). For recording glutamatergic EPSCs electrodes contained (in mM): 125 Cs^+ sulfate, 10 TEA-Cl, 5 EGTA, 0.85 $MgCl_2$, 10 HEPES, 2 QX-314, 4 ATP-Na_2 (pH=7.25). Neurotransmitter receptor antagonists were used to evaluate synaptic contributions of different retinal neurons to RGC light responses (see Supplemental Experimental Procedures).

Light Stimulation

In MEA recordings, we used a 100 W mercury arc lamp filtered through 380 or 500 nm filters (Chroma, Inc), and switched wavelengths with an electronically-controlled shutter and filter wheel (SmartShutter, Sutter Instruments). Unless otherwise indicated, the standard incident light intensity at the retina was 13.4 mW/cm^2 (2.56*10^{16} photons/cm^2/s) for 380 nm and 11.0 mW/cm^2 (2.77*10^{16} photons/cm^2/s) for 500 nm.

PLR Measurement.

Mice were sedated with an intraperitoneal injection of ketamine (6.7mg/ml) and xylazine (0.45 mg/ml) in saline. A glass micropipette was inserted through the sclera into the vitreous cavity to inject a 1 µl bolus of AAQ (80 mM in a saline solution containing 40% DMSO).

Videos of pupillary light responses of mice were recorded before and 3 hours after AAQ injection. White light was derived from halogen dissecting lamp, and intensity was controlled with neutral density filters. Animals were dark-adapted for at least 20 minutes prior to testing. An infrared CCD camera (focused 15 cm from the objective) was used to measure pupil dilation, as described[128].

Locomotory Light Avoidance
Wildtype or *opn4*$^{-/-}$ *rd/rd* mice injected with 80 mM AAQ were dark adapted and placed into a transparent tube. The tube was illuminated with invisible infrared light and mouse movement was recorded with an infrared video camera in darkness and stored for offline analysis. The face of the mouse was illuminated continuously with 385 nm light (log IR 15.7) and at 5 sec intervals flashes of 480 nm light (log IR 15.2) were superimposed. For each mouse we recorded position in the tube pre-injection, and 2 and 24 hours post-injection. Analysis was conducted with an automated image-analysis software. Light avoidance behaviors were determined as rapid aversive movements within 30 seconds of the light stimulus or the beginning of the dark trial.

Open-Field Test
Rd1 mice were placed in a 190 mm x 100 mm circular UV-transparent chamber. The chamber was surrounded by 6 panels of 380 nm LEDs (Roithner Laserteknik), providing uniform illumination with a light intensity of ~7 mW/cm^2 .

The mice were dark adapted in their cages for 1 hr, prior to each experiment. The mice were placed in the experimental chamber and allowed to acclimate for 5 minutes. The behavior was then recorded using an IR sensitive video camera (Logitech C310) for 5 minutes in darkness under IR illumination. After 5 minutes, the chamber was illuminated by the 380 nm LEDs, and behavior was monitored for an additional 5 minutes. The apparatus was cleaned and thoroughly dried prior to each experiment.

After the open-field test, each mouse was given an intravitreal injection of AAQ (20 mM AAQ, 9:1 saline: DMSO), as previously described. The mice were allowed to recover for ~6 hours on a heating pad with open access to food and water in their cage located in the dark room. The behavioral protocol described above was repeated to determine the effect of AAQ. The videos were analyzed utilizing motion tracking video analysis software (Tracker) in order to quantify the average velocity of the mice, the trajectory of motion throughout the test, and the total distance traveled. The animals were then immediately sacrificed and MEA recordings were conducted from their retinas.

Data analysis and statistics
Light-elicited changes in firing rate during test flashes were normalized with respect to initial firing rate and expressed as a Photoswitch Index (PI), defined as follows: PI = (test firing rate – initial firing rate) / (test firing rate + initial firing rate).

Relative pupillary light responses were calculated as 1 - (pupil area minimum during thirty seconds of the light stimulus) / (pupil area minimum during five seconds preceding the stimulus). Relative response data for wild type and *opn4-/- rd/rd* mice were fitted with a three parameter Hill equation (SigmaPlot, Systat Software, Inc.). Data is mean ± s.e.m, unless otherwise indicated. The p-values for open field experiments were calculated using the two tailed unpaired Students T-test. Latencies were calculated for every cell with a PI greater than 0.011, the upper median confidence interval PI of our control experiments (n = 13 retinas; n = 409 cells). For each cell, cellular firing rate was averaged over the first two light periods (dark and 380nm light), with a 10 msec bin size. Cellular basal activity was defined as the upper median confidence interval firing rate in 500 nm light. Cellular latency was then calculated as the time difference between

the onset of 380 nm light and the first bin with a firing rate greater than the cell‟s basal activity. The median cellular latency was 45 msec (n = 10 retinas; n = 368 cells).

All statistics were performed using commercially available algorithms MATLAB (Mathworks). Distributions were first tested for normality using the Shapiro–Wilk test. For non-normal distributions, the Wilcoxon rank sum test was used for pairwise comparisons. The 95% confidence intervals for medians were generated by resampling the original distributions and applying the bias-corrected percentile method[129]. Results with $p < 0.05$ were considered significant.

For all box plots, box limits represent the 25th and 75th percentile, respectively. The red line represents the median and whiskers denote 1.5 times the interquartile range from the limits of the box. Outliers are marked by red + signs.

Supplemental Information

Figure S1

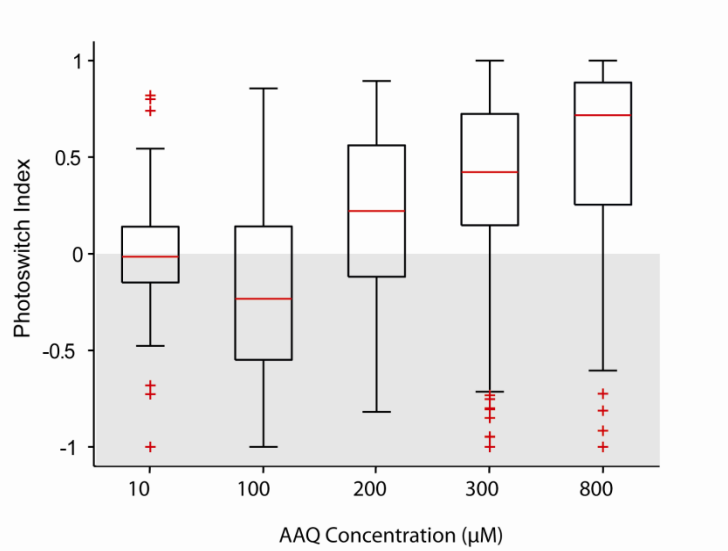

Figure S1, Related to Figure 1: Concentration-dependence of AAQ photosensitization of *rd1* retinas. See **Table S1** for values. Whiskers denote 1.5 times the interquartile range from the 25th and 75th percentile.

Table S1, Related to Figure S1.

Concentration (μM)	# Cells	Median PI	95% Confidence Interval
10	128 (3 retinas)	-0.016	-0.043 to 0.015
100	37 (2 retinas)	-0.233	-0.725 to 0.258
200	38 (1 retina)	0.221	-0.197 to 0.640
300	1025 (21 retinas)	0.423	0.394 to 0.457
800	359 (5 retinas)	0.717	0.627 to 0.762

Figure S2

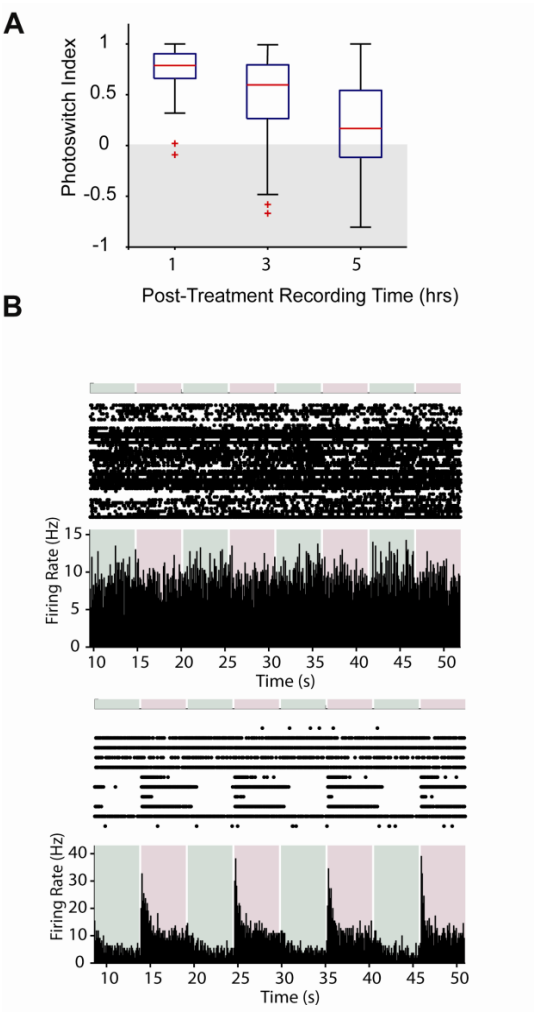

Figure S2, Related to Figure 1. AAQ photosensitization abates slowly after treatment

(**A**) Decay of photosensitization following *ex vivo* treatment of *rd1* retinas. See **Table S2** for values. Whiskers denote 1.5 times the interquartile range from the 25th and 75th percentile.
(**B**) Examples of MEA recordings obtained 12 hrs after intravitreal injection of AAQ *in vivo*.

Table S2, Related to Figure S2.

Time after treatment (hrs)	# Cells	Median PI	95% Confidence Interval
1	51 (1 retina)	0.787	0.728 to 0.841
3	61 (1 retina)	0.597	0.457 to 0.678
5	66 (1 retina)	0.167	-0.314 to 0.649

Figure S3

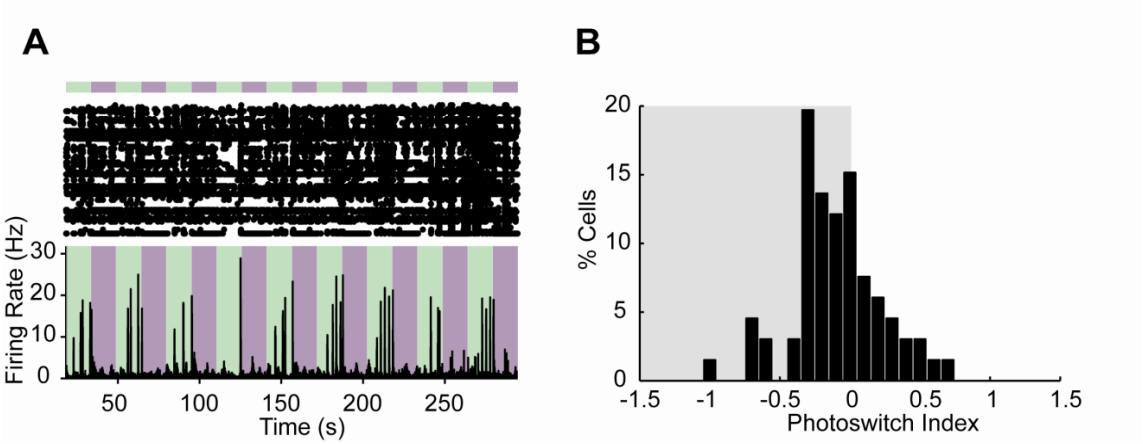

Figure S3, Related to Figure 2. Blocking retinal synapses greatly reduces AAQ photosensitization

(**A**) Top, raster plot of spiking from RGCs; bottom, average RGC firing rate calculated in 100 msec time bins. Color bars represent illumination with 380 nm (violet) or 500 nm light (green). Stimulation of RGC firing in an AAQ treated retina with D-APV, Curare, DNQX, Strychnine, Gabazine, and TPMPA.
(**B**) Analysis of photoswitching of the entire population of RGCs (n = 66) from one treated retina. PI median was -0.063 (95% CI: -0.384 to 0.258).

Figure S4

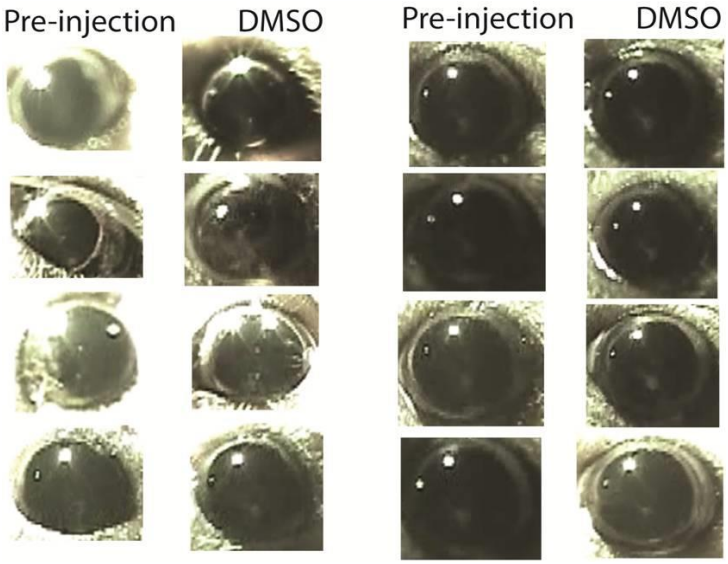

Figure S4, related to Figure 5. Sham injection does not restore the PLR

Sham injection into the eyes of rd/rd;opn4-/- mice with vehicle alone (40% DMSO in saline) did not restore pupillary constriction in response to light. Left panels show pupils in the light, right panels show pupils in the dark.

Movie S1, Related to Figure 5: Intraocular injection of AAQ restores the pupillary light response in mice lacking all retinal photoreceptors.

Exposure to a 30 s flash of white light induced a pupillary constriction in the AAQ-treated eye (right), but not in the untreated eye (left). Movie was recorded 3 hours after intravitreal injection of AAQ (1 μl of 80 mM in DMSO). For movie, see online version of article at: http://www.sciencedirect.com/science/article/pii/S0896627312004886.

Movie S2, **Related to Figure 7: Mice do not respond to 380 nm light in the open field prior to AAQ.**

Movie of a blind mouse before bilateral AAQ injection in the open field test. The mouse was recorded for 5 minutes in darkness immediately followed by a 5 minute recording in 380 nm light. The mouse continues to explore the chamber after it has been illuminated. For movie, see online version of article at:
http://www.sciencedirect.com/science/article/pii/S0896627312004886.

Movie S3, Related to Figure 7. **AAQ restores the light response of mice in the open field.**

Movie of a blind mouse after bilateral AAQ injection in the open field test. The mouse was recorded for 5 minutes in darkness followed immediately by a 5 minute recording in 380 nm light. After the application of AAQ, the mouse shows a dramatic decrease in exploratory

behavior of the test area in 380 nm light compared to in darkness. For movie, see online version of article at: http://www.sciencedirect.com/science/article/pii/S0896627312004886.

Supplemental Experimental Procedures

Animals

Wild-type mice (C57BL/6J strain, Jackson Laboratories) and homozygous *rd1* mice (C3H/HeJ strain, Charles River Laboratories) >3 months old were used for the experiments. *Opn4-/-* and *Opn4-/- rd/rd* mice were a gift of Satchidananda Panda and John Hogenesch. Mutant genotypes were confirmed by PCR of genomic DNA. *Opn4-/- rd/rd* animals were >3 months old and had no pupillary light reflex before treamtne . All animal use procedures were approved by the UC Berkeley or University of Washington Institutional Animal Care and Use Committee, and were in accord with guidelines from the Association of Vision Research in Ophthalmology and the NIH.

Electrophysiology and pharmacology

To block synaptic contributions of different retinal neurons to RGCs, the following neurotransmitter receptor antagonists were used: 4 μM SR-95531 (gabazine) for $GABA_A$ receptors, 10 μM 1,2,5,6 tetrahydropyridin-4-yl)methylphosphinic acid (TPMPA) for $GABA_C$ receptors, 10 μM initroquinoxaline-2,3-dione disodium salt (DNQX) for non-NMDA type glutamate receptors, 50 μM d-(-)-2-Amino-5-phosphonopentanoic acid (AP5) for NMDA-type glutamate receptors, 10 μM strychnine for glycine receptors, 50 μM d-tubocurarine chloride (curare) for nicotinic acetylcholine receptors. To block voltage-gated Na^+ channels we used 1 μM tetrodotoxin (TTX). All of these drugs were purchased from Sigma or Tocris.

Chapter 3: Restoring vision to blind mice with a photoswitch that acts selectively on degenerated retina

The data presented below will be published in the following article which is reprinted in full with permission:

Tochitsky I., Polosukhina A., Degtyar V., Gallerani N., Friedman A., Van Gelder R., Trauner D., Kaufer D., Kramer R.H. "Restoring visual function to blind mice with a photoswitch that exploits electrophysiological remodeling of retinal ganglion cells". *Neuron* 2014.

Author contribution

I.T. and R.H.K. designed the experiments. I.T. and V.D. performed physiological experiments. A.P. and N.G. performed histological experiments. I.T., A.F. and D.K. performed behavioral experiments. D.T. synthesized photoswitch compounds. I.T. and R.H.K. wrote the manuscript. R.H.K. supervised the project.

Abstract

Retinitis pigmentosa (RP) and age-related macular degeneration (AMD) are blinding diseases caused by the degeneration of rods and cones, leaving the remainder of the visual system unable to respond to light. Here we report a chemical photoswitch named DENAQ that restores retinal responses to white light of intensity similar to ordinary daylight. A single intraocular injection of DENAQ photosensitizes the retina for days, restoring electrophysiological and behavioral responses with no toxicity. Experiments on mouse strains with functional, non-functional, or degenerated rods and cones show that DENAQ is effective only in retinas with degenerated photoreceptors. DENAQ confers light sensitivity on a hyperpolarization-activated inward current that is enhanced in degenerated retina, enabling optical control of retinal ganglion cell firing. The acceptable light sensitivity, favorable spectral sensitivity, and selective targeting to diseased tissue make DENAQ a prime drug candidate for vision restoration in patients with end-stage RP and AMD.

Introduction

Degenerative retinal diseases including AMD and RP affect millions of people around the world. At present, there are no effective treatments to prevent the progressive degeneration of rod and cone photoreceptors that characterizes these disorders. Without a means for restoring photoreception, patients with advanced RP face the prospect of irreversible blindness. Several technologies are being developed to confer information about the visual world to the retinal neurons that survive after the rods and cones have degenerated. Surgically implanted electronic retinal prosthetics can electrically stimulate RGC firing[130], restoring some visual perception to blind humans[130]. Transplantation of stem cell-derived photoreceptor progenitors can improve visual function in patients with RP[131]. Viral expression of microbial opsins[79,91,104] or other optogenetic tools[93] can restore visual responses to strains of blind mouse that serve as animal models of RP. All of these strategies have shown promise for restoring visual function, but they are either invasive (i.e. implantation of electronic chips) or irreversible (i.e. transplantation of photoreceptor progenitors or viral expression of optogenetic tools). The potential permanence of stem cell or gene therapies could be a benefit if complications are absent, but the possibility of irreversible adverse effects makes these interventions risky to implement in humans.

We recently introduced another strategy for restoring visual function: adding a synthetic small molecule ‘‘photoswitch’’ to confer light sensitivity onto retinal neurons without involving exogenous gene expression. We showed that a photoswitchable K^+ channel blocker named AAQ could bestow light responses onto RGCs and restore light-elicited behavior in blind mice *in vivo*[132]. As a small drug-like molecule, AAQ has some advantages over the other approaches for vision restoration. Unlike microbial opsin or stem cell-based therapies, the effect of AAQ is reversible, allowing the dosage to be adjusted to maximize efficacy and minimize toxicity. Furthermore, photoswitch compounds diffuse freely and photosensitize neurons throughout the entire retina. This ensures broader coverage and higher spatial resolution than a retinal implant, which covers only a small area of the retina with stimulating electrodes that are spaced further apart than the packing density of RGCs.

Unfortunately, several properties of AAQ limit its potential for therapeutic development. AAQ requires high intensity, UV light and dissipates from the eye within a day after intravitreal injection. The human lens filters out most UV light[133] and repeated exposure to high intensity light can be damaging[134]. AAQ’s short half-life would necessitate daily injections of the compound into the eye, a delivery schedule unsuitable for long-term treatment. Furthermore, AAQ contains a reactive acrylamide moiety and its toxicity *in vivo* is unknown. In an attempt to overcome these shortcomings we have turned to a red-shifted K^+ channel photoswitch, which exhibits *trans* to *cis* photoisomerization with visible light (450-550 nm) and which relaxes rapidly to the *trans* configuration in the dark[48].

Results

DENAQ restores photopic light responses to the degenerating mouse retina.

DENAQ is a red-shifted photoswitch compound (Figure 1A) that confers light sensitivity on voltage-gated ion channels[48]. We tested the action of DENAQ on the retinas of 3-6 month old *rd1* mice, which lose nearly all rods and cones within 1 month after birth[101]. We measured the effect of light on action potential firing by RGCs recorded with an extracellular multi-electrode array (MEA). Before photoswitch application, light caused no significant change in firing rate (Figure 1B). Treatment with 300 µM DENAQ for 30 min photosensitized the retina, such that nearly all RGCs responded to the onset of a 15 sec light flash with an increase in firing rate (Figure 1C). On average, DENAQ-treated RGCs generated a significant firing rate increase within ~20 msec of light onset ($p<0.05$), reaching their peak firing within 400 msec. Thereafter, the firing frequency declined during the flash. Azobenzene photoswitches reach a stable photostationary state with sustained illumination[135], so the decline in firing is likely a consequence of spike frequency adaptation intrinsic to RGCs rather than to photochemical properties of DENAQ. At light offset, the average firing rate across all units returned to baseline within ~600 msec, but >20% of units recovered within 100 msec. The decay of the DENAQ-mediated response at light offset is dependent on fast *cis* to *trans* relaxation[48], in contrast to AAQ, which persists in the *cis* state for >10 minutes and needs to be reset with green light[100].

We next examined the spectral sensitivity of DENAQ-mediated photosensitization of the *rd1* retina. A wide range of wavelengths between ~400 to ~550 nm, can elicit the light response, with blue-green light (480-500 nm) being most effective in the visible range (Figure 1D). The action spectrum of retinal photosensitization closely matches the absorption spectrum of *trans*-DENAQ in solution[48]. Stimulation with broad spectrum white light is also effective. To quantify the degree of photosensitization for each RGC we calculated the Light Response Index (LRI) (previously designated the "photoswitch index"[132]). The LRI is the normalized change in average firing rate upon switching from darkness to white light. RGCs from untreated *rd1* retinas showed no detectable light response (median LRI=0, n=12 retinas); while nearly all RGCs treated with DENAQ were activated by white light (median LRI=0.42, n=12 retinas, $p<0.001$, rank sum test) (Figure 1E). For every untreated retina studied, light caused no significant change in firing rate (n=12, p=0.94) (Figure 1F), while for every DENAQ-treated retina, light elicited a significant increase in firing rate (mean increase=2.4-fold, n=12, $p<0.001$) (Figure 1G).

The light intensity threshold for triggering RGC firing was $4x10^{13}$ photons/cm^2/sec for DENAQ (Figure 2A). More RGCs could be recruited to respond by increasing intensity, with ~1 log unit above threshold ($3x10^{14}$ photons/cm^2/sec) needed to generate a response in >50% of RGCs (Figure 2B). For comparison, the thresholds for responses mediated by AAQ[132], ChR2 expressed in RGCs[104] and halorhodopsin (NpHR) expressed in remnant cones[79] were $4x10^{15}$, $1x10^{14}$, and $2x10^{14}$ photons/cm^2/sec, respectively. Thus, the sensitivity of DENAQ-treated retinas is as high, if not higher, than that of retinas expressing these microbial optogenetic tools. New optogenetic tools with improved light sensitivity[136] are available, but have not yet been tested for vision restoration.

Figure 1

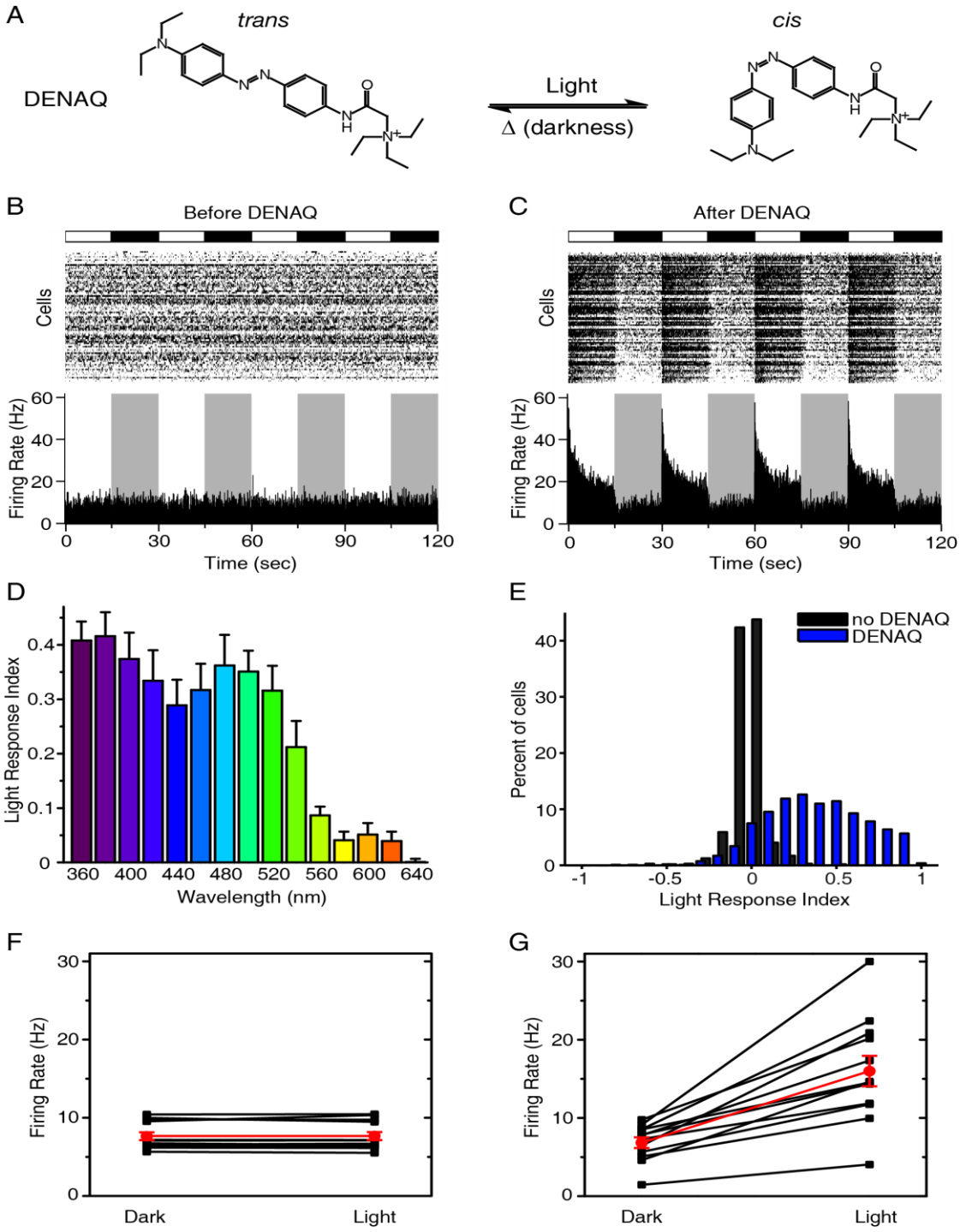

Figure 1. The red-shifted photoswitch DENAQ restores light responses to blind retinas from *rd1* mice.

(**A**) Molecular structure of DENAQ. Light converts DENAQ from the *trans* to the *cis* form, and the compound relaxes back to the *trans* form in the dark.
(**B-C**) MEA recording from an *rd1* retina before DENAQ treatment (**B**) and after treatment with 300μM DENAQ (**C**). Light (white) and dark (black/gray) episodes are shown.
(**D**) Spectral sensitivity of the DENAQ-mediated light response.
(**E**) LRI value distributions for RGCs from untreated (black) (median LRI=0, n=12 retinas) and DENAQ-treated (blue) *rd1* retinas (median LRI=0.42, n=12 retinas, $p<0.001$, rank sum test).
(**F-G**) DENAQ restored light responses in every retina tested. Mean RGC firing rate for each retina in light and darkness before (n=12 retinas, $p=0.94$) (**F**) and after DENAQ treatment (n=12 retinas, $p<0.001$) (**G**). Mean±SEM values are shown in red.

Figure 2

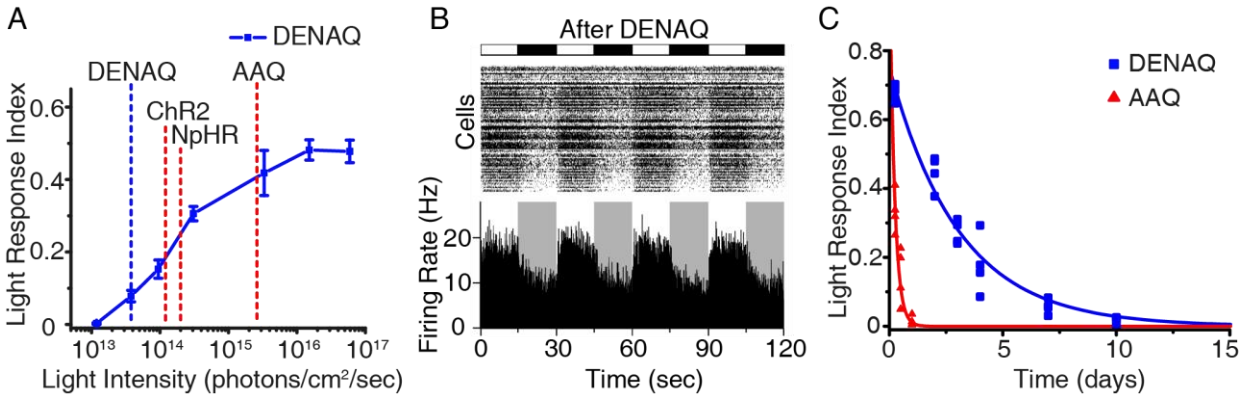

Figure 2. Intensity requirements for restoring light responses and persistence of the red-shifted photoswitches in the eye.

(**A**) Light intensity vs. response curves for DENAQ (n=5 retinas). Data are mean±SEM. Labeled dotted lines represent the thresholds for activation of DENAQ (blue), ChR2[104] (red), NpHR[79] (red) and AAQ[132] (red) in the retina.
(**B**) MEA recording from a DENAQ-treated *rd1* retina stimulated with moderate intensity ($3x10^{14}$ photons/cm^2/sec) white light. Light (white) and dark (black/gray) episodes are shown.
(**C**) Persistence of photosensitization elicited by *in vivo* injection of AAQ (red, half-life=3.6 hours) and DENAQ (blue, half-life=2.1 days). Responses were measured on the MEA *ex vivo*, hours to days after *in vivo* injection of 2 µL of 20mM photoswitch (n=4 retinas per time point). Photoswitch half-life was calculated by fitting the data with a monoexponential decay function.

Photosensitivity can also be conferred to the *rd1* retina by injecting DENAQ into the vitreous cavity of eye *in vivo*. MEA recordings at later times after injection showed that DENAQ photosensitization persists for several days (half-life=2.1 days), in contrast to AAQ, which dissipates within 12 hours after intravitreal injection (half-life=3.6 hours) (Figure 2C). The relative lifetime of the compounds in the eye mirrors their relative lipophilicity, with the more hydrophobic DENAQ persisting longer than AAQ.

We characterized the receptive field properties of DENAQ-treated RGCs. Stimulation of the retina with a small spot of light resulted in an increase in activity in stimulated RGCs (median LRI=0.45, n=16 cells), but the surrounding unilluminated RGCs showing no change in firing rate (median LRI=-0.01, n=741 cells, $p<0.001$, rank sum test) (Figures 3A, 3B and Table S1). Since only targeted neurons near a single electrode showed a light response and since individual RGCs are detected by only one electrode on the MEA (which are spaced 200 μm apart), we can estimate that the DENAQ-mediated RGC collecting area is at most ~200 μm in diameter. Indeed, as we stimulated RGCs with expanding spots of light, the response increased with larger spot size and saturated at an average spot diameter of 240 μm (Figure 3C). No further increase in the light response was observed with spot size greater than 240 μm or full-field stimulation. The estimated receptive field size of DENAQ-treated RGCs matches previous measurements of mouse RGC dendritic fields, which average ~200 μm in diameter[137]. Stimulation with small, 30 μm diameter light spots was sufficient to drive RGC activity, suggesting that neighboring RGCs could, in principle, be manipulated independently with a precise stimulus, offering a basis for high-acuity vision. The receptive field properties are different in AAQ-treated retina, because chemical photosensitization extends to inhibitory amacrine cells, leading to an antagonistic center-surround response in RGCs[132].

DENAQ selectively photosensitizes retinas with degenerated rods and cones

Photoreceptor degeneration in RP progresses from the peripheral to the central retina, which in some patients, can remain disease-free for years[111]. In AMD, the pattern is reversed, with photoreceptor degeneration largely restricted to the central retina[138]. For any technology that restores photosensitivity, it would be preferable if the treatment selectively acted on diseased retinal regions while sparing healthy tissue. To assess the actions of photoswitch compounds on healthy and diseased retina, we compared the effects of DENAQ in wild-type (WT) vs. *rd1* retinas. The light stimulus parameters were the same as those shown in Figure 1. The WT retina is naturally sensitive to light, so not surprisingly almost all RGCs exhibited strong light responses with light-onset triggering an increase in firing in some neurons (ON-RGCs) and a decrease in others (OFF-RGCs) (Figure 4A). However, it was surprising to find that DENAQ treatment caused no change in the light response of the WT retina, with no difference in the number of RGCs generating On vs. Off responses (Figure 4B). To quantify this comparison, we calculated for each RGC the Peak Light Response Index (PLRI), which represents the normalized change in peak firing rate upon switching from darkness to light. Plotting the PLRI for each RGC reveals the distribution of neurons exhibiting primarily On- vs. Off- behavior (Figure 4C). We found no significant difference in the PLRI distribution before and after DENAQ treatment (n=6 retinas, $p=0.34$, rank sum test). Hence, at least according to this measure, DENAQ has no effect on the response properties of the wild-type retina, in stark contrast to its effect on the *rd1* retina.

Figure 3

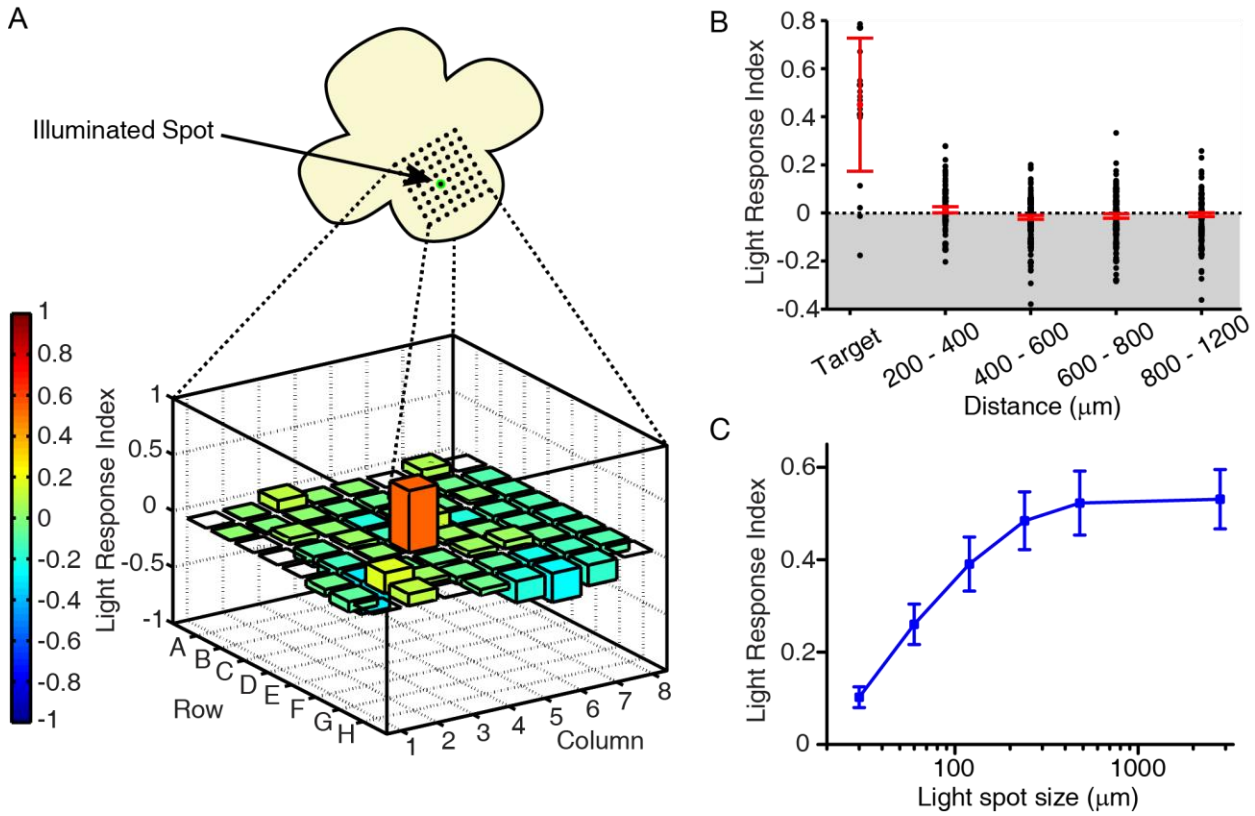

Figure 3. The DENAQ-Treated *rd1* Retina Generates Spatially Precise Light Responses.

(**A**) Targeted illumination of a portion of an *rd1* retina centered on a single MEA electrode (top). Electrode E4 was stimulated with a 60 μm diameter light spot. Only the targeted electrode recorded a large increase in RGC firing in response to white light (bottom). PI values are color-coded (scale at left) and also represented by bar height. The orange bar is electrode E4. Empty squares are electrodes on which no action potentials were recorded.
(**B**) Targeted illumination elicits an increase in activity in stimulated RGCs and has no effect on surrounding RGCs (n = 16 cells and n = 741 cells, respectively, from seven retinas). LRI values of RGCs (black circles) as a function of distance from the target electrode, displayed in 200 μm bins. The red diamonds indicate the median plus or minus the 95% confidence intervals. See Supplemental Table S1 for values.
(**C**) Responses of DENAQ-treated *rd1* RGCs to stimulation with spots of light of increasing diameter. Data are mean±SEM, n=20 cells.

Figure 4

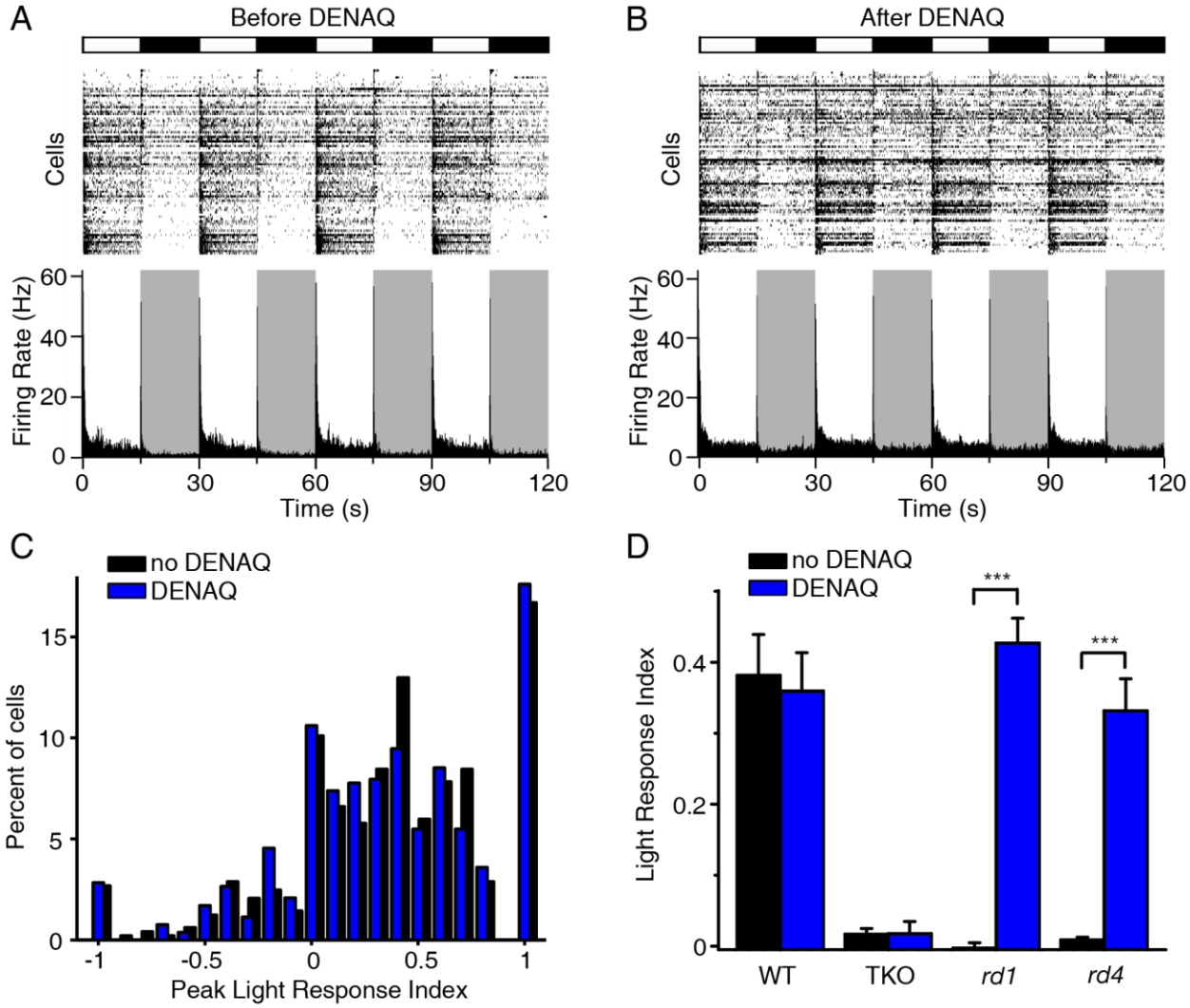

Figure 4. DENAQ only photosensitizes retinas in which rod and cone photoreceptors have degenerated.

(**A-B**) MEA recording from a WT retina before (**A**) and after (**B**) treatment with 300µM DENAQ. Light (white) and dark (black/gray) episodes are shown.
(**C**) RGC PLRI values for WT retinas before (black) and after (blue) DENAQ treatment (n=6 retinas, p=0.34, rank sum test).
(**D**) Light responses of untreated and DENAQ-treated WT (n=6, p=0.72), TKO (n=6, p=0.97), *rd1* (n=12, p<0.001) and *rd4* retinas (n=6, p<0.001). Mean PLRI values are shown for WT retinas and mean LRI values for TKO, *rd1* and *rd4* retinas. Data are mean±SEM.

The *rd1* retina differs from the WT retina in several ways. Not only have the rods and cones degenerated, which leads to changes in growth factor release[139], but the neural circuitry of the retina no longer processes light-driven signals, which leads to homeostatic changes in synaptic transmission and neuronal excitability[74]. To test whether the loss of light-driven signals is sufficient for enabling DENAQ photosensitization, we tested DENAQ on retinas from a triple knockout mouse (TKO) (tra$^{-/-}$ cnga3$^{-/-}$ opn4$^{-/-}$). The TKO mouse has the normal complement of structurally intact rods and cones, but light responsiveness in these cells has been impaired because of the loss of essential phototransduction proteins[140]. Also lacking is melanopsin, the photopigment of intrinsically photosensitive RGCs. As expected, TKO retinas did not respond to white light stimulation. But the retinas remained unresponsive even after DENAQ treatment (n=6 retinas, p=0.21, rank sum test) (Figure 4D). The lack of photosensitization suggests that the mere presence of intact photoreceptors, even if they are not light-sensitive, is sufficient to prevent DENAQ action.

We further tested the role of rod and cone degeneration in DENAQ photosensitization, by evaluating the effectiveness of the photoswitch in a different mouse model of RP. *Rd4* mouse have a null mutation in rod transducin[141], whereas *rd1* mice suffer from a null mutation in rod phosphodiesterase[142]. The rods and cones degenerate soon after birth in both of these mouse strains, leading to complete blindness by 6 weeks of age[101,143]. As expected, untreated retinas from 3-6 month old *rd4* mice did not generate a light response, but DENAQ treatment did confer robust light responses (n=6 retinas, p<0.001, rank sum test) (Figure 4D), just like in the *rd1* retina. Thus, it seems that rod and cone degeneration itself, and not any particular mutation, is what enables DENAQ photosensitization.

Mechanism of degeneration-specific photosensitization by DENAQ

In animal models of RP, degeneration of rods and cones leads to an increase in the spontaneous firing rate of RGCs[144,145]. The mechanism of this electrophysiological remodeling is unknown, but at least part of the hyperactivity is intrinsic to the RGCs themselves[145]. To test whether RGCs are a target for DENAQ in degenerating retina, we applied a cocktail of neurotransmitter antagonists onto DENAQ-treated retinas to block glutamate, GABA, acetylcholine and glycine-mediated synaptic transmission. Under these conditions, RGCs continued to generate an increase in firing frequency in response to light (mean LRI=0.70, n=8 retinas) (Figures 5A and 5C). In fact, rather than being reduced by synaptic blockade, the light response of RGCs was increased, mainly due to a reduction in spontaneous firing in the dark. Similar results were obtained from RGCs in DENAQ-treated *rd4* retina, which also continued to show light responses after synaptic blockade (mean LRI=0.43, n=6 retinas) (Figure 5C). Control experiments showed that the cocktail completely eliminated light-elicited changes in RGC firing mediated by normal rod and cone phototransduction in WT retina (Figure S1), confirming that blockade of retinal synaptic transmission was effective[146].

Figure 5

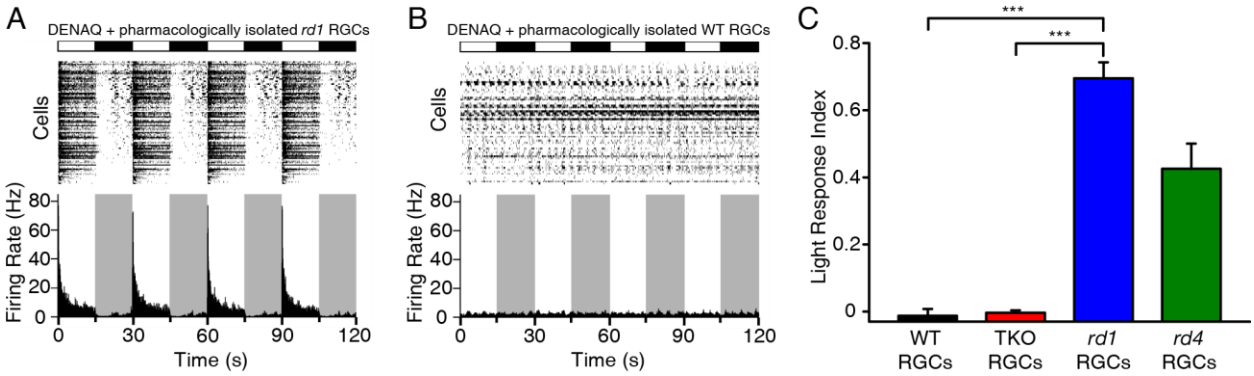

Figure 5. DENAQ selectively photosensitizes RGCs from retinas with degenerated photoreceptors.

(**A-B**) MEA recording from pharmacologically isolated *rd1* (**A**) and WT (**B**) RGCs.
(**C**) Light responses of pharmacologically isolated WT retinas (mean LRI=-0.01, n=10 retinas, $p<0.001$), TKO retinas (mean LRI=0, n=6 retinas, $p<0.001$), *rd1* retinas (mean LRI=0.70, n=8 retinas) and *rd4* retinas (mean LRI=0.43, n=6 retinas).

In contrast to its effects on degenerating retina, DENAQ failed to photosensitize pharmacologically-isolated RGCs in WT retinas (mean LRI=-0.01, n=10 retinas) (Figures 5A and 5C) and in retinas from TKO mice (mean LRI=0, n=6 retinas) (Figure 5C). Hence, while RGCs from degenerated retinas are strongly photosensitized by DENAQ, RGCs from intact retinas are DENAQ-insensitive. These results indicate that the primary cellular locus for DENAQ photosensitization is the RGC. This is different from AAQ photosensitization, which is mediated primarily by amacrine cells[132].

We explored differences between *rd1* and WT retinas that might account for degeneration-specific DENAQ photosensitization. It seemed possible that DENAQ might have greater access to RGCs in degenerating retina, perhaps due to changes in the integrity or permeability of the inner limiting membrane (ILM) or outer limiting membrane (OLM). To test whether the ILM or OLM act as a barrier to prevent DENAQ photosensitization, we disrupted both membranes in the WT retina with a series of transverse cuts made by a sharp razor blade. Subsequent DENAQ treatment of these retinal slices failed to produce any photosensitization (mean LRI=0.03, n=6 retinas, p=0.62) (Figure S2). This experiment indicates that poor accessibility cannot account for the DENAQ-insensitivity of the WT retina.

Since DENAQ access is not the issue, perhaps the selectivity of DENAQ for the degenerating retina is caused by a change in conductances photosensitized by DENAQ. To compare photosensitization of ionic conductances in WT and *rd1* RGCs, we obtained whole-cell patch clamp recordings after DENAQ treatment. We used the same cocktail of receptor antagonists to eliminate synaptic transmission, thereby revealing light-elicited effects on intrinsic conductances. Membrane potential was held at -60 mV and a series of test pulses from -100 mV to 0 mV were delivered to activate voltage-gated channels. Figures 6A-C compare the current-voltage relationships of representative WT and *rd1* RGCs, and Fig. 6D shows average data from all WT and *rd1* RGCs. In the RGC from the WT retina, light resulted in a small increase in the outward current elicited by depolarization above -40 mV, consistent with photoregulation of voltage-gated K^+ current (I_K) (Figures 6A, 6C and S3A). On average, light elicited a 15% increase in I_K (Figure 6D). However, light had no effect on ionic current near the resting potential (-70 mV) nor on the hyperpolarization-activated current, I_h, elicited by steps to -100 mV (Figures 6A, 6C, 6D, S3A).

In contrast, in the RGC from the *rd1* retina, DENAQ conferred light sensitivity on ion channels that were active at both depolarized and hyperpolarized membrane potentials (Figures 6B and 6C). At potentials positive to -40 mV, light resulted in an increase in I_K, not significantly different from the effect of DENAQ on WT RGCs (Figure 6D; mean increase=23%, p=0.2). However, unique to the *rd1* cell, light also increased I_h (Figures 6B, 6C and S3B). On average, light increased I_h by ~20% in 11 RGCs tested (Figure 6D; $p<0.001$). At membrane potentials below -50mV, light caused a steady inward current that would have depolarized the cell, if it was not voltage-clamped. The light-regulated current increased non-linearly between -50 mV and -100 mV, consistent with the properties of I_h described previously in many neurons, including RGCs[147,148]. A comparison of the light-elicited currents in WT and *rd1* RGCs (Figure 6D) shows that DENAQ only affects I_h in *rd1* RGCs. We propose that light-elicited enhancement of I_h is the primary cause of light-elicited RGC firing.

RGCs from *rd1* retina have a more depolarized average resting potential and a higher basal firing rate in darkness than RGCs from WT retinas (Figures 6A, 6B and [144]). We found that the current density of I_h is significantly larger in *rd1* RGCs (6.4 pA/pF) than in WT RGCs (2.9 pA/pF, $p<0.01$) (Figure 6E), consistent with enhanced excitability. However, the ~2-fold increase in current density seems insufficient to fully account for the dramatic difference in the light response, suggesting that there are additional differences in the properties of channels underlying I_h in *rd1* RGCs. I_K is slightly larger in *rd1* RGCs, but the difference from WT RGCs is not statistically significant ($p=0.3$).

To confirm that photosensitization of I_h mediates the DENAQ light response, we obtained MEA recordings from *rd1* retinas treated with three different I_h inhibitors. The light response was completely eliminated by ZD7288 (100 μM), a widely-used blocker of I_h[149]. However, this blocker reduced the basal firing rate of RGCs in darkness (Figure 6F) and is known to inhibit certain voltage-gated Na^+ channels[150]. Therefore we used two other blockers, ivabradine (50 μM) and cilobradine (50 μM), which are more specific for I_h[149] and do not noticeably decrease basal RGC activity (Figure 6F). Both of these drugs completely eliminated the DENAQ-mediated light response (Figures 6F and 6G). Similar results were obtained in DENAQ-treated retinas in the absence of synaptic blockers (Figure S4). Hence blockade of DENAQ-mediated photosensitization by I_h inhibitors is independent of changes in RGC excitability.

DENAQ is non-toxic

In order to assess the safety of DENAQ *in vivo*, we performed a histological analysis of WT retinas at 10 and 30 days post injection (DPI) of phosphate buffer saline (PBS) alone (sham) or PBS containing 5 mM DENAQ. No pathological changes were observed in either the DENAQ-injected or sham-injected retinas (Figure S5A). To determine whether DENAQ caused apoptosis of retinal neurons, we performed a TUNEL assay, which stains cells with nicked DNA, a marker of apoptosis[151]. Apoptotic cells were extremely rare (<0.2%) (Figures S5A and S5B) and did not significantly differ in number between DENAQ and sham injected retinas ($p_{10day}=0.16$, $p_{30day}=0.13$). In contrast, DNase I treated retinas displayed extensive apoptosis, with 70% of retinal neurons staining positive in the TUNEL assay (Figures S5A and S5B). There was no significant difference between sham and DENAQ treated retinas in the thickness of the outer nuclear layer ($p_{10day}=0.92$; $p_{30day}=0.77$) or the inner nuclear layer ($p_{10day}=0.39$, $p_{30day}=0.73$) (Figure S5C). Finally, there was no change RGC density (cells per 100 μm) in the central ($p=0.62$) or peripheral retina ($p=0.1$) (Figure S5D).

Figure 6

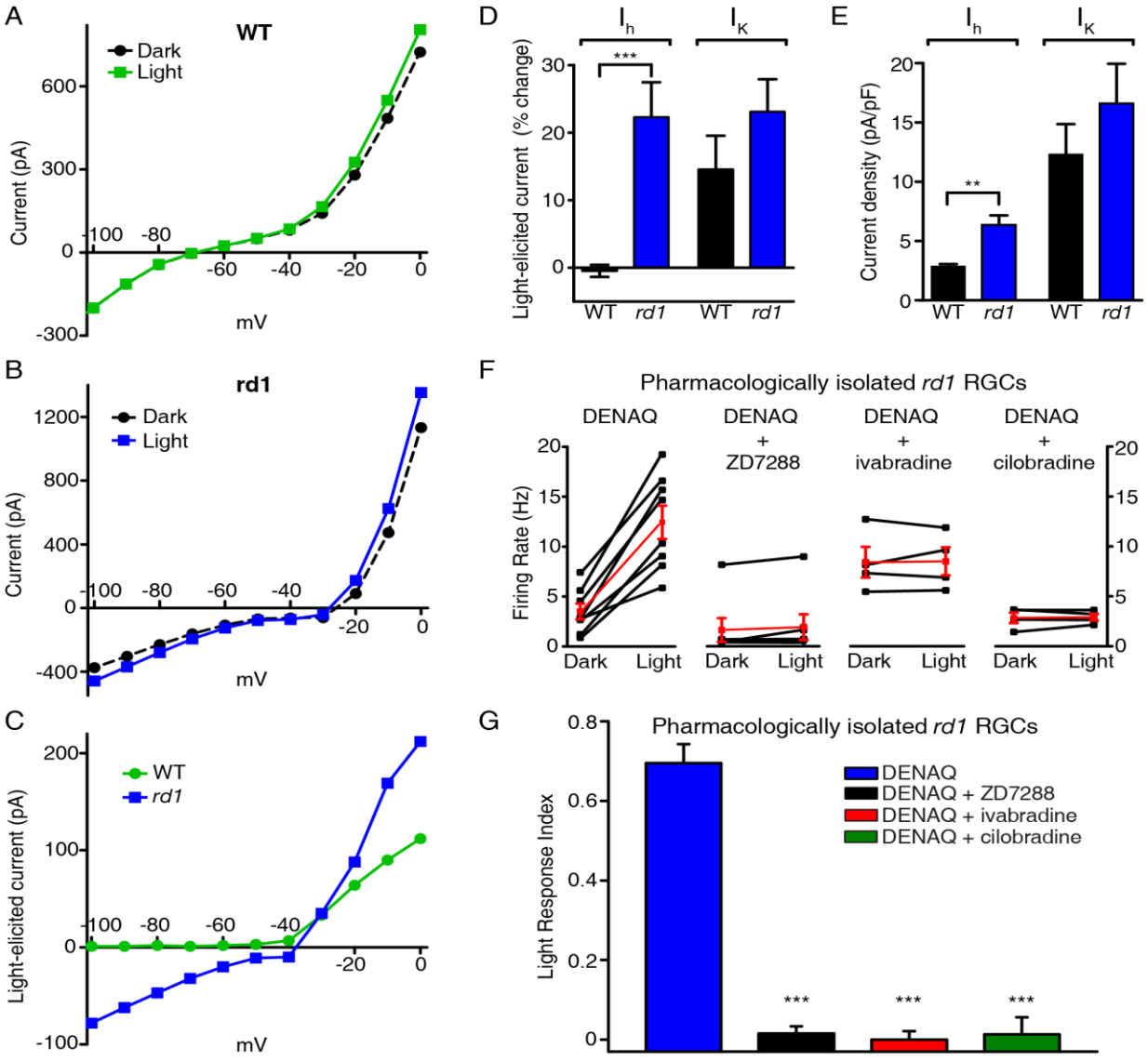

Figure 6. DENAQ selectively photosensitizes I_h in *rd1* but not WT RGCs.

(**A**) I-V curve from a typical WT RGC measured by voltage steps applied from Vh= -60 mV in 10mV increments either in the dark (black) or under 480nm light (green).
(**B**) I-V curve from a typical *rd1* RGC in the dark (black) or under 480nm light (blue).
(**C**) Light-elicited current, defined as difference between currents measured in light and dark in the WT RGC (from panel A) (green squares & line) and in the *rd1* RGC (from panel **B**).
(**D**) Light-elicited change in I_h (left), and in I_K (right) in WT RGCs (black) (n=11) and in *rd1* RGCs (blue) (n=9), shown as percent difference. I_h was photoregulated in *rd1* (mean=22%) RGCs, but not in WT RGCs (mean=-0.3, $p<0.001$). I_K is not differentially photosensitized (WT mean=15%, *rd1* mean=23%, p=0.2).

(**E**) I_h and I_K densities measured in WT (black) (n=7 cells) and *rd1* (blue) (n=13) RGCs. I_h density was significantly higher in *rd1* RGCs (mean=6.4 pA/pF) than in WT RGCs (mean=2.9 pA/pF, $p<0.01$). I_K density was not significantly different (WT mean=12.3 pA/pF, *rd1* mean=16.6 pA/pF, p=0.3).
(**F**) Firing rate in light and in the dark of DENAQ-treated *rd1* RGCs (n=8 retinas, mean firing rate increase (MFRI) = 3.5x, $p<0.001$) (left) and DENAQ-treated *rd1* RGCs subsequently treated with I_h blockers - 100μM ZD7288 (n=7 retinas, MFRI=1.18, p=0.38) (second from left), 50μM ivabradine (n=4 retinas, MFRI=1.01, p=0.87) (second from right) and 50μM cilobradine (n=4 retinas, MFRI=1.02, p=0.81) (right). Mean±SEM firing rates are shown in red.
(**G**) Light response indices of DENAQ-treated *rd1* RGCs (mean LRI=0.7) (blue), and DENAQ-treated *rd1* RGCs treated with ZD7288 (mean LRI=0.02, $p<0.001$) (black), ivabradine (mean LRI=0, $p<0.001$) (red) and cilobradine (mean LRI=0.01, $p<0.001$). Data are mean±SEM.

DENAQ enables innate and learned behavioral light responses in blind mice.

We next evaluated the ability of DENAQ to restore light-elicited behavior *in vivo*. Blind *rd1* mice showed no difference in exploratory behavior during 5 minutes spent in green light versus 5 minutes in darkness in an open field locomotory assay (Figures 7A and 7B). Six hours after intravitreal injection of DENAQ, individual mice displayed an increase in locomotory activity in light as compared to darkness (Figures 7A and 7B). Before DENAQ treatment the average velocity of movement for 20 mice tested was the same in darkness as in light, whereas after treatment their movement was faster in light than darkness (Figure 7C). The greatest increase in exploratory behavior was observed in the first 100 seconds of the light (mean ratio=1.74, n=20, $p<0.001$) (Figure 7C) and then diminished at later time points, most likely due to habituation. This increase in light-elicited locomotion is consistent with previously reported results from *rd1* mice expressing ChR2 in ON-bipolar cells[91]. Sham injection of PBS produced no significant change in basal activity or relative activity in light versus darkness (n=6, p=0.88) (Figure 7C).

Whatever vision restoration technology is ultimately employed, regaining normal sensory perception, including visual object recognition, will almost certainly require learning. To test whether *rd1* mice can use the DENAQ-mediated light response as a stimulus for a learned behavior, we used a visual-cued fear conditioning assay. In normally sighted mice, this classical conditioning paradigm associates a light cue with an electric foot shock, such that subsequent exposure to the light stimulus alone elicits a learned fear response ("freezing" behavior)[150]. We used 3 groups of animals for these studies: WT mice and *rd1* mice injected with either DENAQ or sham at 6 hours before training. On day 1 (training day), we exposed animals to either paired (3 trials of 10 s light stimuli, each co-terminating with a 2 s shock) or unpaired stimuli (the same light and shock stimuli interleaved rather than overlapping). On day 2 (recall day), we presented the light stimulus alone (Figure 8A). Sample recall trial movement traces of individual sham-injected *rd1* mice (left, black), DENAQ-injected *rd1* mice (middle, blue) and WT mice (right, red), all of whom had been exposed to paired conditioning during day 1, are shown in Figure 8B. WT mice that had received paired stimuli showed a decrease in locomotor activity in response to light on recall day (n=10, $p<0.001$) (Figures 8B and 8C). In contrast, sham-injected *rd1* mice showed no change in locomotor activity in response to light (n=9, p=0.98) (Figures 8B and 8C). However, DENAQ-injected *rd1* mice that had received paired conditioning showed a decrease in locomotor activity (i.e. freezing) in response to light (n=10, $p<0.001$), to the same extent as conditioned WT mice (n=10, p=0.51) (Figures 8B and 8C). DENAQ-injected *rd1* mice that had received unpaired stimuli showed no change in locomotor activity in response to light. These results demonstrate that the light perception conferred by DENAQ allows for visual learning, first enabling mice to associate light with a fearful stimulus on day 1, and then mediating the recall of the memory on day 2.

Figure 7

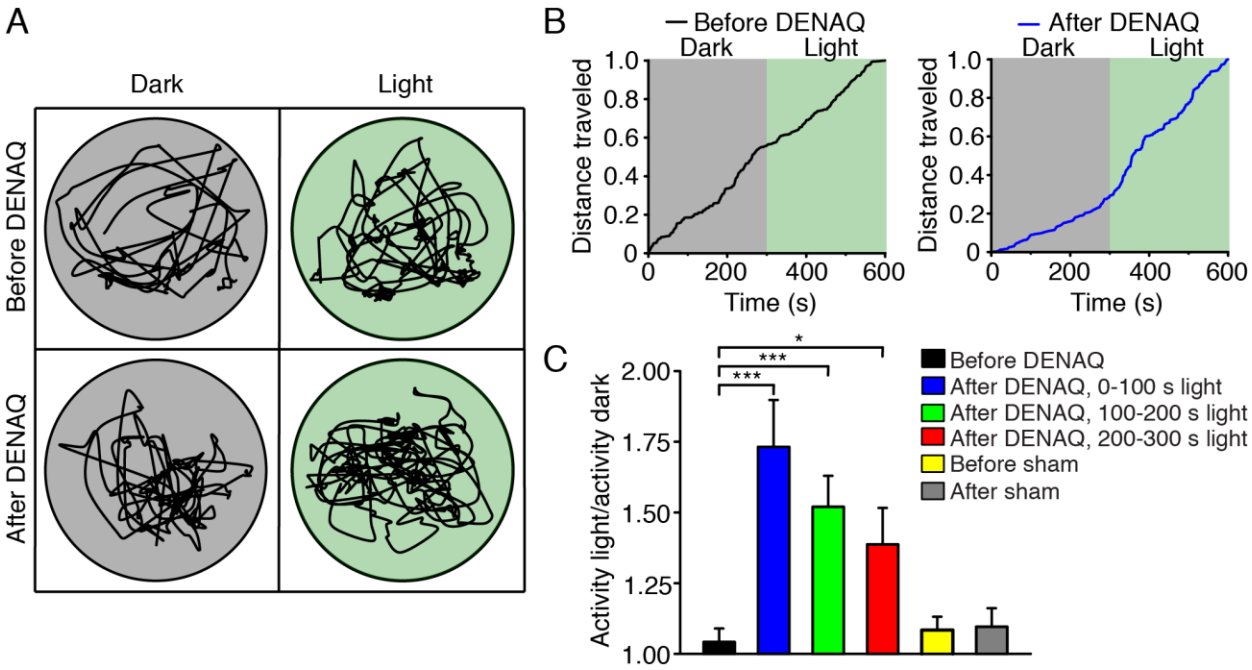

Figure 7. DENAQ restores light-modulated open-field locomotor behavior in blind mice.

(**A**) Movement trajectory of the same *rd1* mouse exploring an open cylindrical cage in the dark (gray) and under 500 nm light (green) before (top) and after (bottom) DENAQ injection.
(**B**) Cumulative distance traveled by an *rd1* mouse before (left) and after (right) DENAQ injection.
(**C**) Bar graph of activity in the light divided by activity in darkness before (black) (n=20 mice, mean=1.04) and after intravitreal injection of DENAQ and before (yellow) or after (gray) sham injection (n=6 mice, p=0.88). Activity ratios for the first 100 seconds of exploratory behavior of DENAQ-injected mice (blue) (mean =1.73, $p<0.001$), 100-200 seconds in the light (green) (mean=1.52, $p<0.001$) and the final 100 seconds in the light (red) (200-300 sec) (mean=1.39, $p<0.05$). The amount of exploratory activity decreased with time. Data are mean±SEM.

Figure 8

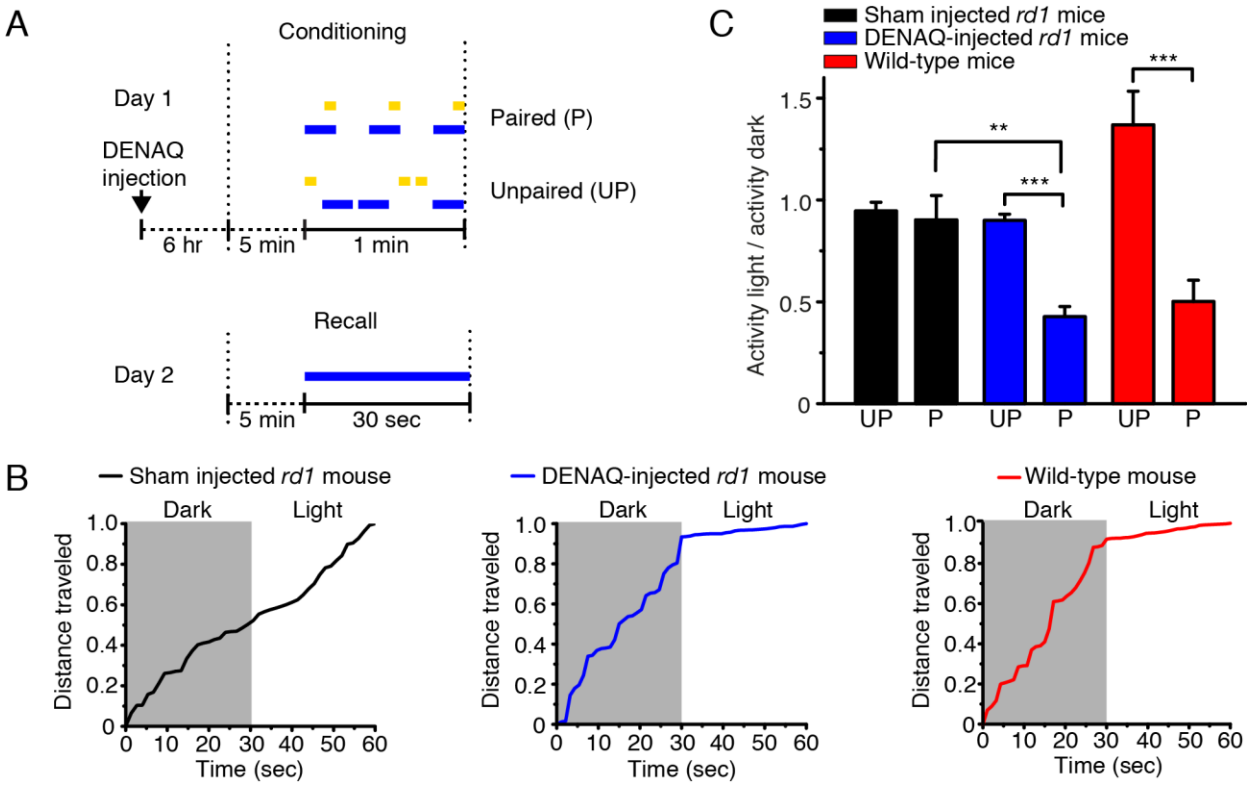

Figure 8. DENAQ enables visual learning in blind mice.

(**A**) Diagram of the paired, unpaired conditioning and recall protocols for the visual fear conditioning assay. Electric foot shock (yellow) and light flash (blue) episodes are shown.
(**B**) Cumulative distance traveled by a paired-conditioned sham-injected *rd1* mouse (left, black), a paired-conditioned DENAQ-injected *rd1* mouse (middle, blue) and a paired-conditioned WT mouse (right, red) in the 30 seconds of darkness preceding the light flash and the subsequent 30 seconds in the light during the recall trial.
(**C**) Bar graph of activity in light divided by activity in darkness for sham-injected *rd1* (n=9, p=0.71), DENAQ-injected *rd1* (n=10, p<0.001) and WT mice (n=10, p<0.001) during the recall trial. Data are mean±SEM.

Discussion

DENAQ as a potential treatment for degenerative blinding disease

DENAQ has none of the serious shortcomings exhibited by AAQ. DENAQ has a red-shifted absorbance spectrum and therefore photoisomerizes from *trans* to *cis* with light in the 400-550 nm range, instead of the UV light required by AAQ. DENAQ photosensitizes the blind *rd1* retina to moderately bright white light, similar in intensity to ordinary daylight. The compound lasts in the eye for days following a single intravitreal injection. TUNEL staining and histological analyses show no evidence of adverse effects on the mouse retina. These features make DENAQ a favorable photoswitch candidate for preclinical development as a potential therapeutic for human use. Additional studies will be needed to assess acute toxicity potential in large mammals having eyes that are structurally and functionally closer to humans. Both safety and efficacy of photosensitization can be assessed in several animal models of RP including blind strains of dogs[152] and pigs[153]. There are no suitable primate models of RP, but laser ablation of photoreceptors can generate local scotomas that have features in common with human blinding disease[154].

We delivered DENAQ *in vivo* by injecting it into the vitreous cavity of the eye. Intravitreal drug administration in humans has become commonplace. For example, anti-angiogenesis drugs for AMD are often administered in monthly injections[155], which have proven to be safe[156]. DENAQ persists in the eye for up to a week after a single injection. A slow release formulation involving biodegradable polymer encapsulation[122] may extend the release lifetime of DENAQ to enable less frequent treatments (perhaps monthly) to sustain photosensitization.

Nonetheless, the transient nature of DENAQ photosensitization could be advantageous for minimizing possible adverse effects. The impermanence would allow for adjustment of dosage in individual patients to optimize vision restoration outcomes. In addition to potentially restoring visual function to end-stage RP patients with no light perception, DENAQ might be useful for enhancing visual performance in low vision patients with advanced RP or AMD. Moreover, acute RGC photosensitization with DENAQ might be useful for evaluating the functional integrity of the visual system in the brain before employing more permanent therapies, such as retinal implants.

Our results demonstrate that DENAQ can restore innate and learned visual behavioral responses in blind mice. We do not know whether these mice are capable of visually recognizing objects, but object recognition has not yet been demonstrated for any vision restoration technology implemented in blind mice. It is likely that whatever technology is used, training will lead to improvement in visual performance over time. Object recognition in human RP patients receiving a retinal implant improves dramatically with training[77], similar to the progressive improvement of hearing of profoundly deaf patients outfitted with cochlear implants[157]. It is thus encouraging that light perception conferred by DENAQ is sufficient for visual learning and recall in blind mice.

Ideally, vision restoration technologies should enable the blind retina to respond to acceptable light intensities with sufficiently rapid kinetics to enable detection of moving objects. The

kinetics of DENAQ-mediated responses are dependent on light intensity, with bright light maximizing the speed of response onset to as brief as 50 msec, and dim light allowing reliable responses to more frequent flashes. Spontaneous relaxation of DENAQ from *cis* to *trans* in darkness ($t_{1/2}$) takes ~300 ms[48], consistent with the DENAQ-mediated RGC light response decaying within 1 sec, on average. However, the response kinetics vary considerably and some RGCs consistently turn off much quicker (<50 ms). In part, the speed of movement detection will depend on how the visual system weighs these different RGC responses. Novel azobenzene derivatives with nanosecond thermal relaxation kinetics have been developed[158] and photoswitches incorporating these compounds may enable very high frequency optical stimulation of neuronal firing.

The RGCs of DENAQ-treated blind mice all generate the same polarity light response, in contrast to the dual On vs. Off light responses generated by RGCs in normal functioning retinas, but this should not be a serious problem for visual perception. In human RP patients, electronic retinal implants can restore object recognition, even though the implants indiscriminately stimulate On- and Off-RGCs[77]. DENAQ might enable some degree of visual perception under real-world photopic illumination conditions. However, image-altering projection goggles could improve perception by tuning the intensity, wavelength, refresh rate, and image complexity to optimize the visual experience.

Implications of degeneration-specific photosensitization

DENAQ has a profound effect on photoreceptor-degenerated retinas from *rd1* or *rd4* mice, while having little or no effect on healthy retinas from WT or TKO mice. The degeneration-dependent action suggests that DENAQ might selectively impart photosensitivity when cell death is constrained to a particular region, e.g. the peripheral retina in RP or the central retina in AMD. Our results imply that DENAQ will not interfere with normal phototransduction and visual processing in regions of the retina that are still healthy. The selective targeting of photosensitization to diseased tissue could be an important clinical advantage.

Our experiments indicate that RGCs are the primary cellular target for DENAQ photosensitization in the retina. The DENAQ-mediated light response is fully retained in RGCs after blocking all synaptic transmission, indicating that bipolar and amacrine cells are not required. We previously showed that the dominant cell type for AAQ-mediated photosensitization is the amacrine cell[132]. Light relieves AAQ blockade of K^+ channels in amacrine cells, hyperpolarizing the membrane potential, but because amacrine cells are inhibitory, the net effect is to enhance RGC firing. There are possible advantages in converting RGCs into the direct transducers of light input, rather than relying on presynaptic neurons to transmit this information. In principle, the latency of signaling to the brain will be shorter with direct RGC stimulation. And the signal generated directly in RGCs is downstream of retinal circuit remodeling that occurs during degeneration[74,159], which could distort spatial representation of images.

Our results indicate that degeneration of rods and cones in the outer retina somehow leads to changes in the electrophysiology of RGCs in the inner retina, enabling DENAQ photosensitization. We do not know whether the change in RGCs is triggered by the loss of light-

driven synaptic input or trophic factor signaling. Morphological and electrophysiological changes in RGCs, resulting from degeneration, have been reported[74,145,159,160], but our results point to a previously unrecognized change in I_h as being the crucial alteration that enables DENAQ photosensitization.

I_h is a hyperpolarization-activated inward current that generates rebound depolarization after spikes, sustaining repetitive activity in cardiac myocytes and neurons[161]. Our results show a ~2-fold increase of I_h in *rd1* RGCs, helping to explain why these neurons are hyperactive in degenerating retina. However, it is unclear whether the increase in current density alone accounts for the enormous increase in DENAQ photosensitivity, or whether additional changes in channel properties are involved. There are four hyperpolarization-activated cyclic nucleotide-gated (HCN) channel subunits, HCN1-4, that underlie I_h in different cell types[149,161]. RGCs normally express HCN1 and HCN4[148] and both of these channels can be photosensitized by DENAQ when expressed as homomultimers in HEK-293 cells (unpublished observations). In addition to changes in channel expression, it is possible that a change in HCN channel localization, subunit composition or a change in auxiliary subunits, such as TRIP8b[162] might alter the sensitivity of I_h to DENAQ.

DENAQ photosensitizes I_h and voltage gated K^+ channels in RGCs from *rd1* retina. Unlike K^+ channels, which are found in virtually every cell type in the eye, HCN channels are highly restricted to neurons[163]. Different azobenzene photoswitches have overlapping but distinct selectivities for voltage-gated ion channels[164]. Thus, it may be possible to engineer a photoswitch compound that is specific for I_h, either by modifying chemical moieties in DENAQ, or by adding a light-sensitive azobenzene to a selective HCN ligand, such as ivabradine. A photoswitch specific for I_h would have the advantage of enabling photoregulation of neurons while having no effect on other cell types. By targeting I_h we have uncovered a new strategy for restoring visual function, based on exploiting changes in the endogenous electrophysiology of neurons that have remodeled during the progression of retinal degeneration.

Materials and methods

Chemicals

Photoswitch compounds were synthesized as formate salts in accordance with previously described protocols[48,100]. All other chemicals were purchased from Sigma-Aldrich or Tocris Bioscience.

Animals

WT mice (C57BL/6J strain, Jackson Laboratory), homozygous *rd1/rd1* mice (C3H/HeJ strain, Charles River Laboratories), heterozygous *rd4/+* mice (In56Rk-*Rd4* strain, Jackson Laboratory) and triple knockout mice (tra$^{-/-}$ cnga3$^{-/-}$ opn4$^{-/-}$, gift of King-Wai Yau, Johns Hopkins University) 3-6 months old were used in the MEA experiments. All animal use procedures were approved by the UC Berkeley Institutional Animal Care and Use Committee.

Multielectrode array recordings

Mouse retinas were dissected and kept in physiological saline (ACSF) at 37^{0}C containing (in mM) 119 NaCl, 2.5 KCl, 1 KH_2PO_4, 1.3 $MgCl_2$, 2.5 $CaCl_2$, 26.2 $NaHCO_3$, and 20 D-glucose, aerated with 95% O_2 / 5% CO_2. In order to pharmacologically isolate RGCs from outer retinal synaptic inputs, a solution containing (in μM) 10 AP4, 40 DNQX, 30 AP5, 10 SR-95531 (GABAzine), 50 TPMPA, 10 strychnine, 50 tubocurarine was used. For extracellular recordings, a flat-mounted retina, or a series of 400 μm wide transverse retinal sections made with a sharp razor blade, were placed ganglion cell layer down onto a multielectrode array system (MEA 1060-2-BC, Multi-Channel Systems). The MEA electrodes were 30 μm in diameter, spaced 200 μm apart and arranged in an 8x8 rectangular grid. Retinas were treated with 300 μM DENAQ in the MEA chamber for 30 min, followed by a 15 min wash. In order to pharmacologically isolate RGCs, the synaptic blocker cocktail (in physiological saline) was subsequently perfused for 15 min. I_h was blocked by a 30 min perfusion of 100 μM ZD7288, 50μM ivabradine, or 50μM cilobradine (in saline with or without synaptic blockers). Extracellular spikes were high-pass filtered at 200 Hz and digitized at 20 kHz. A spike threshold of 4SD was set for each channel. Typically, each electrode recorded spikes from one to three RGCs. Principal component analysis of the spike waveforms was used for sorting spikes generated by individual cells (Offline Sorter, Plexon).

Patch-clamp electrophysiology

Borosilicate glass electrodes with resistance of 4-6 MΩ were used for all voltage clamp recordings. Access resistance was 5-14 MΩ. For measuring voltage-gated I_h and K^+ currents, electrodes contained (in mM) 116 K^+ gluconate, 6 KCl, 2 NaCl, 20 HEPES, 0.5 EGTA, 4 ATP-Mg, 0.3 GTP-Na_2, 10 Phosphocreatine-Na_2. The ACSF solution was the same as the one used in the MEA experiments. Flat-mounted retinas were treated with 200 μM DENAQ for 40 min in ACSF at 25^{0}C, followed by a 15 min wash. Synaptic inputs were blocked with a solution containing the same synaptic blockers as those used in the MEA experiments in addition to 1μM TTX-citrate. Current amplitudes for I-V relationships were measured as averages over 50ms at the end of voltage test pulses applied from the holding potential V_h=-60 mV to -100mV, then stepping up to 0 mV in 10mV increments every 1s. Two sets of I-V measurements were made in the dark and under 480nm light and averaged to calculate percent change in current. Photoregulation of I_h was quantified at -100mV and photoregulation of I_K at 0 mV.

Light Stimulation

A 100W arc lamp (Ushio USH-103D) was used for MEA light stimulation. The photon flux equivalent for DENAQ-treated retinas was calculated using 470 nm (photoswitch absorbance peak) photon energy. The incident white light intensity for *rd1*, WT and TKO retinas was $3.3x10^{15}$ photons/cm^2/sec, and $3x10^{14}$ photons/cm^2/sec for *rd4* retinas, unless stated otherwise. AAQ-treated retinas were stimulated with filtered 380 nm and 500 nm light from the same lamp using narrow-band filters (Chroma, Inc), with the same light intensity as previously described[132]. A Polychrome V (Till Photonics GmbH) monochromator was used to determine the action spectrum of DENAQ in the retina and to stimulate RGCs in patch clamp experiments. The action spectrum was corrected for photon flux at each individual wavelength. A typical stimulation protocol consisted of 10 cycles of alternating 15 sec light/dark intervals.

Data Analysis and Statistics

We calculated the average RGC firing rate for individual retinas in light and in darkness in some experiments. In order to normalize light-elicited changes in firing rate of individual RGCs in *rd1*, *rd4* and TKO retinas, we calculated the LRI = (mean firing rate in the light – mean firing rate in darkness) / (mean firing rate in the light + mean firing rate in darkness). Light-elicited changes in firing rate of individual RGCs in WT retinas were calculated as PLRI = (peak firing rate in the light – peak firing rate in darkness) / (peak firing rate in the light + peak firing rate in darkness). The first second of the light and dark intervals was used to measure the peak firing rate. Pairwise comparisons of LRI and PLRI distributions were performed using the Wilcoxon rank sum test (Matlab). All other statistical significance (p value) calculations were performed using the two tailed unpaired Student's t test. Results with $p<0.05$ were considered significant.

Intravitreal injections

Before injection, animals were anesthetized with isoflurane (2%) and their pupils were dilated with tropicamide (1%). An incision was made through the sclera, below the ora serrata with a 30 gauge needle and 2 µl of either DENAQ (2 µl of various concentrations of DENAQ in 90% PBS / 10% DMSO) or vehicle only (sham) (2 µl of 90% PBS / 10% DMSO) were injected into the vitreous with a blunt ended 32 gauge Hamilton syringe. The mice were allowed to recover for 6 hr after injection with open access to food and water in their cage.

Cryosections

WT mice were euthanized by CO_2 asphyxiation and cervical dislocation 10 or 30 days after intravitreal injection. For each mouse, one eye was injected with 5mM DENAQ, while the other eye was injected with sham. For retinal cross sections, the animals were enucleated, the cornea and lens were removed, and the resulting eye-cups were fixed in 4% paraformaldehyde for 1 hour at room temperature. The tissues were then cryoprotected in 30% sucrose overnight at 40C and frozen in OCT compound (Tissue-TEK, Sakura) with dry-ice ethanol slurry. Retinal sections were cut (15 µm) with a Microm HM550 cryostat (Thermo Scientific) and collected on Superfrost Plus slides (Menzel–Glaser).

Histology

Terminal deoxynucleotidyl transferase (TdT) mediated dUTP nick end labeling, or TUNEL, was used to assess apoptosis in retinal slices. Slides were treated using an In Situ Cell Death Detection Kit, Fluorescein (Roche) following the manufacturer's instructions for cryopreserved

tissue. Positive and negative TUNEL control sections (DNAse I treated sections and sections without TdT) were included on each slide. Slides were then stained with 1 µM DAPI in PBS (GIBCO, pH 7.4). Fluoromount-G (Southern Biotech) was used to mount coverslips (Fisherbrand 22x50-1.5) onto slides. Slides were imaged on an Olympus VS120 slide scanner through a 40x air objective using DAPI and FITC filters. Images were analyzed using ImageJ. Each section was broken up into 250x250 µm fields of roughly equal cell number, and three fields from each section were randomly chosen. Apoptotic cells were identified by colocalized DAPI and fluorescein signals. Thickness of nuclear layers was measured at four equidistant positions along the image and averaged. Retinal ganglion cells were counted over a 100 µm section. Two counts were made and averaged.

Open-Field Test

Rd1 mice were placed in a 190 x 100 mm circular chamber. The chamber was surrounded by six panels of 500 nm LEDs (Roithner Laserteknik), providing uniform illumination with a light intensity of $2.5x10^{16}$ photons/cm^2/sec. The mice were dark-adapted for 1 hour and habituated to the experimental chamber for 5 min prior to each experiment. Exploratory behavior was recorded using an IR sensitive video camera (Logitech C310) for 5 min in darkness under IR illumination, then the chamber was illuminated by the 500 nm LEDs, and mouse locomotion was monitored for an additional 5 min. The apparatus was cleaned after each experiment. Each mouse was tested once before intravitreal injection and again 6 hours after injection of either 20mM DENAQ or sham. Videos were analyzed with motion tracking software (Tracker) to record the animals' velocity and position. The ratio of activity light / activity dark was defined as mean velocity in the light / mean velocity in darkness.

Visual Fear Conditioning Test

Fear conditioning was conducted in a 12 x 10 x 12 inch chamber with an electrified metal bar floor (Coulbourn Instruments). Prior to the experiment, animals were habituated by handling intervals interspersed over two days and with a 5 minute exposure to the chamber. On day one, groups of WT mice, sham-injected *rd1* mice, or DENAQ-injected *rd1* mice (6 hours after intravitreal injection of 10 mM DENAQ or sham) were subjected to paired stimuli or unpaired stimuli. Paired conditioning consisted of a 5 min habituation period in the dark, followed by three 10 s white light stimuli each co-terminating with a 2 s foot shock, with 15 s between light flashes. Unpaired conditioning was identical except the three foot shocks and three light stimuli were interleaved with 5-12 s between stimuli. On day two the mice were tested for recall of the light-cued conditioning. The recall trial consisted of a 5 min habituation period in the dark followed by a 30 s white light stimulus. The apparatus was cleaned after each experiment. Two house lights provided very dim illumination ($1x10^{13}$ photons/cm^2/sec) sufficient to allow video recording throughout the experiment, but below the threshold for DENAQ activation. The bright light cue was provided by two white LED arrays attached to the inner chamber ceiling ($1.1x10^{15}$ photons/cm^2/sec). Locomotor activity was analyzed as in the open field assay.

Supplemental Information

Figure S1

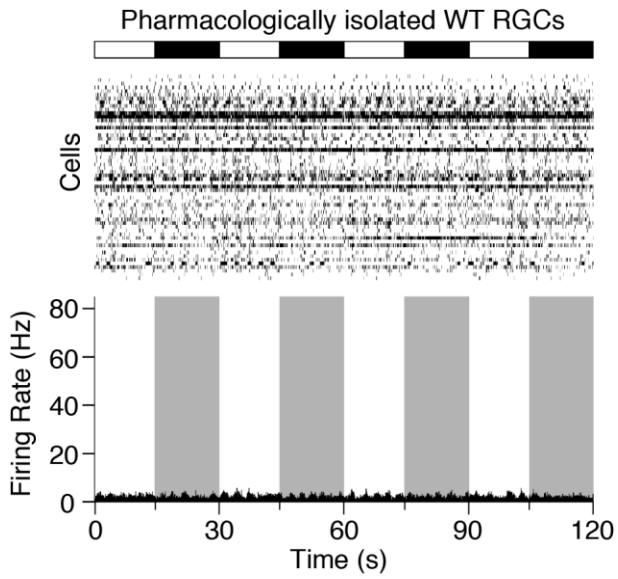

Figure S1, related to Figure 5: Pharmacological blockade of synaptic inputs onto WT RGCs blocks photoreceptor-mediated light responses.

MEA recording from pharmacologically isolated WT RGCs. Light (white) and dark (black/gray) episodes are shown. Neither the ON-light response, nor the OFF-light response is present (mean LRI=0.03).

Figure S2

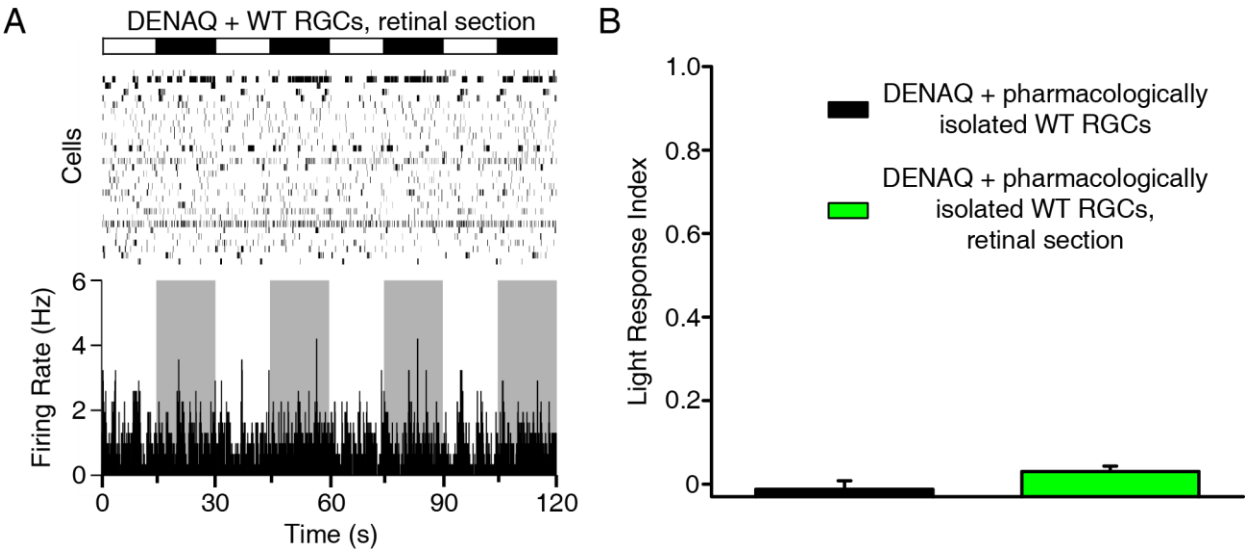

Figure S2, related to Figure 5: ILM/OLM disruption in WT retina does not promote DENAQ photosensitization of pharmacologically isolated WT RGCs.

(**A**) MEA recording from pharmacologically isolated WT RGCs in a transverse retinal slice treated with 300 µM DENAQ. Light (white) and dark (black/gray) episodes are shown. No light response is evident (mean LRI=-0.01).
(**B**) Light responses of DENAQ-treated, pharmacologically isolated WT RGCs from intact WT retinas (black) (n=10 retinas, mean LRI=-0.01) and from transverse WT retinal sections (green) (n=6 retinas, mean LRI=0.03) are not significantly different (p=0.62). Data are mean±SEM.

Figure S3

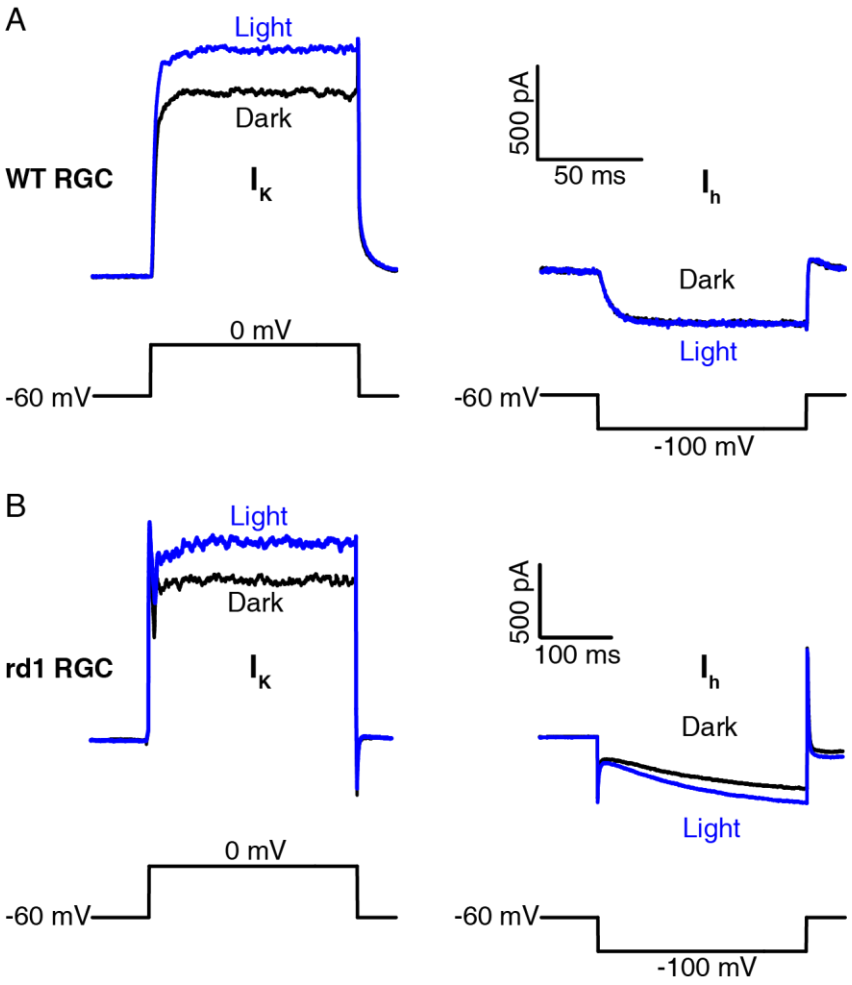

Figure S3, related to Figure 6: DENAQ selectively photosensitizes a hyperpolarization activated inward current in pharmacologically isolated *rd1* but not WT RGCs.

(**A**) Current traces from a DENAQ-treated WT RGC in response to depolarizing (V_h=-60 mV to 0 mV) voltage steps for measuring I_K (left) and hyperpolarizing (V_h=-60 mV to -100 mV) voltage steps for measuring I_h (right) in the light (blue) and in the dark (black). Only I_K increased in the light (20% increase).
(**B**) Current traces from a DENAQ-treated *rd1* RGC in response to the same depolarizing (left) and hyperpolarizing (right) voltage steps in the light (blue) and in the dark (black). Both I_K and I_h increased in the light (increase in I_K=21%, increase in I_h=24%)

Figure S4

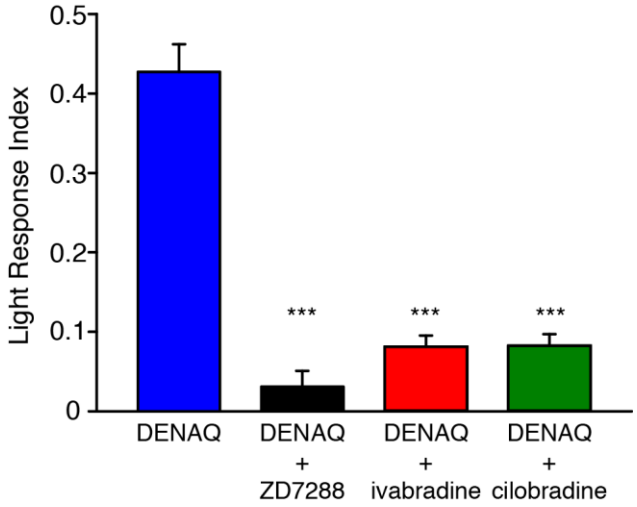

Figure S4, related to Figure 6: I_h blockers eliminate DENAQ-mediated photoswitching in *rd1* retina.

DENAQ treatment confers light sensitivity onto *rd1* retinas (blue) (n=12 retinas, mean LRI=0.43). Subsequent treatment with I_h blockers - ZD7288 (black) (n=6 retinas, mean LRI=0.03, $p<0.001$), ivabradine (red) (n=6 retinas, mean LRI=0.08, $p<0.001$) or cilobradine (green) (n=6 retinas, mean LRI=0.08, $p<0.001$) almost entirely eliminates the light response. Data are mean±SEM.

Figure S5

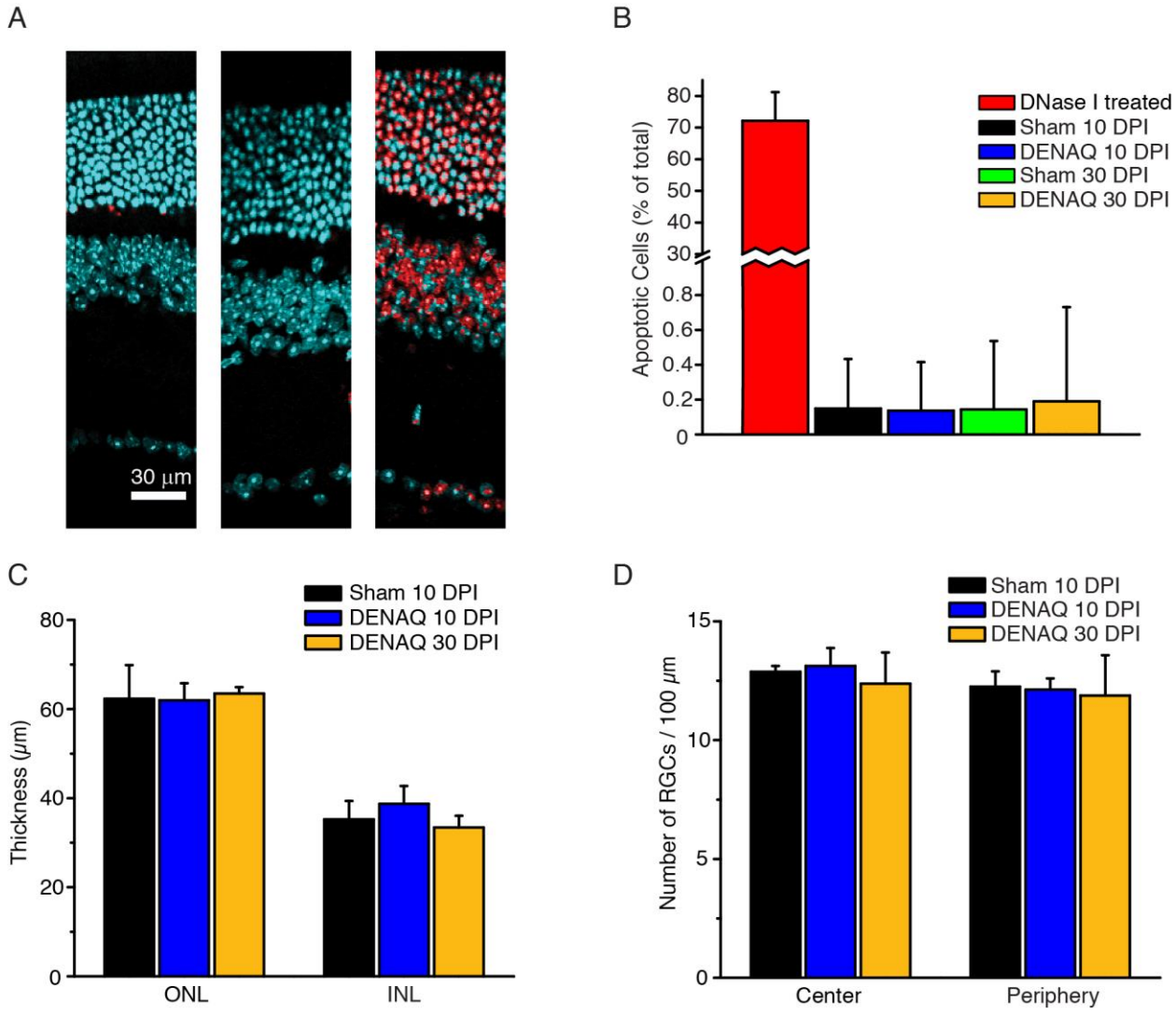

Figure S5: DENAQ has no apparent toxic effects on the mouse retina.

(**A**) Retinal cross sections 10 days post injection (DPI), after TUNEL assay and DAPI counterstain. Apoptotic cells are marked red (pseudocolor for visibility), nuclei are cyan. Sham injected retina (left), DENAQ injected retina (center), sham injected retina treated with DNAse I during TUNEL assay (right).
(**B**) Percent apoptotic cells after sham or DENAQ injection, at 10 DPI (black/blue) and 30 DPI (green/yellow). DNAse I treated percentage shown in red.
(**C**) Outer nuclear layer (ONL) and inner nuclear layer (INL) thickness 10 DPI of sham (black) and DENAQ (blue) and 30 DPI of DENAQ (yellow).
(**D**) RGC count per 100 µm of retina 10 DPI of sham (black) and DENAQ (blue) and 30 DPI of DENAQ (yellow).

Supplemental Table 1, related to Figure 3

Distance (μm)	No. of Cells	Median LRI	95% Confidence Interval
Target	16	0.4504	0.1733 to 0.7276
200-400	110	0.0101	0.0007 to 0.0262
400-600	213	-0.0175	-0.0266 to -0.0098
600-800	242	-0.0106	-0.0222 to 0.0031
800-1200	176	-0.0068	-0.0148 to 0.0005

Table S1. Center and Surround RGC Responses under Targeted Illumination

References

1. Crick, F. The impact of molecular biology on neuroscience. *Philosophical transactions of the Royal Society of London. Series B, Biological sciences* **354**, 2021-2025 (1999).
2. Djamgoz, M.B.A., Archer, S.N. & Vallerga, S. *Neurobiology and clinical aspects of the outer retina*, (Chapman & Hall, London ; New York, 1995).
3. Kaplan, J.H., Forbush, B., 3rd & Hoffman, J.F. Rapid photolytic release of adenosine 5'-triphosphate from a protected analogue: utilization by the Na:K pump of human red blood cell ghosts. *Biochemistry* **17**, 1929-1935 (1978).
4. Nerbonne, J.M., Richard, S., Nargeot, J. & Lester, H.A. New photoactivatable cyclic nucleotides produce intracellular jumps in cyclic AMP and cyclic GMP concentrations. *Nature* **310**, 74-76 (1984).
5. Walker, J.W., McCray, J.A. & Hess, G.P. Photolabile protecting groups for an acetylcholine receptor ligand. Synthesis and photochemistry of a new class of o-nitrobenzyl derivatives and their effects on receptor function. *Biochemistry* **25**, 1799-1805 (1986).
6. Callaway, E.M. & Katz, L.C. Photostimulation Using Caged Glutamate Reveals Functional Circuitry in Living Brain-Slices. *P Natl Acad Sci USA* **90**, 7661-7665 (1993).
7. Banghart, M.R. & Sabatini, B.L. Photoactivatable Neuropeptides for Spatiotemporally Precise Delivery of Opioids in Neural Tissue. *Neuron* **73**, 249-259 (2012).
8. Kramer, R.H., Mourot, A. & Adesnik, H. Optogenetic pharmacology for control of native neuronal signaling proteins. *Nature neuroscience* **16**, 816-823 (2013).
9. Dürr, H. & Bouas-Laurent, H. *Photochromism : molecules and systems*, (Elsevier, Amsterdam ; Boston, 2003).
10. Banghart, M., Borges, K., Isacoff, E., Trauner, D. & Kramer, R.H. Light-activated ion channels for remote control of neuronal firing. *Nature neuroscience* **7**, 1381-1386 (2004).
11. Volgraf, M., *et al.* Allosteric control of an ionotropic glutamate receptor with an optical switch. *Nat Chem Biol* **2**, 47-52 (2006).
12. Levitz, J., *et al.* Optical control of metabotropic glutamate receptors. *Nature neuroscience* **16**, 507-516 (2013).
13. Boyden, E.S., Zhang, F., Bamberg, E., Nagel, G. & Deisseroth, K. Millisecond-timescale, genetically targeted optical control of neural activity. *Nature neuroscience* **8**, 1263-1268 (2005).
14. Zhang, F., *et al.* Multimodal fast optical interrogation of neural circuitry. *Nature* **446**, 633-639 (2007).
15. Lin, J.Y., Knutsen, P.M., Muller, A., Kleinfeld, D. & Tsien, R.Y. ReaChR: a red-shifted variant of channelrhodopsin enables deep transcranial optogenetic excitation. *Nature neuroscience* **16**, 1499-1508 (2013).
16. Christie, J.M., Gawthorne, J., Young, G., Fraser, N.J. & Roe, A.J. LOV to BLUF: flavoprotein contributions to the optogenetic toolkit. *Molecular plant* **5**, 533-544 (2012).
17. Tye, K.M. & Deisseroth, K. Optogenetic investigation of neural circuits underlying brain disease in animal models. *Nature reviews. Neuroscience* **13**, 251-266 (2012).
18. Fehrentz, T., Schonberger, M. & Trauner, D. Optochemical genetics. *Angew Chem Int Ed Engl* **50**, 12156-12182 (2011).

19. Taly, A., Corringer, P.-J., Guedin, D., Lestage, P. & Changeux, J.-P. Nicotinic receptors: allosteric transitions and therapeutic targets in the nervous system. *Nat Rev Drug Discov* **8**, 733-750 (2009).
20. Albuquerque, E.X., Pereira, E.F.R., Alkondon, M. & Rogers, S.W. Mammalian nicotinic acetylcholine receptors: from structure to function. *Physiological Reviews* **89**, 73-120 (2009).
21. Kew, J.N.C. & Davies, C.H. *Ion Channels: From Structure To Function*, (Oxford University Press, Oxford, 2010).
22. Neher, E. & Sakmann, B. Single-channel currents recorded from membrane of denervated frog muscle fibres. *Nature* **260**, 799-802 (1976).
23. Unwin, N. Refined structure of the nicotinic acetylcholine receptor at 4A resolution. *J Membr Biol* **346**, 967-989 (2005).
24. Nowak, M.W., *et al.* Nicotinic receptor binding site probed with unnatural amino acid incorporation in intact cells. *Science* **268**, 439-442 (1995).
25. Noda, M., *et al.* Primary structure of alpha-subunit precursor of *Torpedo californica* acetylcholine receptor deduced from cdna sequence. *Nature* **299**, 793-797 (1982).
26. Noda, M., *et al.* Primary structures of beta-subunit and delta-subunit precursors of *Torpedo californica* acetylcholine-receptor deduced from cdna sequences. *Nature* **301**, 251-255 (1983).
27. Kramer, R.H., Fortin, D.L. & Trauner, D. New photochemical tools for controlling neuronal activity. *Current Opinion in Neurobiology* **19**, 544-552 (2009).
28. Fortin, D.L., *et al.* Optogenetic photochemical control of designer K+ channels in mammalian neurons. *Journal of Neurophysiology* **106**, 488-496 (2011).
29. Mourot, A., *et al.* Probing the reorganization of the nicotinic acetylcholine receptor during desensitization by time-resolved covalent labeling using [3H]AC5, a photoactivatable agonist. *Molecular Pharmacology* **69**, 452-461 (2006).
30. Hunt, R. & Renshaw, R.R. Some effects of derivatives of betaine amide and of choline ethers on the autonomic nervous system. *Journal of Pharmacology and Experimental Therapeutics* **35**, 99-128 (1929).
31. Wong, K.C. & Long, J.P. Nicotinic and muscarinic activity of phenacyl and phenylalkyl trimethylamines. *J Pharmacol Exp Ther* **137**, 70-75 (1962).
32. Gotti, C., *et al.* 4-Oxystilbene compounds are selective ligands for neuronal nicotinic αBungarotoxin receptors. *British Journal of Pharmacology* **124**, 1197-1206 (1998).
33. Celie, P.H.N., *et al.* Nicotine and carbamylcholine binding to nicotinic acetylcholine receptors as studied in AChBP crystal structures. *Neuron* **41**, 907-914 (2004).
34. Le Novère, N., Grutter, T. & Changeux, J.-P. Models of the extracellular domain of the nicotinic receptors and of agonist- and Ca2+-binding sites. *Proc. Natl. Acad. Sci. USA* **99**, 3210-3215 (2002).
35. Brejc, K., *et al.* Crystal structure of an ACh-binding protein reveals the ligand-binding domain of nicotinic receptors. *Nature* **411**, 269-276 (2001).
36. Hansen, S.B., *et al.* Structures of *Aplysia* AChBP complexes with nicotinic agonists and antagonists reveal distinctive binding interfaces and conformations. *EMBO J* **24**, 3635-3646 (2005).
37. Chavez-Noriega, L.E., *et al.* Pharmacological characterization of recombinant human neuronal nicotinic acetylcholine receptors hα2β2, hα2β4, hα3β2, hα3β4, hα4β2, hα4β4

and hα7 expressed in *Xenopus* oocytes. *Journal of Pharmacology and Experimental Therapeutics* **280**, 346-356 (1997).

38. Gotti, C., Zoli, M. & Clementi, F. Brain nicotinic acetylcholine receptors: native subtypes and their relevance. *Trends in Pharmacological Sciences* **27**, 482-491 (2006).
39. Nishimura N., *et al.* Thermal cis-to-trans isomerization of substituted azobenzenes II. Substituent and solvent effects. *Bulletin of the Chemical Society of Japan* **49**(1976).
40. Pozhidaeva, N., Cormier, M.E., Chaudhari, A. & Woolley, G.A. Reversible photocontrol of peptide helix content: adjusting thermal stability of the cis state. *Bioconjug Chem* **15**, 1297-1303 (2004).
41. Bartels, E., Wassermann, N.H. & Erlanger, B.F. Photochromic activators of the acetylcholine receptor. *Proc. Natl. Acad. Sci. USA* **68**, 1820-1823 (1971).
42. Lester, H.A., Krouse, M.E., Nass, M.M., Wassermann, N.H. & Erlanger, B.F. A covalently bound photoisomerizable agonist: comparison with reversibly bound agonists at *Electrophorus* electroplaques. *J Gen Physiol* **75**, 207-232 (1980).
43. Barrantes, F.J. Modulation of acetylcholine receptor states by thiol modification. *Biochemistry* **19**, 2957-2965 (1980).
44. Cox, R.N., Kawai, M., Karlin, A. & Brandt, P.W. Voltage fluctuations at the frog sartorius motor endplate produced by a covalently attached activator. *J Membr Biol* **51**, 145-159 (1979).
45. Chabala, L.D. & Lester, H.A. Activation of acetylcholine receptor channels by covalently bound agonists in cultured rat myoballs. *J Physiol* **379**, 83-108 (1986).
46. Gorostiza, P., *et al.* Mechanisms of photoswitch conjugation and light activation of an ionotropic glutamate receptor. *Proc. Natl. Acad. Sci. USA* **104**, 10865-10870 (2007).
47. Sadovski, O., Beharry, A.A., Zhang, F.Z. & Woolley, G.A. Spectral tuning of azobenzene photoswitches for biological applications. *Angew Chem Int Edit* **48**, 1484-1486 (2009).
48. Mourot, A., *et al.* Tuning photochromic ion channel blockers. *ACS chemical neuroscience* **2**, 536-543 (2011).
49. Corringer, P.-J., *et al.* Atomic structure and dynamics of pentameric ligand-gated ion channels: new insight from bacterial homologues. *J Physiol* **588**, 565-572 (2010).
50. Bocquet, N., *et al.* A prokaryotic proton-gated ion channel from the nicotinic acetylcholine receptor family. *Nature* **445**, 116-119 (2007).
51. Hilf, R.J.C. & Dutzler, R. X-ray structure of a prokaryotic pentameric ligand-gated ion channel. *Nature* **452**, 375-379 (2008).
52. Law, R.J., Henchman, R.H. & McCammon, J.A. A gating mechanism proposed from a simulation of a human alpha7 nicotinic acetylcholine receptor. *Proc. Natl. Acad. Sci. USA* **102**, 6813-6818 (2005).
53. Sullivan, D.A. & Cohen, J.B. Mapping the agonist binding site of the nicotinic acetylcholine receptor. Orientation requirements for activation by covalent agonist. *J Biol Chem* **275**, 12651-12660 (2000).
54. Hibbs, R.E. & Gouaux, E. Principles of activation and permeation in an anion-selective cys-loop receptor. *Nature* **474**, 54-60 (2011).
55. Langmead, C.J., Watson, J. & Reavill, C. Muscarinic acetylcholine receptors as CNS drug targets. *Pharmacol Therapeut* **117**, 232-243 (2008).

56. Dani, J.A. & Bertrand, D. Nicotinic acetylcholine receptors and nicotinic cholinergic mechanisms of the central nervous system. *Annual Review of Pharmacology and Toxicology* **47**, 699-729 (2007).
57. Aravanis, A.M., *et al.* An optical neural interface: in vivo control of rodent motor cortex with integrated fiberoptic and optogenetic technology. *J Neural Eng* **4**, S143-156 (2007).
58. Thomas, K.R. & Capecchi, M.R. Site-directed mutagenesis by gene targeting in mouse embryo-derived stem cells. *Cell* **51**, 503-512 (1987).
59. Mourot, A., Bamberg, E. & Rettinger, J. Agonist- and competitive antagonist-induced movement of loop 5 on the alpha subunit of the neuronal alpha4beta4 nicotinic acetylcholine receptor. *J Neurochem* **105**, 413-424 (2008).
60. Friesner, R.A., *et al.* Glide: a new approach for rapid, accurate docking and scoring. 1. Method and assessment of docking accuracy. *J Med Chem* **47**, 1739-1749 (2004).
61. Eldridge, M.D., Murray, C.W., Auton, T.R., Paolini, G.V. & Mee, R.P. Empirical scoring functions: I. The development of a fast empirical scoring function to estimate the binding affinity of ligands in receptor complexes. *J Comput Aided Mol Des* **11**, 425-445 (1997).
62. Baxter, C.A., Murray, C.W., Clark, D.E., Westhead, D.R. & Eldridge, M.D. Flexible docking using Tabu search and an empirical estimate of binding affinity. *Proteins: Structure, Function, and Bioinformatics* **33**, 367-382 (1998).
63. Larkin, M.A., *et al.* Clustal W and Clustal X version 2.0. *Bioinformatics* **23**, 2947-2948 (2007).
64. Goujon, M., *et al.* A new bioinformatics analysis tools framework at EMBL-EBI. *Nucleic Acids Res* **38**, W695-W699 (2010).
65. Chatrenet, B., *et al.* Photoactivatable Agonist of the Nicotinic Acetylcholine-Receptor - Potential Probe to Characterize the Structural Transitions of the Acetylcholine Binding-Site in Different States of the Receptor. *Molecular Pharmacology* **41**, 1100-1106 (1992).
66. Hilf, R.J.C. & Dutzler, R. X-ray structure of a prokaryotic pentameric ligand-gated ion channel. *Nature* **452**, 375-U312 (2008).
67. Haghbeen, K. & Tan, E.W. Facile synthesis of catechol azo dyes. *J Org Chem* **63**, 4503-4505 (1998).
68. Bunker, C.H., Berson, E.L., Bromley, W.C., Hayes, R.P. & Roderick, T.H. Prevalence of Retinitis Pigmentosa in Maine. *Am J Ophthalmol* **97**, 357-365 (1984).
69. Klein, R., *et al.* Prevalence of Age-Related Macular Degeneration in the US Population. *Arch Ophthalmol-Chic* **129**, 75-80 (2011).
70. Gonzalez-Cordero, A., *et al.* Photoreceptor precursors derived from three-dimensional embryonic stem cell cultures integrate and mature within adult degenerate retina. *Nat Biotechnol* **31**, 741-+ (2013).
71. Carr, A.J., *et al.* Protective Effects of Human iPS-Derived Retinal Pigment Epithelium Cell Transplantation in the Retinal Dystrophic Rat. *Plos One* **4**(2009).
72. Li, Y., *et al.* Long-term safety and efficacy of human-induced pluripotent stem cell (iPS) grafts in a preclinical model of retinitis pigmentosa. *Molecular medicine* **18**, 1312-1319 (2012).
73. Schwartz, S.D., *et al.* Embryonic stem cell trials for macular degeneration: a preliminary report. *Lancet* **379**, 713-720 (2012).
74. Jones, B.W., *et al.* Retinal remodeling. *Japanese journal of ophthalmology* **56**, 289-306 (2012).

75. Dagnelie, G. Retinal implants: emergence of a multidisciplinary field. *Current opinion in neurology* **25**, 67-75 (2012).
76. da Cruz, L., *et al.* The Argus II epiretinal prosthesis system allows letter and word reading and long-term function in patients with profound vision loss. *The British journal of ophthalmology* **97**, 632-636 (2013).
77. Humayun, M.S., *et al.* Interim results from the international trial of Second Sight's visual prosthesis. *Ophthalmology* **119**, 779-788 (2012).
78. Mourot, A., Tochitsky, I. & Kramer, R.H. Light at the end of the channel: optical manipulation of intrinsic neuronal excitability with chemical photoswitches. *Frontiers in molecular neuroscience* **6**, 5 (2013).
79. Busskamp, V., *et al.* Genetic reactivation of cone photoreceptors restores visual responses in retinitis pigmentosa. *Science* **329**, 413-417 (2010).
80. Hacein-Bey-Abina, S., *et al.* A serious adverse event after successful gene therapy for X-linked severe combined immunodeficiency. *The New England journal of medicine* **348**, 255-256 (2003).
81. Jimenez, A.J., Garcia-Fernandez, J.M., Gonzalez, B. & Foster, R.G. The spatio-temporal pattern of photoreceptor degeneration in the aged rd/rd mouse retina. *Cell and tissue research* **284**, 193-202 (1996).
82. Marc, R.E., Jones, B.W., Watt, C.B. & Strettoi, E. Neural remodeling in retinal degeneration. *Progress in retinal and eye research* **22**, 607-655 (2003).
83. Punzo, C. & Cepko, C. Cellular responses to photoreceptor death in the rd1 mouse model of retinal degeneration. *Investigative ophthalmology & visual science* **48**, 849-857 (2007).
84. Strettoi, E. & Pignatelli, V. Modifications of retinal neurons in a mouse model of retinitis pigmentosa. *Proc Natl Acad Sci U S A* **97**, 11020-11025 (2000).
85. Chader, G.J., Weiland, J. & Humayun, M.S. Artificial vision: needs, functioning, and testing of a retinal electronic prosthesis. *Progress in brain research* **175**, 317-332 (2009).
86. Gerding, H., Benner, F.P. & Taneri, S. Experimental implantation of epiretinal retina implants (EPI-RET) with an IOL-type receiver unit. *J Neural Eng* **4**, S38-49 (2007).
87. Shire, D.B., *et al.* Development and implantation of a minimally invasive wireless subretinal neurostimulator. *IEEE transactions on bio-medical engineering* **56**, 2502-2511 (2009).
88. Humayun, M.S., *et al.* Visual perception in a blind subject with a chronic microelectronic retinal prosthesis. *Vision research* **43**, 2573-2581 (2003).
89. Yanai, D., *et al.* Visual performance using a retinal prosthesis in three subjects with retinitis pigmentosa. *Am J Ophthalmol* **143**, 820-827 (2007).
90. Bi, A., *et al.* Ectopic expression of a microbial-type rhodopsin restores visual responses in mice with photoreceptor degeneration. *Neuron* **50**, 23-33 (2006).
91. Lagali, P.S., *et al.* Light-activated channels targeted to ON bipolar cells restore visual function in retinal degeneration. *Nature neuroscience* **11**, 667-675 (2008).
92. Tomita, H., *et al.* Channelrhodopsin-2 gene transduced into retinal ganglion cells restores functional vision in genetically blind rats. *Exp Eye Res* **90**, 429-436 (2010).
93. Caporale, N., *et al.* LiGluR restores visual responses in rodent models of inherited blindness. *Molecular therapy : the journal of the American Society of Gene Therapy* **19**, 1212-1219 (2011).

94. Lin, B., Koizumi, A., Tanaka, N., Panda, S. & Masland, R.H. Restoration of visual function in retinal degeneration mice by ectopic expression of melanopsin. *Proc Natl Acad Sci U S A* **105**, 16009-16014 (2008).
95. Lamba, D.A., Gust, J. & Reh, T.A. Transplantation of Human Embryonic Stem Cell-Derived Photoreceptors Restores Some Visual Function in Crx-Deficient Mice. *Cell Stem Cell* **4**, 73-79 (2009).
96. Winter, J.O., Cogan, S.F. & Rizzo, J.F. Retinal prostheses: current challenges and future outlook. *J Biomat Sci-Polym E* **18**, 1031-1055 (2007).
97. Chaudhry, G.R., *et al.* Fate of Embryonic Stem Cell Derivatives Implanted into the Vitreous of a Slow Retinal Degenerative Mouse Model. *Stem Cells Dev* **18**, 247-258 (2009).
98. Beltran, W.A., *et al.* rAAV2/5 gene-targeting to rods: dose-dependent efficiency and complications associated with different promoters. *Gene Ther* **17**, 1162-1174 (2010).
99. Banghart, M.R., *et al.* Photochromic Blockers of Voltage-Gated Potassium Channels. *Angewandte Chemie-International Edition* **48**, 9097-9101 (2009).
100. Fortin, D.L., *et al.* Photochemical control of endogenous ion channels and cellular excitability. *Nature methods* **5**, 331-338 (2008).
101. Sancho-Pelluz, J., *et al.* Photoreceptor cell death mechanisms in inherited retinal degeneration. *Molecular neurobiology* **38**, 253-269 (2008).
102. Meister, M., Pine, J. & Baylor, D.A. Multi-neuronal signals from the retina: acquisition and analysis. *Journal of neuroscience methods* **51**, 95-106 (1994).
103. Hattar, S., Liao, H.W., Takao, M., Berson, D.M. & Yau, K.W. Melanopsin-containing retinal ganglion cells: architecture, projections, and intrinsic photosensitivity. *Science* **295**, 1065-1070 (2002).
104. Thyagarajan, S., *et al.* Visual function in mice with photoreceptor degeneration and transgenic expression of channelrhodopsin 2 in ganglion cells. *The Journal of neuroscience : the official journal of the Society for Neuroscience* **30**, 8745-8758 (2010).
105. Panda, S., *et al.* Melanopsin is required for non-image-forming photic responses in blind mice. *Science* **301**, 525-527 (2003).
106. Johnson, J., *et al.* Melanopsin-dependent light avoidance in neonatal mice. *P Natl Acad Sci USA* **107**, 17374-17378 (2010).
107. Kandel, G.L., Bedell, H.E., Walker, R. & Wolf, B.M. Negative Phototaxis in Pigmented, Albinotic and Rcs Rat Pups Measured with a New Technique. *Clin Vision Sci* **1**, 357-366 (1987).
108. Ecker, J.L., *et al.* Melanopsin-expressing retinal ganglion-cell photoreceptors: cellular diversity and role in pattern vision. *Neuron* **67**, 49-60 (2010).
109. Farrow, K. & Masland, R.H. Physiological clustering of visual channels in the mouse retina. *J Neurophysiol* **105**, 1516-1530 (2011).
110. Carcieri, S.M., Jacobs, A.L. & Nirenberg, S. Classification of retinal ganglion cells: a statistical approach. *J Neurophysiol* **90**, 1704-1713 (2003).
111. Milam, A.H., Li, Z.Y. & Fariss, R.N. Histopathology of the human retina in retinitis pigmentosa. *Progress in retinal and eye research* **17**, 175-205 (1998).
112. Ivanova, E., Hwang, G.S., Pan, Z.H. & Troilo, D. Evaluation of AAV-mediated expression of Chop2-GFP in the marmoset retina. *Investigative ophthalmology & visual science* **51**, 5288-5296 (2010).

113. Vandenberghe, L.H., *et al.* Dosage thresholds for AAV2 and AAV8 photoreceptor gene therapy in monkey. *Science translational medicine* **3**, 88ra54 (2011).
114. Hauswirth, W.W., *et al.* Treatment of Leber Congenital Amaurosis Due to RPE65 Mutations by Ocular Subretinal Injection of Adeno-Associated Virus Gene Vector: Short-Term Results of a Phase I Trial. *Hum Gene Ther* **19**, 979-990 (2008).
115. Greenberg, K.P., Pham, A. & Werblin, F.S. Differential targeting of optical neuromodulators to ganglion cell soma and dendrites allows dynamic control of center-surround antagonism. *Neuron* **69**, 713-720 (2011).
116. Schiller, P.H., Sandell, J.H. & Maunsell, J.H. Functions of the ON and OFF channels of the visual system. *Nature* **322**, 824-825 (1986).
117. Sekirnjak, C., *et al.* Loss of responses to visual but not electrical stimulation in ganglion cells of rats with severe photoreceptor degeneration. *J Neurophysiol* **102**, 3260-3269 (2009).
118. Kessel, L., Lundeman, J.H., Herbst, K., Andersen, T.V. & Larsen, M. Age-related changes in the transmission properties of the human lens and their relevance to circadian entrainment. *J Cataract Refr Surg* **36**, 308-312 (2010).
119. Degenaar, P., *et al.* Optobionic vision-a new genetically enhanced light on retinal prosthesis. *Journal of Neural Engineering* **6**(2009).
120. Nagel, G., *et al.* Channelrhodopsin-2, a directly light-gated cation-selective membrane channel. *Proc Natl Acad Sci U S A* **100**, 13940-13945 (2003).
121. Govorunova, E.G., Spudich, E.N., Lane, C.E., Sineshchekov, O.A. & Spudich, J.L. New channelrhodopsin with a red-shifted spectrum and rapid kinetics from Mesostigma viride. *mBio* **2**, e00115-00111 (2011).
122. London, N.J., Chiang, A. & Haller, J.A. The dexamethasone drug delivery system: indications and evidence. *Advances in therapy* **28**, 351-366 (2011).
123. Ahuja, A.K., *et al.* Blind subjects implanted with the Argus II retinal prosthesis are able to improve performance in a spatial-motor task. *The British journal of ophthalmology* **95**, 539-543 (2011).
124. Benav, H., *et al.* Restoration of useful vision up to letter recognition capabilities using subretinal microphotodiodes. *Conference proceedings : ... Annual International Conference of the IEEE Engineering in Medicine and Biology Society. IEEE Engineering in Medicine and Biology Society. Conference* **2010**, 5919-5922 (2010).
125. Feldbauer, K., *et al.* Channelrhodopsin-2 is a leaky proton pump. *P Natl Acad Sci USA* **106**, 12317-12322 (2009).
126. Sjulson, L. & Miesenbock, G. Photocontrol of neural activity: biophysical mechanisms and performance in vivo. *Chemical reviews* **108**, 1588-1602 (2008).
127. Huberman, A.D., Feller, M.B. & Chapman, B. Mechanisms underlying development of visual maps and receptive fields. *Annual review of neuroscience* **31**, 479-509 (2008).
128. Van Gelder, R.N. Nonvisual ocular photoreception in the mammal. *Methods in enzymology* **393**, 746-755 (2005).
129. Efron, B. & Tibshirani, R. Bootstrap Methods for Standard Errors, Confidence Intervals, and Other Measures of Statistical Accuracy. *Statistical Science* **1**, 54-75 (1986).
130. Weiland, J.D., Cho, A.K. & Humayun, M.S. Retinal prostheses: current clinical results and future needs. *Ophthalmology* **118**, 2227-2237 (2011).
131. Lamba, D.A., Karl, M.O. & Reh, T.A. Strategies for retinal repair: cell replacement and regeneration. *Progress in brain research* **175**, 23-31 (2009).

132. Polosukhina, A., *et al.* Photochemical restoration of visual responses in blind mice. *Neuron* **75**, 271-282 (2012).
133. Artigas, J.M., Felipe, A., Navea, A., Fandino, A. & Artigas, C. Spectral transmission of the human crystalline lens in adult and elderly persons: color and total transmission of visible light. *Investigative ophthalmology & visual science* **53**, 4076-4084 (2012).
134. Noell, W.K., Walker, V.S., Kang, B.S. & Berman, S. Retinal damage by light in rats. *Investigative ophthalmology* **5**, 450-473 (1966).
135. Fischer, E., Frankel, M. & Wolovsky, R. Wavelength Dependence of Photoisomerization Equilibria in Azocompounds. *The Journal of Chemical Physics* **23**, 1367-1367 (1955).
136. Chow, B.Y., *et al.* High-performance genetically targetable optical neural silencing by light-driven proton pumps. *Nature* **463**, 98-102 (2010).
137. Ren, L., Liang, H., Diao, L. & He, S. Changing dendritic field size of mouse retinal ganglion cells in early postnatal development. *Dev Neurobiol* **70**, 397-407 (2010).
138. Khandhadia, S., Cherry, J. & Lotery, A.J. Age-related macular degeneration. *Advances in experimental medicine and biology* **724**, 15-36 (2012).
139. Amendola, T., Fiore, M. & Aloe, L. Postnatal changes in nerve growth factor and brain derived neurotrophic factor levels in the retina, visual cortex, and geniculate nucleus in rats with retinitis pigmentosa. *Neuroscience letters* **345**, 37-40 (2003).
140. Hattar, S., *et al.* Melanopsin and rod-cone photoreceptive systems account for all major accessory visual functions in mice. *Nature* **424**, 76-81 (2003).
141. Kitamura, E., *et al.* Disruption of the gene encoding the beta1-subunit of transducin in the Rd4/+ mouse. *Investigative ophthalmology & visual science* **47**, 1293-1301 (2006).
142. Bowes, C., *et al.* Retinal degeneration in the rd mouse is caused by a defect in the [beta] subunit of rod cGMP-phosphodiesterase. *Nature* **347**, 677-680 (1990).
143. Roderick, T.H., Chang, B., Hawes, N.L. & Heckenlively, J.R. A new dominant retinal degeneration (Rd4) associated with a chromosomal inversion in the mouse. *Genomics* **42**, 393-396 (1997).
144. Stasheff, S.F. Emergence of sustained spontaneous hyperactivity and temporary preservation of OFF responses in ganglion cells of the retinal degeneration (rd1) mouse. *J Neurophysiol* **99**, 1408-1421 (2008).
145. Sekirnjak, C., *et al.* Changes in physiological properties of rat ganglion cells during retinal degeneration. *J Neurophysiol* **105**, 2560-2571 (2011).
146. Wong, K.Y., Dunn, F.A., Graham, D.M. & Berson, D.M. Synaptic influences on rat ganglion-cell photoreceptors. *J Physiol* **582**, 279-296 (2007).
147. Lee, S.C. & Ishida, A.T. Ih Without Kir in Adult Rat Retinal Ganglion Cells. *Journal of Neurophysiology* **97**, 3790-3799 (2007).
148. Stradleigh, T.W., *et al.* Colocalization of hyperpolarization-activated, cyclic nucleotide-gated channel subunits in rat retinal ganglion cells. *The Journal of Comparative Neurology* **519**, 2546-2573 (2011).
149. Postea, O. & Biel, M. Exploring HCN channels as novel drug targets. *Nat Rev Drug Discov* **10**, 903-914 (2011).
150. Li, Y.K., *et al.* Aquaporin-4 deficiency impairs synaptic plasticity and associative fear memory in the lateral amygdala: involvement of downregulation of glutamate transporter-1 expression. *Neuropsychopharmacology : official publication of the American College of Neuropsychopharmacology* **37**, 1867-1878 (2012).

151. Loo, D. In Situ Detection of Apoptosis by the TUNEL Assay: An Overview of Techniques. in *DNA Damage Detection In Situ, Ex Vivo, and In Vivo*, Vol. 682 (ed. Didenko, V.V.) 3-13 (Humana Press, 2011).
152. Petersen-Jones, S. Advances in the molecular understanding of canine retinal diseases. *The Journal of small animal practice* **46**, 371-380 (2005).
153. Li, Z.Y., *et al.* Rhodopsin transgenic pigs as a model for human retinitis pigmentosa. *Investigative ophthalmology & visual science* **39**, 808-819 (1998).
154. Hunter, J.J., *et al.* The susceptibility of the retina to photochemical damage from visible light. *Progress in retinal and eye research* **31**, 28-42 (2012).
155. Comparison of Age-related Macular Degeneration Treatments Trials Research, G., *et al.* Ranibizumab and bevacizumab for treatment of neovascular age-related macular degeneration: two-year results. *Ophthalmology* **119**, 1388-1398 (2012).
156. Ladas, I.D., *et al.* Safety of repeat intravitreal injections of bevacizumab versus ranibizumab: our experience after 2,000 injections. *Retina* **29**, 313-318 (2009).
157. Stacey, P.C., *et al.* Effectiveness of computer-based auditory training for adult users of cochlear implants. *International journal of audiology* **49**, 347-356 (2010).
158. Garcia-Amoros, J., Diaz-Lobo, M., Nonell, S. & Velasco, D. Fastest thermal isomerization of an azobenzene for nanosecond photoswitching applications under physiological conditions. *Angew Chem Int Ed Engl* **51**, 12820-12823 (2012).
159. Marc, R.E., Jones, B.W., Watt, C.B. & Strettoi, E. Neural remodeling in retinal degeneration. *Progress in retinal and eye research* **22**, 607-655 (2003).
160. Jones, B.W., *et al.* Retinal remodeling triggered by photoreceptor degenerations. *The Journal of Comparative Neurology* **464**, 1-16 (2003).
161. Lewis, A.S. & Chetkovich, D.M. HCN channels in behavior and neurological disease: Too hyper or not active enough? *Molecular and Cellular Neuroscience* **46**, 357-367 (2011).
162. Santoro, B., *et al.* TRIP8b Splice Variants Form a Family of Auxiliary Subunits that Regulate Gating and Trafficking of HCN Channels in the Brain. *Neuron* **62**, 802-813 (2009).
163. Müller, F., *et al.* HCN channels are expressed differentially in retinal bipolar cells and concentrated at synaptic terminals. *European Journal of Neuroscience* **17**, 2084-2096 (2003).
164. Mourot, A., Tochitsky, I. & Kramer, R.H. Light at the end of the channel: Optical manipulation of intrinsic neuronal excitability with chemical photoswitches. *Frontiers in Molecular Neuroscience* **6**(2013).